HEAT TRANSFER AND PRESSURE DROP STUDIES OF GAS-SOLID FLOW IN ADIABATIC PIPES USING A VARIABLE GAS PROPERTY TWO-FLUID MODEL

A Thesis submitted in the partial fulfillment of the requirements for

the award of the degree of

Doctor of Philosophy

in

Mechanical Engineering

by

Brundaban Patro

(Roll No. 716122)

Under the Supervision of

Dr. K. Kiran Kumar, Associate Professor

&

Dr. D. Jaya Krishna, Associate Professor

Department of Mechanical Engineering

National Institute of Technology Warangal

Telangana – 506 004 (India)

July 2021

Dedicated

to

- *My beloved father and mother*
- *My wife Madhusmita Patro*

Department of Mechanical Engineering
National Institute of Technology Warangal
Telangana, India – 506 004

CERTIFICATE

This is to certify that the thesis entitled, **"Heat Transfer and Pressure Drop Studies of Gas-Solid Flow in Adiabatic Pipes using a Variable Gas Property Two-Fluid Model",** being submitted by **Mr. Brundaban Patro (Roll No. 716122)** to the Department of Mechanical Engineering, National Institute of Technology Warangal, for the partial fulfillment of the award of the degree of Doctor of Philosophy, is a record of bonafide research work carried out by him under our supervision and guidance. This thesis, in our opinion, is worthy of consideration for the award of the degree of Doctor of Philosophy in accordance with the regulation of the institute. To the best of our knowledge, the results embodied in this thesis have not been submitted to any other University or Institute for the award of any degree or diploma.

Date: 14.07.2021

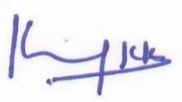

Supervisor
Dr. K. Kiran Kumar
Associate Professor
Department of Mechanical Engineering
National Institute of Technology Warangal
Telangana, India- 506 004

Co-Supervisor
Dr. D. Jaya Krishna
Associate Professor
Department of Mechanical Engineering
National Institute of Technology Warangal
Telangana, India- 506 004

DECLARATION

I hereby declare that the matter embodied in the thesis entitled **"Heat Transfer and Pressure Drop Studies of Gas-Solid Flow in Adiabatic Pipes using a Variable Gas Property Two-Fluid Model"** is the result of research carried out by me under the supervision of **Dr. K. Kiran Kumar** and **Dr. D. Jaya Krishna** in the Department of Mechanical Engineering, National Institute of Technology Warangal, Telangana, India. This work or part of this work has not been submitted to any other University or Institute for the award of any other degree or diploma.

Date: 14.07.2021
Place: Warangal

(Brundaban Patro)
Research Scholar
Roll No. 716122

ACKNOWLEDGEMENTS

I would like to express my deep and sincere gratitude to my supervisor Dr. K. Kiran Kumar and co-supervisor Dr. D. Jaya Krishna for their guidance, motivation, and good wishes. Their interests in the topic, convenience of the discussion sessions, and appropriate suggestions have been the main source of inspiration for the present research work. I am grateful to my supervisors for giving me ample freedom for generating new ideas.

I would like to express my thanks to university authorities, Prof. N.V. Ramana Rao, Director, National Institute of Technology Warangal, and others for giving me an opportunity to carry out this research work.

I would like to express my deep sense of gratefulness to the members of my Doctors Scrutiny Committee (DSC), Prof. Adepu Kumar (HOD); Prof. S. Srinivas Rao; Dr. Karthik Balasubramanian of the Mechanical Engineering Department and Dr. G. Uday Bhaskar Babu of the Chemical Engineering Department, for thoughtful advice during the discussion sessions. I sincerely thank all faculties and staff of the Mechanical Engineering Department for their kindness to me.

I also prompt my thankfulness to all friends including research scholars at National Institute of Technology Warangal for supporting me. Especially, I would like to thank Mr. Ramesh Babu Bejam, Mr. Ranga Babu, Mr. Sai Sudheer, Mr. P. Mahesh, Mr. Nandan Hegde, and Mr. Raghuvaran for making my stay at National Institute of Technology Warangal memorable and pleasant. I am also thankful to all those people who have directly or indirectly helped me to carry out this research work.

I am also grateful to my parents and family members for their support. Especially, I am very much thankful my wife Mrs. Madhusmita Patro and my elder brother Dr. Pandaba Patro for continuous encouragement and motivation.

I am always thankful to my institute National Institute of Technology Warangal, where I learned many things along with the research. I am also thankful to all supporting and technical staff of the Mechanical Engineering Department, who have directly or indirectly helped me

during the research work. Moreover, I am thankful to the library staff and administrative staff of National Institute of Technology Warangal for their cooperation.

NIT Warangal (Brundaban Patro)

14th July 2021

Abstract

Gas-solid flows occur in several industrial processes, for example, drying and/or preheating, separation, pneumatic conveying, and fluidization. Poor handling of solid particles may result in poor system performance. Therefore, it is necessary to effectively design the system based on various factors such as type of material, solid loading ratio (SLR), particle size, gas velocity, and many others. The heat transfer and pressure drop studies of gas-solid flows have been conducted in horizontal and vertical, adiabatic pipes, using a **variable gas property two-fluid model**. The present computational model is satisfactorily validated with the benchmark experimental data and other theoretical results. **The computational results show that the variable gas properties model meaningfully affects both heat transfer and pressure drop when compared with the constant gas properties model in the case of the horizontal pipe**. However, in the case of the vertical pipe, there is an insignificant deviation in the results of heat transfer, and there is a significant deviation in the pressure drop results between the variable and constant gas properties models.

The Nusselt number and pressure drop have been studied in horizontal and vertical pipes with respect to particle size, SLR, and gas Reynolds number. **Two correlations have been generated to predict the average gas-solid Nusselt number, one for the horizontal pipe and the other for the vertical pipe.** Similarly, the local heat transfer studies (temperature profiles of the gas and solid, local logarithmic mean temperature difference, local Nusselt number, and thermal effectiveness of the gas and solid) have been conducted in horizontal and vertical pipes. The local heat transfer studies show similar trends in both horizontal and vertical pipes.

The heat transfer and pressure drop results are compared using plastic, sand, and glass particles in horizontal and vertical pipes. The gas temperature is higher for air-glass flow and lower for air-plastic flow along with the axial distance for both horizontal and vertical pipes. However, the particle temperature is higher for air-glass flow and lower for air-plastic flow in the equilibrium temperature region. Up to a part of the initial length, the particle temperature is higher for air-sand flow and lower for air-glass flow. For both horizontal and vertical flows, the Nusselt number is higher for glass particles. But the lower Nusselt number shows different behavior based on the particle size, SLR and gas velocity in the horizontal flow. The Nusselt

number is lower for plastic particles for the vertical flow. For both horizontal and vertical flows, the pressure drop is higher for glass particles and lower for plastic particles with respect to the particle diameter, inlet SLR, and inlet gas velocity.

A new concept which is called the **heat properties ratio** is defined for gas-solid flows. The heat properties ratio is defined as the ratio of the multiplication of the density, specific heat, and thermal conductivity of the solid to the gas. **The heat properties ratio is useful when different solid particles having different properties are used, which affect significantly the effective gas properties.** It is observed that a higher value of heat properties ratio results in a higher Nusselt number. Finally, the Comparison of heat transfer and pressure drop results between the horizontal pipe flow and vertical pipe flow is carried out.

Keywords: *gas-solid flow; two-fluid model; Nusselt number; pressure drop; logarithmic mean temperature difference; thermal effectiveness; solid loading ratio.*

Table of Contents

List of Figures

List of Tables

Nomenclature

Abbreviations

CFB	circulating fluid bed
CFD	computational fluid dynamics
DEM	discrete element model
FCC	fluid catalytic cracking
HTC	heat transfer coefficient
L/D	length to diameter ratio
LMTD	logarithmic mean temperature difference
SC	specularity coefficient
SLR	solid loading ratio
SVF	solid volume fraction

English symbols

a_1, a_2, a_3, a_4	regression parameters for the horizontal pipe
A_s	particle heat transfer area (m^2)
b_1, b_2, b_3, b_4	regression parameters for the vertical pipe
A, B, C, D, E, F, G, H	coefficients
$C_{1\varepsilon}, C_{2\varepsilon}, C_{3\varepsilon}, C_\mu, \sigma_k, \sigma_\varepsilon$	turbulence model constants
C_D	drag coefficient
C_L	lift coefficient
C_p	specific heat at constant pressure (J/kgK)
d_s	particle diameter (m)
D	pipe inner diameter (m)
e_{ss}	particle-particle restitution coefficient
e_{sw}	particle-wall restitution coefficient
f	friction factor
F_L	lift force (N)
$\vec{g}$	acceleration due to gravity (m/s^2)
$g_{0,ss}$	radial distribution function

$G_{k.g}$	production of turbulent kinetic energy of gas (kg/ms^3)
$h_{gs,}$ h_{sg}	heat transfer coefficient between phases (W/m^{2}K)
$\bar{\bar{I}}$	unit tensor
k	thermal conductivity (W/mK)
k_{eff}	effective thermal conductivity of the gas (W/mK)
k	turbulent kinetic energy (m^2/s^2)
K	constant
K_{gs}, K_{sg}	momentum exchange coefficient between gas-solid (kg/m^{3}s)
l	axial distance along the length (m)
Δl, Z	distance from the inlet (m)
L	pipe length (m)
L/D	pipe length to diameter ratio
m	solid loading ratio
$\dot{m}$	flow rate (kg/s)
M_s	solid holdup (kg)
Nu_{avg}	average gas-solid Nusselt number
Nu_l	local gas-solid Nusselt number
Nu_s	particle Nusselt number
P_{op}	operating pressure (Pa)
$\bar{p}$	mean pressure (Pa)
$\bar{p_s}$	mean solid pressure (Pa)
Δp	pressure drop (Pa)
Pr	Prandtl number
r	radial position (m)
R	pipe radius (m)
R_A	gas constant (J/kgK)
Re_g	gas-phase Reynolds number
Re_s	particle Reynolds number
S	thermal effectiveness
t	time unit (s)
T	temperature (K)

ΔT	temperature difference between phases (K)
q	heat flux (W/m^2)
$\vec{v}$	mean velocity (m/s)
$\vec{v}_{gc}$	centreline gas velocity (m/s)
U	overall gas-solid heat transfer coefficient (W/m^2K)

Greek symbols

α	volume fraction of the phase
$\alpha_{s,max}$	maximum packing limit
$\gamma\theta_s$	energy dissipation due to collisions (kg/ms^3)
ε	dissipation rate due to turbulent kinetic energy (m^2/s^3)
η	effectiveness factor
θ_s	granular temperature (m^2/s^2)
$\kappa_{\theta s}$	diffusion coefficient
λ	bulk viscosity (kg/ms)
μ	shear viscosity (kg/ms)
μ_{gn}	normal dynamic viscosity of the gas (kg/ms)
$\mu_{t,g}$	turbulent viscosity of the gas (kg/ms)
$\Pi_{k,g}$	impact of the solid on the gas for turbulent kinetic energy (kg/ms^3)
$\Pi_{\varepsilon,g}$	impact of the solid on the gas for turbulent kinetic energy dissipation rate (kg/ms^4)
ρ	density (kg/m^3)
$\bar{\bar{\tau}}$	stress tensor (kg/ms^2)
ϕ_{gs}	energy exchange between the phases (kg/ms^3)

Subscripts

coll	collisional
ε	turbulent kinetic energy dissipation rate
g	gas phase
i	inlet
j	gas or solid

k	turbulent kinetic energy
kin	kinetic
n	at any location of the pipe
o	outlet
s	solid phase

Superscripts

T	transpose of the vector

Chapter 1

Introduction

1.1 Background

The transportation of fluids through pipes is not a modern concept and has been started several years back. For example, the Roman people used lead pipes for water supply and sewerage disposal. The Chinese people used bamboo tubes for conveying natural gas from one location to another. Similarly, solid materials have been conveyed by gaseous suspensions for many years without the proper knowledge of transporting mechanism. The main intention was to convey the solid particles from one place to another. The first pneumatic conveying of solids using air was started with the commencement of fans in 1866. The negative and positive pressure conveying was started in the mid-1920s for the transportation of grains. Since then, the exercise of pneumatic conveying has grown principally and has extended to include a diversity of solid materials.

Then, the simultaneous heat transfer in pneumatic conveying was started slowly. The simultaneous heat transfer in pneumatic conveying added much complexity to the system. The topic of heat transfer in gas-solid flows entered into scientific importance during the 1950s. During that time, seeding the flow with particles was well-thought-out as a heat transfer enhancement method. Moreover, during that period, graphite suspensions were used to act as cooling media in nuclear reactors. The earlier works involved in gas-solid flows were the development of correlations for the suspension heat transfer coefficient (HTC) and suspension properties. Then, the experimental works were started on this topic, as the gas-solid flow applications raised to circulating fluid bed (CFB) and transport reactors. The gas-solid flow topic was further advanced.

During the years, theoretical and experimental efforts were used to predict the suspension HTC with different values of solid loading ratio (SLR). Several correlations have been generated to predict the HTC using the empirical approaches, which showed contradictory trends of variations, as reported by Maeda et al. [1]. Again, the theoretical efforts failed in justifying these discrepancies. Then, a renewed interest in the form of CFBs appeared in the literature for heat transfer.

In the last three decades, the upward flow CFBs have been developed as new types of gas-solid reactors, whose applications are found in chemical and process industries. Further, concurrent downward flow CFBs were proposed as alternatives to upward flow CFBs. Despite many years of research, the so-called theory of gas-solid flows, including heat transfer is still in the development stage, because of the diversity of materials to be conveyed.

1.2 Gas-solid flow and its applications

The transportation of solid particles in a flowing gas stream is known as a gas-solid flow. The applications of gas-solid flows are seen in numerous industries such as power plants, chemical, food, process, pharmaceutical, and metallurgical industries. The applications include pneumatic conveying [2,3], CFBs [4], and powder handling [5].

Pneumatic conveying is a major example of gas-solid flows because of its widespread applicability in industries, to transport a wide variety of solid particles. The pneumatic conveying approach was first developed in the middle of the 19^{th} century to transport grains. In most cases, the gas used is usually air. Nevertheless, different gases are used in special conditions such as fire hazards, risk of explosion, and health. In pneumatic conveying, solid materials are transported from one location to another with the help of a gas. The solid materials may be suspended in nature or like a sliding bed. The solid particles are not prone to damage by contact with the pipe wall during the transportation process. Solid particles such as coal, flour, lime, soda ash, plastic pellets, gunpowder, ores, grains, and granular chemicals are generally transported by pneumatic conveying [6–10]. The major benefit of pneumatic conveying is the flexibility of the line location and the ability to tap the line at arbitrary locations.

A fluidized bed is another significant example of gas-solid flow and is a major part of many chemical processes [11]. The fluidization system is one of the most often used systems involving heat and mass transfer. The heat and mass transfer behavior in fluidized beds are important when there occur processes such as drying, polymerization, and chemical synthesis. In fluidized beds, there exists a large heat exchange between the solids and gas, due to the essential thorough gas-solid contact and/or quick mixing of both phases.

Drying is one of the major applications of gas-solid flow, which encompasses heat and mass transfer. Drying of solid particles is found in chemical, process, pharmaceutical, polymer, and many other industries. The drying of solid particles such as powdered and granular materials can be done utilizing a hot flowing gas. The gas used is usually air because of its free suitability. Hence, air drying is one of the widely used drying techniques available in recent particulate systems. Many mineral processing operations require simultaneous pneumatic conveying and drying. It is reported that the conventional transport theory is sufficient for numerical modeling of solids drying process [12]. Further, Kaensup et al. [13] reported that the pneumatic conveying drying is better than the fluidized bed drying from the point of energy consumption.

The cooling of a nuclear reactor can be improved with the help of a coolant like gas with suspended solid particles in it. Such types of coolants may be applied in gas-cooled reactors to enhance heat transfer by several times [14,15]. Moreover, the gas-solid suspensions are beneficial when used in Brayton cycle systems [16].

Other applications of gas-solid flow include roasting of ores, disposal of solid wastes, and preheating of solids. The practice of pneumatic conveying as a gas-solid heat exchanger in the form of preheater and dryer is found in pharmaceutical, metal, and cement industries. Preheating of solid materials is one of the pre-treatment processes. The metal scraps can be preheated using the waste heat of flue gas. There is a significant reduction in the processing time of metals (up to 20 minutes) when the scraps are heated before charged into the melting zone [17].

Heat transfer has an important influence on the performance of the conveying system. Some industrial applications that involve heat transfer in gas-solid flow are:

- Conveyance of hot particles with a gas from one place to another

- In a bagging plant, transportation of polyethylene solids from dryer
- Transportation of pulverized fuel ash for disposal
- Drying and/or preheating of solid particles with the help of flue gas of furnaces
- Preheating of coal before carbonization in a coking plant
- Heat recovery from waste hot flue gas-catalyst mixtures with waste heat boilers in a petrochemical industry

Therefore, heat transfer acts a major role in designing such systems and has been a repeated and interesting topic of research. Heat transfer of gas-solid flows is the main interest of chemical, mechanical, process, and environmental engineers. In the late 1950s, many experimental as well as theoretical works have been carried out by several researchers to simplify the mechanisms and characteristics of heat transfer of particulate flows. Depew and Kramer [18] extensively carried out reviews on heat transfer of particulate flows.

Moreover, previous works have reported that the introduction of solids in a flowing gas enhances heat transfer [19–21]. The heat transfer increases due to the increased volumetric heat capacity of the working fluid, because of the decreased axial temperature difference and gas-side HTC. Because of this, gas-solid suspensions are being considered as coolants for nuclear reactors.

The demerits of the use of solid particles in a gaseous stream as a heat transfer augmentation technique are the cleaning and erosion issues. Nevertheless, the topic of heat transfer has attracted major attention in pneumatic conveying and solids drying process [22]. Moreover, the heat transfer has been a great interest topic in drying and conveying powdered materials in the design of transport reactors [23].

1.3 Dilute phase versus dense phase gas-solid flows

The gas-solid flows may be classified as a dilute phase or a dense phase, based on the concentration of solid particles in a gas. A dilute phase gas-solid flow is the one in which the particle motion is controlled by the drag and lift forces. On the other hand, a dense phase gas-solid flow is the one in which the particle motion is mainly controlled by the particle-particle collisions. In a dilute phase gas-solid flow, the solids are suspended in a flowing gas. Hence,

the dilute phase gas-solid flow is also known as the suspension flow. The characteristics of dilute phase and dense phase gas-solid flows are presented in Table 1.1 [24].

Table 1.1: Characteristics of dilute phase and dense phase gas-solid flows

Dilute phase	**Dense phase**
High velocity flow	Low velocity flow
(12 m/s to 17 m/s for fine particles)	(typical 3 m/s)
High attrition	Low attrition
Large pipe size	Small pipe size
Low pressure	High pressure
(less than 100 kPa)	(typically 100 kPa to 600 kPa)
Low SLRs (up to 15)	High SLRs (more than 100)

1.4 Gas-solid flow through pipes

Gas-solid flow through pipes is seen in numerous industries such as chemical, process, pharmaceutical, polymer industries, and many others. The applications include pneumatic conveying, fluidized beds, drying and preheating, etc. Horizontal and vertical pipes are the simplest form of pipes used in industries for various applications, for example, pneumatic conveying of solids from one location to another. A schematic of gas-solid flow through pipes showing various parameters is given in Figure 1.1.

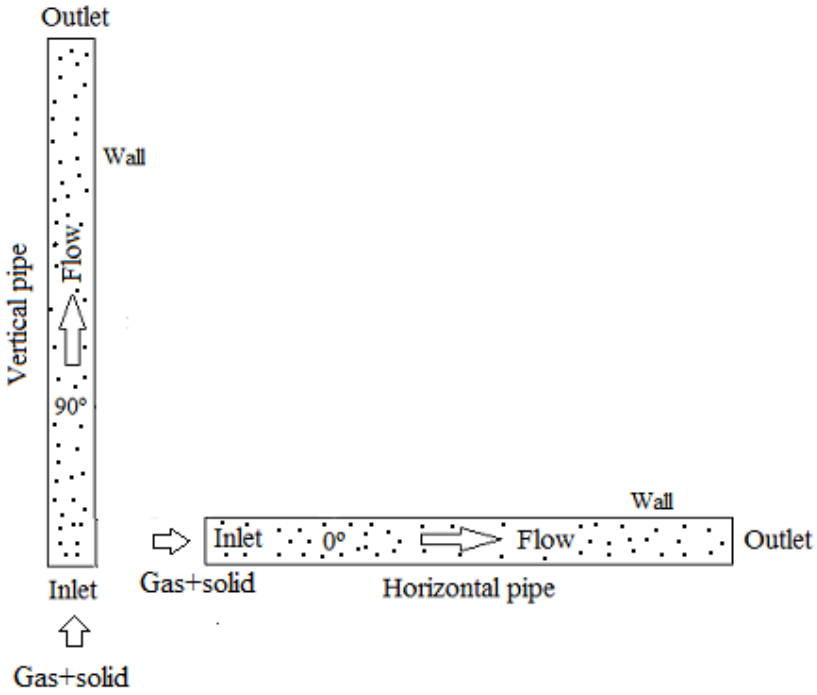

Figure 1.1: A schematic of gas-solid flow through pipes

In horizontal flows, the particle motion is not always straight in horizontal direction. Hence, horizontal gas-solid flows have always been a challenge due to particles accumulate at the bottom of the pipe by gravity, further collisions, and reenter the gas flow. The particle-particle and particle-wall collisions act a dominant role in horizontal flows and significantly affect the flow phenomena [25]. On the other hand, the upward vertical gas-solid flows are always against the gravitational forces, which significantly affect the flow behavior.

The gas-solid flows through pipes are complex, especially when heat transfer comes into play. Hence, special provisions are required in the design of such systems. Several factors such as SLR, gas velocity, pipe size and configuration, particle size, particle density, particle shape and distribution, particle feeding device, and transport direction affect gas-solid flows [26]. Moreover, several researchers [27–29] found that SLR, particle size, and flow Reynolds number significantly affect thermo-hydrodynamics of particulate flows.

The system of transporting solid particles by gaseous suspensions in pipes has been used broadly for many years. The particle-fluid interactions are very important for the design of transportation systems and are still not well understood. If heat transfer plays a role in these systems, the process will be very complicated from the energy exchange point of view.

With the advance in the understanding of the hydrodynamics, the heat transfer of gas-solid flows has been studied by several researchers. It has been revealed from the previous research studies that the heat transfer behavior is controlled by the hydrodynamics of gas-solid flows [30–37].

The use of solids in gases in heat transfer systems (i.e., through pipes) may show to be useful when an intensification in the heat transfer rate is looked for with a minimum pressure drop.

1.5 Computational fluid dynamics (CFD)

Most of the experiments in gas-solid flows are carried out on the laboratory scale, and the actual setups are not possible, because of the requirement of high costs and space. Moreover, the direct experimental validation of gas-solid flows with heat transfer is crucial, particularly in drying process, as reported by Li et al. [38,39], after successfully carried out discrete modeling. Hence, in these situations, computational fluid dynamics (CFD) studies are beneficial.

CFD is the process of solving the governing equations of flow and/or heat transfer using mathematical modeling. It solves the equations numerically using computational power. With the rise of high-speed computers and high-efficient algorithms, CFD became a powerful tool among researchers to solve fluid flow problems. Therefore, it is now possible to solve the complex, turbulent gas-solid flow equations with the use of CFD.

In CFD software, a mathematical model of the physical problem and a numerical method is used. A mathematical model varies with the type of the problem such as heat transfer, mass transfer, change of phase, chemical reactions, and others. Nevertheless, the validation of the mathematical model is very important.

The CFD analysis process is outlined below.

- Formulate the fluid flow problem
- Model the computational domain
- Set the initial and boundary conditions
- Generate the mesh
- Establish the simulation procedure

- Perform the simulation
- Monitor the simulation for the convergence
- Post-processing of the simulation (to get the results)
- Validation of the simulation results (compare the simulation results with the experimental or analytical results)
- Repeat the simulation process to examine the sensitiveness
- Documentation of the findings of the analysis

1.6 Numerical modeling of gas-solid flows

With the development of high-performance computers during the previous two decades and efficient algorithms, numerical computations came into existence to treat the complex, turbulent gas-solid flows. Usually, two models are available for numerical modeling of gas-solid flows. One is the Euler-Euler model, and the other is the Euler-Lagrange model. The Euler-Euler model (also well known as the two-fluid model) treats both phases as continuum, whereas the Euler-Lagrange model (for example, particle-in-cell, discrete element model (DEM), and discrete phase model) treats the solid phase as a discrete phase. Nevertheless, the CFD-DEM began to flourish because of the immense advances in the computer's abilities.

The disadvantage of the Euler-Lagrange model is that the time taken to compute a problem is much higher than the Euler-Euler model [40]. The time required to solve a problem is related to the number of particles in the computational domain. The two-fluid model is the appropriate model for numerical modeling of gas-solid flows [41,42]. The two-fluid model has been used by several investigators [43–45] to study pneumatic drying of solid particles. Therefore, the two-fluid model is used in the present work.

1.7 Organization of the thesis

The present thesis consists of seven chapters, and the prominent features are enunciated in each chapter.

Chapter one provides a general introduction of the research topic, including the applications undertaken in the present thesis. This chapter also defines the broad organization of the thesis,

which clearly states what is expected in each of the chapters for better understanding and reading.

Chapter two deals with an extensive literature survey on the research topic undertaken in the current thesis. After the extensive literature survey, conclusions are drawn and the research gaps are identified. Then, the research objectives are derived and the research methodology is presented.

Chapter three deals with the mathematical model of the present research work. All the governing and constitutive equations are presented in this chapter. This chapter also includes various initial and boundary conditions used in the present work. Finally, the numerical procedure is explained.

Chapter four focuses on the heat transfer and pressure drop studies of gas-solid flow through a horizontal, adiabatic pipe. First, the grid and time-step independence tests for the horizontal pipe are presented here, followed by the numerical sensitivity studies. The numerical model is validated concerning the bench-mark experimental results available in the literature and other theoretical results. Then, the effect of various flow parameters such as SLR, particle size, and gas velocity is considered to determine the heat transfer and pressure drop. Moreover, a correlation is generated to calculate the average gas-solid Nusselt number in the horizontal pipe, based on the studied parameters. Finally, three different solid particles such as plastic, sand, and glass are used to compare the heat transfer and pressure drop in the horizontal pipe.

Similar to chapter four, chapter five focuses on the heat transfer and pressure drop studies of gas-solid flows through a vertical., adiabatic pipe. The grid and time-step independence tests are conducted at the beginning for the vertical pipe, followed by the numerical sensitivity studies. Moreover, the simulation results for the vertical pipe are validated concerning the bench-mark experimental results available in the literature and other theoretical results. The heat transfer and pressure drop studies are predicted based on the various SLR, particle size, and gas velocity. Moreover, a correlation is generated to calculate the average gas-solid Nusselt number in the vertical pipe, based on the studied parameters. Finally, three different solid particles such as plastic, sand, and glass are used to compare the heat transfer and pressure drop in the vertical pipe.

Chapter six emphasizes the comparative studies of heat transfer and pressure drop between the horizontal pipe and vertical pipe.

Chapter seven provides the overall conclusions derived from the present research topic and scope for future work.

1.8 Closure

The current chapter clearly expresses the background and motivation regarding the research problem considered in the current thesis. It also briefly explains all the chapters of the thesis to present a clear idea to readers.

Chapter 2

Literature Survey

2.1 Introduction

The hydrodynamics and heat transfer behavior of suspended particles in a gaseous stream has been studied for several years. There are numerous studies are available for gas-solid flows without heat transfer, i.e., in cold conditions. Therefore, the studies of gas-solid flows with heat transfer are considered in the present research work, due to the associate and interest of the present research work in this topic. The first published research study relating to heat transfer in gas-solid flows was found in the literature in the early 1960s. And over the years, widespread research works in terms of experimental and numerical studies have been done in this research topic, and various theoretical frameworks have been established to demonstrate the numerous thermo-hydrodynamics phenomena involved in this.

2.2 Literature of gas-solid flow in horizontal pipes with heat transfer

Numerous research studies have been conducted in the past to analyze gas-solid flows with heat transfer through horizontal pipes. These are briefly explained below including the latest studies.

Tien [46] carried out the first analytical attempt to study the heat transfer analysis of turbulent gas-solid flows in a circular pipe. He used SLRs of less than one. He found satisfactory agreement with the existing experimental results. He gave a clear understanding of the effect of solid particles on temperature distribution and heat transfer rate. He found that the average

Nusselt number increases with the SLR at different values of pipe length to diameter ratio (L/D). He also noticed that the heat transfer is more pronounced at a low L/D than a high L/D. The local Nusselt numbers were found to increase with increasing the SLR.

Briller and Peskin [47] experimentally studied the suspension heat transfer in heated and cooled gas-solid flows at a high Reynolds number of 130,000. They found that the suspension HTC is the same as the pure gas at the high Reynolds number. The suspension HTC was noticed to be independent of the particle diameter, SLR, and heating/cooling.

Depew and Cramer [48] carried out the thermo-hydrodynamics studies of particulate flow, using an experimental setup. They used two sizes of spherical glass particles such as 30 μm and 200 μm. The SLR was up to a value of 7, and the gas Reynolds number range was 10,000 to 30,000. They noticed larger Nusselt numbers at the pipe bottom than the top for the 30 μm particles. However, the 200 μm particles showed insignificant effects. The 200 μm particles produced more pressure drop than the 30 μm particles. They found no asymmetry of the wall temperature distribution for SLRs of less than one.

Sunderesan and Clark [49] experimentally studied the local HTCs of gas-solid flows on the circumference of a heated horizontal tube, using four types of Geldart-B particles. They found different heat transfer rates at various angular locations around the pipe. They found the presence of the stagnant zone on the top of the tube at low gas velocities. The bubble frequency and heat transfer rates were found to increase with an increase of the gas velocity.

Aihara et al. [50] experimentally carried out the heat transfer studies of gas-solid flows, using glass particles of size 43 μm. They used SLRs from 0 to 3 and gas Reynolds numbers from 30,000 to 120,000. They observed that the radial distributions of air temperature are affected by the addition of solid particles to air flow in both thermal and hydro-dynamically developed regions. The air temperature distribution was found to be complex variations with the increase of the SLR and air Reynolds number. They also found asymptotic Nusselt numbers in the azimuthal directions. The thermal boundary layer was observed to retard monotonously with the increase of the SLR at the top of the pipe. Also, the boundary layer development at the bottom of the pipe was found to increase with the increase of the SLR of above 1. Finally, they noticed that the gas Reynolds number and SLR significantly affect the heat transfer.

Li and Mason [40] computationally investigated the unsteady state heat transfer studies of dilute and dense phase flows of granular particles using the DEM and successfully validated with their experimental work. They modeled the gas phase as the continuum, whereas the particle phase as the discrete particles. They used 3-mm-sized polyethylene pellets as the solid phase. They reported the influence of particle concentration on the system performance.

Li and Mason [51] conducted numerical studies of drying of solids by air in a horizontal pipe, using the DEM. They found that the application of this technique is conceivable in the drying of solids. They found that the fine solid particles follow the temperature of the gas, although, there is a temperature difference between the particles and gas, during the drying of solids. Finally, they found that experimental validation is crucial.

Using a two-dimensional CFD-DEM, Li et al. [38] studied the crucial consequence of the particle transverse motion on heat transfer, while studying air drying of solids. They found that the transversal motion of the rebounding of the particles changes the gas temperature. The particle transversal motion was found to affect the thermal energy transport by the rebounding of the particles, and it modified the thermal boundary layer. They suggested that the experimental validation of the result was crucial.

Again, using a coupled CFD and DEM, Li et al. [39] noticed that the temperature difference between the pipe top and bottom is a direct consequence of the uneven distribution of the solids. They also found thermal energy transport due to the rebounding of particles as well as the alteration of the thermal boundary layer of the gas. Finally, they suggested that the above technique is capable of modeling air drying of solids; however, the experimental validation is a critical task.

Zheng et al. [52] investigated the gas-to-solid heat transfer by simulation and experiment, using a single barley particle. They presented the heat transfer from the wall to the gas and then from the gas to the particle. They noticed that the gas phase reaches thermal equilibrium and has a certain value after a short time when the pipe wall temperature is constant. The transient region was longer for the high-velocity particles. They also noticed that the particle temperature rises over the time spent in the heated region.

Brosh and Levy [53] modeled the heat transfer in gas-particle flows using the combined CFD-DEM, considering the particle temperature distribution. They noticed that the two-way coupling model produces better results than the one-way coupling model. The highest temperature was found to appear in the particle crust, which is valid for temperature-sensitive materials.

Zheng et al. [54] experimentally and numerically analyzed the heat transfer mechanism in a dense phase gas-solid flow. They noticed that the surface HTC increases with the increased gas velocity and a higher solid volume fraction (SVF) value produces a higher peak of the surface HTC. They found that the HTC is a function of the SLR.

Patro et al. [55] numerically (using the two-fluid model) studied the effect of SLR, particle size, and gas Reynolds number on heat transfer and pressure drop in dilute gas-solid flows, subjected to a heated wall. They found that increasing the SLR and particle size increases the pressure drop and heat transfer; however, increasing the gas Reynolds number increases the pressure drop and shows inconsistent behavior on heat transfer. They noticed that the circumferential heat transfer distribution is not symmetric; therefore, the heat transfer is nonuniform in horizontal gas-solid flows. They found that the maximum heat transfer takes place at the bottom part of the pipe. Finally, they found that the temperature of the solid and gas phases remains unchanged up to some distance, which depends on the gas velocity.

Patro [56] studied the thermo-hydrodynamics studies of gas-particle flows in a heated pipe, considering a higher value of the SVF (0.1), having particle sizes from 20 μm to 80 μm. It was observed that the pressure drop as well as the heat transfer increases with the SVF. The particle size had shown an insignificant influence on pressure drop and heat transfer at an SVF value of 0.001. For an SVF value of 0.1, the Nusselt number was found to decrease continuously and the pressure drop was found to increase, reaches a maximum value, and after that decreases with the increased particle size.

Senapati and Dash [57] numerically studied the thermo-hydrodynamics behavior in dilute particulate flows in a heated wall pipe, using particles of size from 2 μm to 20 μm and SVF values from 0.001 to 0.1. They found that the particle-particle collisions significantly affect the pressure drop. They also noticed an increased Nusselt number and pressure drop with

increasing the SVF. The Nusselt number was found to increase and the pressure drop was found to decrease with increasing the inlet slip ratio.

It is noticed from the above literature survey that most of the research studies in horizontal pipe gas-solid flows have been done for heated walls, and the research studies in gas-solid flows for horizontal, adiabatic walls are less. It is also noticed that the earlier numerical studies in horizontal pipes deal with either the constant properties of the gas or only the variable gas density. There is rare literature available to date to numerically model the gas-solid heat transfer in vertical, adiabatic pipes, considering the variable properties of the gas.

2.3 Literature of gas-solid flow in vertical pipes with heat transfer

Like the gas-solid flows through horizontal pipes, numerous studies have been conducted in the past to analyze gas-solid flows with heat transfer through vertical pipes. These are briefly explained below including the latest studies.

Farbar and Morley [19] first investigated the gas-solid flow heat transfer using alumina-silica catalyst particles and noticed a significant increase in the heat transfer rate. Furthermore, they noticed that the presence of solids affects the boundary layer and heat capacity of the mixture. They found that the temperature ratio (ratio of the solid temperature rise to the gas temperature rise) is independent of the SLR and is a constant value at a uniform gas flow rate. The temperature ratio was found to decrease with increase of the gas flow rate or decrease of the particle residence time.

Gorbis and Bakhtiozin [21] investigated the convection heat transfer in gas-graphite suspension flows. They noticed that the intensity of heat transfer declines with increasing the gas Reynolds number, due to a reduction in the turbulence. They also found that the Reynolds number equally affects the single-phase flow and the flow with solid particles. Moreover, the reduced particle size enhanced the heat transfer.

Depew and Farbar [58] experimentally reported the heat transfer in pneumatic conveying of spherical glass particles of size 30 μm and 200 μm. They used gas Reynolds numbers of 13,500 and 27,400 and SLRs of up to 7. They noticed large effects in the local Nusselt

numbers for 30 μm particles, but small effects for 200 μm particles. They also noticed a negligible heat transfer rate when the SLR is less than 0.5.

Farbar and Depew [59] investigated the heat transfer in gas-solid suspensions using glass particles of size 30 μm to 200 μm. They used SLRs from 0 to 10 and gas Reynolds numbers from 15,300 to 26,500. They noticed that there is a considerable increase in the HTC for 30 μm particles, and the increment in the HTC reduces as the particle size increases. They found an insignificant enhancement in the heat transfer for 200 μm particles. They also reported that the heat transfer rises with the increased SLR, and there is a linear relationship between the heat transfer factor and SLR.

Pfeffer et al. [16] generated two possible correlations for the convective HTC in gas-solid suspensions, after reviewing and analyzing several papers. For this, they considered several variables such as SLR, particle size, gas Reynolds number, and specific heat ratio of solid to gas. From the correlations, they noticed that the suspension HTC increases with the SLR and specific heat ratio; however, it decreases with an increase in the gas Reynolds number. The suspension HTC was found to be unaffected by the particle size.

Boothroyd and Haque [60] experimentally investigated the heat transfer in gas-zinc suspension flows in three different pipe sizes of 1 inch, 2 inches, and 3 inches bore. They used zinc particles of size up to 40 μm, SLRs up to 17, and gas Reynolds numbers from 35,000 to 1,00,000. They noticed a small increase in the HTC by reason of the presence of solid particles. They also observed the suppression of the turbulence due to particles for the small pipe, with the high Reynolds numbers. But they noticed a substantially higher Nusselt number than the single-phase flow, for the large pipe with the small Reynolds numbers.

Sadek [61] generated a correlation of the HTC in turbulent air-solid suspension flows, after analyzing several published data. The correlation was valid for the Reynolds number range 4,000 to 80,000, particle size range 20 μm to 600 μm, and SLRs up to 300. They found that a single parameter (average number of particles per unit gas volume in the pipe × square of the particle diameter × pipe diameter) correlates the data to an increase in the HTC. Danziger and Sadek [62] attempted to compare the correlation with the industrial data (Danziger 1963) [20]. Sadek [63] produced modified equations considering the corrected operating pressures, as reported by Danziger [64], and still got significant differences.

Matsumoto et al. [65] investigated the flow dynamics and heat transfer characteristics of gas-solid suspension flows, using glass and copper particles. They used particles of size 72 μm to 1130 μm, gas Reynolds numbers from 12,000 to 24,000, and SLRs up to 10. They observed a slight increase in the suspension HTC for glass particles at a higher SLR. They noticed insignificant effects for copper particles. They also developed a new correlation to calculate the HTC, under uniform wall temperature conditions.

Kim and Seader [66] experimentally studied the heat transfer to concurrently downward gas-solid suspension flows, under the uniform heat flux conditions. They used 329 μm glass particles in the air at SLRs up to 20. The gas Reynolds number range was 9,800 to 29,500. They observed that the suspension Nusselt number decreases with an increase in the SLR at high Reynolds numbers. They noticed a little effect of the gas alone flow at low Reynolds numbers. Again, they compared the suspension Nusselt numbers for the downward flow with the upward flow and found that the downward flow has a lower suspension Nusselt number than the upward flow.

Michaelides [67] developed a phenomenological model to study the heat transfer in gas-solid flows, having SLRs up to 10. In the model, he considered the gas-solid mixture as turbulent and single-phase with a variable density and variable heat capacity. The developed model was found to be in well matched with other experimental outcomes and correlations.

Han et al. [68] (using the two-fluid model) and Haim et al. [69] (using the Eulerian-Lagrangian model) carried out the heat transfer analysis of gas-solid suspension flows and found that there are two factors such as the viscous sublayer thickness and heat capacity-density ratio (ratio of the multiplication of the density and specific heat at a constant pressure of the particle to the gas), which are very much responsible for the heat transfer increase or decrease. They also found that the viscous sublayer size is important at a low SLR, and the effect of heat capacity-density ratio is dominant at a high SLR.

Park [70] experimentally studied the heat transfer in countercurrent gas-particle flows, using sand particles of size 1 mm and 1.7 mm. He observed that there exists an optimum SLR at which the heat transfer is maximum. He also noticed an increase in the HTC of up to 62% with the addition of particles. He observed a relatively small pressure drop.

Molodtsof [71] theoretically and experimentally investigated the thermo-hydrodynamics studies of dilute gas-solid flows. He observed a sudden transition to dense phase flow after a critical value of the solid concentration. Molodtsof and Muzyka [72] theoretically derived a general form of the suspension HTC as a function of the SLR and found it reliable with the experimental data.

Avila and Cervantes [27] numerically predicted the average HTC in turbulent air-solid flows using the Eulerian-Lagrangian model. The particle sizes were from 70 μm to 200 μm. They noticed that the large particles of size 200 μm do not increase the HTC, however, the small particles show a linear increase in the HTC. The suspension HTC was found to increase beyond the SLR of one. They observed that the suspension HTC is a function of the SLR, particle size, and flow Reynolds number.

Boulet et al. [73] numerically (using the two-fluid model) found that the particles strongly affect wall to suspension heat transfer. They also noticed that the heat transfer decreases at low SLRs (less than 2) and a further increase if more particles are introduced.

Kim et al. [74] investigated the bed-to-wall heat transfer in a downer reactor, using an experimental set up. They noticed an increased heat transfer with an increased suspension density (up to 19 kg/m^3) and with a decreased particle size (236 μm to 83 μm). They suggested a model for the calculation of the bed-to-wall HTC.

Ma and Zhu [75] experimentally studied the effects of distributor design in a downer reactor, using fluid catalytic cracking (FCC) particles. They found that the distributor structure suggestively affects the gas-solid flow at the entrance region. Further, Ma and Zhu [76] experimentally carried out comparative studies of heat transfer between concurrent downer and concurrent riser of a CFB, using FCC particles. They noticed that the different heat transfer in both cases is closely related to the hydrodynamics and distinct flow structure. They noticed that the operating conditions play a vital role in producing different results in both cases.

Sorensen et al. [77] investigated the thermo-hydrodynamics characteristics of concurrent, upward gas-solid flows, using suspended coal particles, and compared the results with the concurrent downward flows. They observed that the frictional pressure drop for the upward

flow is more than the downward flow. The Nusselt number was found to be slightly lower than the single-phase flow. However, the Nusselt number was found to be slightly more than the downward flow. They noticed that the particle Nusselt number value depends on the value of the gas Reynolds number as well as the SLR and nearly equal to the downward flow.

Bourloutski et al. [78] compared the heat transfer results in turbulent gas-solid flows using two modeling approaches such as the Eulerian-Lagrangian approach and the Eulerian-Eulerian approach. They found that the Eulerian-Lagrangian approach is limited to very low SLR and the accuracy of the solution decreases when the SLR increases, due to the significance of particle-particle collisions. They found that the calculation time increases as much as 3 to 5 times with the Eulerian-Lagrangian approach, as compared to the Eulerian-Eulerian approach.

Chagras et al. [79] numerically studied the effects of the diameter ratio of the particle to the pipe in non-isothermal, upward gas-solid flows, using the Euler-Lagrange method. They found that this ratio has an important role in the flow and temperature field. They noticed that the smaller particles increase the turbulence attenuation. They noticed that the suspension Nusselt number slightly decreases at moderate SLR with increasing the particle size.

Jin-song et al. [80] studied the influence of the SLRs on heat transfer in dilute gas-particle cross flows. They found an increased heat transfer in the case of high SLRs and a decreased heat transfer in the case of very low SLRs (less than 0.05). They developed a suitable correlation to predict the heat transfer from the experimental results, considering various SLR, particle size, and flow Reynolds number.

Mansoori et al. [81] developed a thermo-mechanical model to study heat transfer in gas-solid flows with a heated wall, using the Eulerian-Lagrangian method. They adopted a four-way interaction to consider the particle-particle and particle-wall collisions. They used 500 μm to 900 μm sand particles with SLRs up to 4. They noticed that the particle collisions significantly affect the thermal turbulence intensity and heat transfer. They found that the particle-particle collisions diminish the thermal turbulence intensity close to the wall. They noticed that the conduction heat transfer due to the particle-particle collisions is negligible.

Mansoori et al. [28] modeled heat transfer in upward, turbulent gas-solid flows with a heated wall, using the two-way Eulerian-Lagrangian approach. They studied the HTC variations at a gas Reynolds number of 20,000, using 200 μm sand particles, and found that the HTC varies with the SLR, particle diameter, and flow Reynolds number. They found that the HTC goes to a minimum value at a specific SLR, where the temperature fluctuation near the wall is minimum.

Mansoori et al. [82] experimentally and numerically studied the heat transfer in gas-solid flows at different particle temperatures, using a four-way Eulerian-Lagrangian approach. They found that the addition of hot particles (of size 600 μm to 1200 μm) to suspension flow can alter the HTC, and this effect depends upon the particle size and gas Reynolds number. They also found an increased heat transfer for the large-sized particles at a low gas velocity when introducing the hot particles to the gas flow.

Namkung and Cho [83] experimentally investigated the hydrodynamics studies of gas-solid flows in a pneumatic conveying dryer, using iron ore particles. They found that the pressure drop decreases in the acceleration region; however, it is constant in the fully developed region. The axial pressure drop profiles were unaffected by the inlet gas temperatures. They also noticed that the drying rate increases with increasing the gas velocity and gas temperature, but it decreases with increasing the SLR.

Mansoori et al. [84] studied the particle-particle heat transfer in gas-solid flows, considering the Euler-Lagrange method. They used hot and cold particles. They noticed that the particle-particle heat transfer is significant when the particle sizes are small, the flow Reynolds number is low, and the SLR is high. They found that the thermal properties of the solid particles do not affect the particle-particle heat transfer and the suspension heat transfer is unresponsive to the particle-particle heat transfer.

Everaert et al. [85] experimentally investigated the heat transfer in a single tube of a dilute CFB riser. They found a constant HTC for a low SLR at a constant gas flow rate, followed by an increasing HTC with an increasing SLR. The HTC was found to decrease with increasing the gas flow rate at a constant SLR.

Rajan et al. [86] numerically studied the heat transfer in a pneumatic conveyor with hot gas supplied and multiple gas inlets, using the two-fluid model (one-dimensional). They found higher heat recovery with more number gas inlets and lower gas to solid mass flow ratios.

Haim et al. [69] numerically studied the effects of geometrical and flow parameters on gas and solid temperature profiles, convection HTC, and thermal entry length in gas-solid flows with a heated wall, using a two-way Eulerian-Lagrangian model. They noticed an extended thermal entry length and a decreased bulk temperature, particle temperature, and convective HTC with increasing the particle size. Increasing the pipe diameter directed to decrease the thermal entry length, bulk and particle temperatures, and Nusselt number. Increasing the SLR was found to decrease the wall and bulk temperatures and increase the thermal entry length and convective HTC.

Narimatsu et al. [87] numerically investigated the drying of coarse particles in a pneumatic conveying dryer, considering the continuum model (one-dimensional), and found that the maximum HTCs are obtained at the point of minimum pressure drop velocity. They found that the gas-solid Nusselt number depends upon the particle Reynolds number, SVF, and Prandtl number. But they did not observe the dependence of the Nusselt number on the particle morphology.

Rajan et al. [88] proposed a two-fluid model to study the heat transfer in dilute phase pneumatic conveying. They noticed the effect of particle size on the flow behavior and heat transfer.

Saffar-Avval et al. [89] numerically studied the effect of collisions in upward gas-solid flows, using the Eulerian-Lagrangian method. They found flatter profiles of solids concentration, velocity, and temperature, due to the particle-particle collisions. From the study, they noticed that the particle-particle collisions play a major role in particle fluctuation velocity. Increasing the SLR led to the attenuation of the turbulence by the particle-particle collisions in the central region of the pipe.

Haim and Kalman [90] numerically developed a criterion whether to consider the internal particle conductivity or not in dilute gas-solid flows. They found that the convective HTC decreases by 45% by increasing the particle size by a factor of five.

Rajan et al. [91] experimentally studied the thermal effectiveness of gas-solid flows, using gypsum particles (200 μm to 800 μm in size). They noticed that the thermal effectiveness of the gas increases with the solid feed rate and it decreases with the gas velocity. They noticed that the thermal effectiveness of the solid decreases with the solid feed rate. They found an optimum gas velocity at which the maximum thermal effectiveness of solid occurs. Finally, they developed a correlation for the thermal effectiveness of the solid.

Rajan et al. [92] experimentally found that the air-particle heat transfer increases with an increase in the SLR in pneumatic conveying, using gypsum particles. Nevertheless, the air-solid heat transfer rate first increases with air velocity and then goes to a maximum value before a decrease in its value with an increase in the air velocity. The gas-solid HTC was found to increase at higher SLRs. They proposed a correlation to find the particle Nusselt number.

Mansoori et al. [93] performed three-dimensional simulations in turbulent gas-solid flows, using the four-way Eulerian-Lagrangian method, and found that the particle-particle collisions and SLR have a prominent effect on the simulation results. Increasing the SLR caused a more flattening of the gas velocity profiles and a decreased turbulence intensity of the gas and a velocity fluctuation of the solid phase. The particle-particle collisions made the solid phase temperature and velocity profiles more smooth. They suggested that the three-dimensional simulations provide better results for a higher SLR.

Behzad et al. [94] developed a thermal stochastic collision model for particulate flows, including a four-way coupling, to eliminate the higher simulation time of the Eulerian-Lagrangian model. They suggested that the developed model can be used in nearly dense gas-solid flows for SLRs up to 8.

Hamzehei et al. [95] carried out experimental and numerical studies of hydrodynamics and heat transfer in an upward gas-solid fluidized bed reactor, using the Eulerian-Eulerian model. They found a decreased gas temperature and an increased particle temperature in the upward direction. They found that the gas temperature decreases and the solid temperature increases with increasing the gas velocity. Finally, they suggested that the numerical model can predict the hydrodynamics and heat transfer behavior in fluidized bed reactors.

Rajan et al. [96] experimentally studied the thermal conductance of gas-solid flows, using sand and gypsum particles. They used the particle size range 200 μm to 800 μm, solid feed rate range 1 g/s to 14.1 g/s at low gas velocities (4–6 m/s). They found that the thermal conductance increases with increase of the gas velocity and SLR. They proposed a correlation for thermal conductance.

El-Behery et al. [97] investigated the flow behavior and heat transfer in dilute gas-solid flows, considering the Eulerian-Lagrangian model. They found that the heat transfer rate increases with an increase in the SLR and the Nusselt number increases with an increase in the pipe size. They noticed significant roles of the particle-particle collisions, turbulence dispersion, and lift force in the concentration distribution.

Azizi et al. [98] carried out a two-dimensional heat transfer modeling of gas-solid flows, considering the two-fluid approach. They found that the solids concentration is constant near the wall and a maximum value at the central region. They observed a flatter gas velocity profile at the center and a sharper around the wall. The solid temperature was found to increase uniformly towards the center of the pipe. Finally, they noticed that the addition of particles to the gas flow enhances the convective HTC.

El-Behery et al. [99] experimentally and numerically noticed that the flow conditions significantly affect the equilibrium temperature and equilibrium distance in gas-solid flows. The outcomes reported that there is a rise in the pressure drop in the dilute phase flow and a decrease in the pressure drop in the dense phase flow when the hot solids are added in the cold gas flow. However, a reverse effect was attained when colder solids are added to the hot gas flow.

Ibrahim et al. [100] experimentally and numerically studied the effect of swirling in the pneumatic conveying dryer, using the Eulerian-Lagrangian model. They observed that the swirling increases the drying process. However, the pressure drop in the swirling flow was found to be more than the non-swirling flow. The experimental results of Zheng et al. [101] proposed that the HTC in dense phase gas-solid flows with a heated wall shows a linear relationship with the SLR, and a higher value of the SLR consequences a higher value of the HTC.

Patro [29] numerically studied the wall to suspension heat transfer in gas-particle flows, considering the four-way coupled Eulerian-Eulerian model. He found a significant increase in the heat transfer with increasing the SLR and gas Reynolds number than the single-phase flow. The gas-solid Nusselt number was increased by increasing the SLR, particle size, and gas Reynolds number.

Bertoli et al. [102] established a mathematical model to study the heat transfer analysis of co-current moving bed gas-solid flows, having adiabatic walls. They used the lumped parameter analysis. They suggested that the developed method is in general use and can be applied to other engineering problems.

El-Behery et al. [103] predicted the pressure drop in pneumatic conveyors considering the two-fluid model. They noticed an increased pressure drop with increasing the SLR, particle size, and particle density. They noticed that the phase change (dense to dilute) happens at the lowest pressure drop.

Sahu et al. [104] studied the temperature effects on the hydrodynamics of dense air-coal particle flows, using the two-fluid model. They noticed that the variation of the minimum fluidization velocity with temperature depends on the particle diameter. The minimum fluidization velocity was decreased for small particles (0.5 mm in size) and it was increased for large particles (2.5 mm size) with increasing the temperature. They noticed that the operating temperature affects the gas-solid momentum exchange coefficient.

Arvind et al. [105] experimentally studied the effect of SLR, pipe height, and particle diameter on heat transfer. They observed that the heat transfer rate increases with the solid feed rate and particle size. The thermal effectiveness was found to increase with the pipe height, and it was decreased with the solid feed rate.

Dhurandhara et al. [106] carried out the comparative studies of hydrodynamics and heat transfer between a converging riser and an equivalent uniform riser. They found that the converging shape of the riser enhances the heat transfer. The pressure drop was noticed to be more for converging riser.

Watkins and Gould [107] experimentally studied the effect of flow rate and temperature (up to 1000 ºC) on heat transfer of gravity-driven dense flows. They observed that the HTC

increases with increasing the temperature. They found that the flow rate has a nominal impact on heat transfer. The radiation heat transfer did not come into play, due to smaller-sized 300 μm particles.

Wanchan et al. [108] investigated the wall-to-bed heat transfer in fluidized beds, applying the two-fluid model. They noticed that the HTC increases with increasing the SLR and it decreases with increasing gas velocity and particle size. Finally, they developed two correlations for FCC particles of 90 μm in size to calculate the HTC, considering the operating parameters, such as the SLR, superficial gas velocity, and solid diameter.

Tawfik et al. [109] investigated the hydrodynamics and heat transfer in a swirling gas-solid flow, using polyethylene beads of size 6 mm. The results showed that increasing the mass flow rate of polyethylene beads increases the pressure drop and decreases the HTC. The HTC was decreased with increasing the bed height. The heat transfer was enhanced and the bed pressure drop was decreased by introducing a cone-shaped metallic central body.

Popuri and Garimella [110] experimentally studied the effect of the solid feed rates and gas velocity on the heat transfer, using sand (480 μm in size), limestone (98 μm in size), and chalcopyrite (240 μm in size) particles. They calculated the overall HTCs and rate of heat transfer at different solid feed rates (0.0084 kg/s - 0.0329 kg/s). Finally, they developed a correlation to find the Nusselt number in terms of Reynolds number and Prandtl number.

Li et al. [111] studied the influence of hydrodynamics on heat transfer in a riser having external solids circulation, using the packet renewal model. They found that the mean residence time of packet (particle clusters) significantly affects heat transfer. They found that the packet renewal model can be used to predict the HTCs in fluidized beds with external solids circulation.

It is noticed from the above literature survey that most of the research studies on gas-solid flows with heat transfer are with vertical, heated pipes. Gas-solid flows with heat transfer in vertical, adiabatic pipes are limited. The temperature variable gas properties have not been used by previous researchers in gas-solid flow numerical works through vertical pipes. Some researchers have used the constant gas properties and some researchers have used only the

variable gas density in their numerical works. The consideration of variable gas properties in numerical studies of vertical flows is not available in the literature.

2.4 Literature of gas-solid flow in both horizontal and vertical pipes with heat transfer

This subsection deals with the studies of gas-solid flow with heat transfer in both horizontal and vertical pipes. These are briefly explained below including the latest studies.

Wahi [112] experimentally found that the large particles of 200 μm in size do not affect the heat transfer; but the small particles of 30 μm in size suggestively affect the heat transfer. In the case of 30 μm particles, the Nusselt number was first decreased up to an SLR of 1 and then increased with further increase in the SLR. Additionally, they found a noteworthy increment in the thermal entry length with increasing the SLR. The local Nusselt numbers were higher by 2% to 25% for the downward flows than the upward flows. This is due to the better thermal equilibrium in case of vertical downward flows as reported. Similarly, the horizontal flow results were higher than the upward flows by 2% to 13%. This is due to the stable heat transfer as a result of suspension flow in case of horizontal flows as reported.

Kane and Pfeffer [113] experimentally studied the HTCs of gas-solid flows, using air-glass, argon-glass, and argon-aluminum suspensions. They used particle sizes from 21.6 μm to 36 μm, gas Reynolds numbers from 11,000 to 21,000, and SLRs from 0 to 2.5. They noted a decrease in the HTC with the presence of particles. They found that, in the case of a horizontal pipe, this is because of the particle deposition at the pipe bottom, and in the case of a vertical pipe, this is due to the increased viscous sublayer thickness.

Chagras et al. [114] employed the four-way coupled Eulerian-Lagrangian method to model the gas-solid flows in heated tubes, having SLRs up to 10. They found that the role of collisions is significant in the flow dynamics of gas-solid flows that leads to a significant alteration in the thermal exchange rate. They noticed a negligible thermal exchange with the direct solid-solid contacts. The overall heat transfer was found to increase by 8% in the vertical flow, due to the particle-particle collisions.

2.5 Literature of gas-solid flow in inclined pipes with heat transfer

Finally, the gas-solid flow studies with heat transfer in inclined pipes are briefly explained in this subsection, including the latest studies.

Ebadi et al. [115] numerically studied the effect of wall roughness on heat transfer and temperature profiles at different inclination angles starting from 0° to 90°, using the four-way coupled Eulerian-Lagrangian model. They noticed a reduction in the Nusselt number at the bottom part of the pipe. The gas temperature was reduced in the pipe core and it was increased near the wall. They noticed that the presence of the wall roughness enhances the heat transfer.

Pishvar et al. [116] numerically studied the heat transfer characteristics of turbulent gas-solid flows in heated pipes, using the four-way coupled Lagrangian-Eulerian method. They applied a three-dimensional model with constant wall flux. They found an asymmetric nature of the gas velocity and thermal turbulence intensity profiles and an increased SVF at the bottom of the pipe. They found a significant increment in the Nusselt number and pressure at an inclination angle of lower than 90 ºC. They also noticed the influence of the SLR on the optimal inclination angle.

Mokhtarifar et al. [117] carried out the experimental modeling of heat transfer characteristics of gas-solid flows in adiabatic pipes. They found that the gas-solid Nusselt number decreases at lower SLRs, and it increases at higher SLRs in dilute gas-solid flows. In horizontal pipe gas-solid flows, they found that the gas and solid temperatures decrease with the increase in the SLR (0.413-0.568). The thermal effectiveness of air was noticed to increase with the solids feed rate (15-25 g/s). But the thermal effectiveness of solid was noticed to decrease up to 22 g/s solid feed rate, and at 25 g/s solid feed rate, an increasing trend was observed. Moreover, they found that the highest Nusselt number occurs at an angle of 45°. At 45° pipe angle with fixed gas velocity and SLR, the heat transfer rate is maximum and the driving force is minimum, hence the highest Nusselt number occurs at 45°.

2.6 Identification of research gaps from the literature survey

Based on the literature review, the following research gaps are identified.

i. Most of the research studies on gas-solid flows with heat transfer are with heated pipes. Gas-solid flows with heat transfer in adiabatic pipes are limited.
ii. The numerical modeling of gas-solid flows with heat transfer in adiabatic pipes is less.
iii. The temperature variable gas properties have not been used by previous researchers in gas-solid flow numerical works. Some researchers have used the constant gas properties and some researchers have used only the variable gas density in their numerical works. The consideration of variable gas properties in numerical studies is not available in the literature.
iv. The pressure drop studies of non-isothermal gas-solid flows in adiabatic pipes are less.
v. The detailed studies of several flow parameters such as SLR, particle size, and gas Reynolds number on heat transfer and pressure drop in gas-solid flows in adiabatic pipes are less.
vi. The studies of local heat transfer characteristics of gas-solid flows considering the effects of SLR, particle size, and gas velocity in adiabatic pipes are less.
vii. The correlation studies of heat transfer in gas-solid flows in adiabatic pipes are less.
viii. The comparative studies of heat transfer and pressure drop in gas-solid flows using different solid materials in adiabatic pipes are less.

2.7 Objectives of the present study

Based on the above research gaps, the following research objectives are formulated in the present research work.

i. Mathematical modeling of gas-solid flow heat transfer in adiabatic pipes and validation of the numerical model
ii. Studies of average gas-solid Nusselt number and pressure drop in gas-solid flow in a horizontal, adiabatic pipe, using sand particles
iii. Studies of average gas-solid Nusselt number and pressure drop in gas-solid flows in a vertical, adiabatic pipe, using sand particles
iv. Studies of local heat transfer characteristics of gas-solid flow in a horizontal, adiabatic pipe, using sand particles

v. Studies of local heat transfer characteristics of gas-solid flow in a vertical, adiabatic pipe, using sand particles
vi. Comparison of results of heat transfer and pressure drop in a horizontal, adiabatic pipe, using three different solid particles such as plastic, sand, and glass
vii. Comparison of results of heat transfer and pressure drop in a vertical, adiabatic pipe, using three different solid particles such plastic, sand, and glass
viii. Comparison of heat transfer and pressure drop results between horizontal pipe flow and vertical pipe flow

2.8 Research methodology

In the present research work, the numerical simulations based on the two-fluid model of ANSYS FLUENT 15.0 are carried out to study the gas-solid flow behavior through horizontal and vertical, adiabatic pipes. A nine-step research methodology is used in the present work and is presented below.

i. First, carrying out an extensive literature review
ii. Find out the research gaps and derive the research objectives, based on the literature review
iii. Mathematical modeling: Governing equations (such as continuity, momentum, and energy equations) and constitutive equations
iv. Geometric modeling and meshing
v. Providing initial and boundary conditions
vi. Simulation procedure
vii. Grid and time-step independent tests and numerical sensitivity studies
viii. Validation with the benchmark experimental data and other theoretical results
ix. Accomplishing the research objectives and results and discussions

2.9 Closure

A comprehensive review of the literature associated with gas-solid flows with heat transfer through pipes is presented. In some cases, a definite pattern is observed, and in some other cases, contradictory results are noticed. After an exhaustive literature survey, the research

gaps are identified and the research objectives are derived. Finally, the research methodology is explained.

Chapter 3

Mathematical Model

3.1 Introduction

A mathematical model of the flow problem is required to solve the problem numerically. The mathematical model consists of the governing equations as well as the constitutive equations. In the present study, the two-fluid model is used. The two-fluid model is based on the Eulerian-Eulerian approach, where the gas phase as well as the solid phase is assumed as continuum. Therefore, the two-fluid model may also be known as the Eulerian granular model, where the Eulerian-Eulerian approach is used.

The mathematical model of the gas-solid flow consists of the Eulerian- Eulerian model of ANSYS FLUENT 15.0, to solve the governing equations of the conservation of the mass, momentum, and energy. Moreover, various constitutive equations are required to close the governing equations. In dilute gas-solid flows, the gas phase is the primary phase and the solid phase is the dispersed phase. In the present work, the gas phase stresses are modeled by the standard $k-\varepsilon$ turbulence model [118], and the solid phase stresses are modeled using the kinetic theory of granular flow [119]. The gas properties such as density, dynamic viscosity, thermal conductivity, and specific heat are defined with the temperature of the gas in the computational domain.

The model assumptions are presented below.

i. The gas phase (air) is assumed as an incompressible, ideal gas.
ii. The mass transfer between the phases or source terms is neglected.
iii. The virtual mass force and external body forces are neglected.

iv. The radiation heat transfer is neglected. Since the system temperatures in the present study are less than 811K, the radiation effects are negligible [120].
v. The particles are assumed as spherical and monodispersed.
vi. The solid properties are assumed as constant with temperature.
vii. The particle velocity is equal to the gas velocity due to suspension flow.
viii. The moisture present in the particle phase is negligible.

3.2 Model equations

3.2.1 Governing equations

The equations have been taken from the two-fluid model of ANSYS FLUENT 15.0 and are presented below.

3.2.1.1 Continuity equations

The continuity equation for each phase is

$$\frac{\partial}{\partial t}\left(\alpha_j \rho_j\right) + \nabla \cdot \left(\alpha_j \rho_j \vec{v}_j\right) = 0 \tag{3.1}$$

where the subscript 'j' is either gas or solid.
Here, the mass transfer between the phases or source terms is neglected.

$$\sum \alpha_j = 1 \tag{3.2}$$

3.2.1.2 Momentum equations

The momentum equation for the gas phase is

$$\frac{\partial}{\partial t}\left(\alpha_g \rho_g \vec{v}_g\right) + \nabla \cdot \left(\alpha_g \rho_g \vec{v}_g \vec{v}_g\right) = -\alpha_g \nabla \bar{p} + \nabla \cdot \bar{\bar{\tau}}_g + \alpha_g \rho_g \vec{g} + K_{sg}\left(\vec{v}_s - \vec{v}_g\right) + F_{L,g} \tag{3.3}$$

Here, the subscript 'g' refers to the gas phase, and the subscript 's' refers to the solid phase.

The momentum equation for the solid phase is

$$\frac{\partial}{\partial t}\left(\alpha_s \rho_s \vec{v}_s\right) + \nabla \cdot \left(\alpha_s \rho_s \vec{v}_s \vec{v}_s\right) = \tag{3.4}$$

$$-\alpha_s \nabla \bar{p} - \nabla \overline{p_s} + \nabla \cdot \bar{\bar{\tau}}_s + \alpha_s \rho_s \vec{g} + K_{gs}(\vec{v}_g - \vec{v}_s) + F_{L,s}$$

Here, the virtual mass force and external body forces are neglected.

3.2.1.3 Energy equations

The energy equation for the gas phase is

$$\alpha_g \rho_g C_{pg} \left(\frac{\partial T_g}{\partial t} + \vec{v}_g . \nabla T_g \right) = -\nabla . q_g + h_{gs}(T_s - T_g) \tag{3.5}$$

The energy equation for the solid phase is

$$\alpha_s \rho_s C_{ps} \left(\frac{\partial T_s}{\partial t} + \vec{v}_s . \nabla T_s \right) = -\nabla . q_s - h_{gs}(T_s - T_g) \tag{3.6}$$

Here, the heat transfer due to radiation effects is neglected.

3.2.2 Constitutive equations

3.2.2.1 Stress tensor

The gas phase and solid phase stress tensors are

$$\bar{\bar{\tau}}_g = \alpha_g \mu_g (\nabla \vec{v}_g + \nabla \vec{v}_g^T) + \alpha_g \left(\lambda_g - \frac{2}{3} \mu_g \right) \nabla . \vec{v}_g \bar{\bar{I}} \tag{3.7}$$

$$\bar{\bar{\tau}}_s = \alpha_s \mu_s (\nabla \vec{v}_s + \nabla \vec{v}_s^T) + \alpha_s \left(\lambda_s - \frac{2}{3} \mu_s \right) \nabla . \vec{v}_s \bar{\bar{I}} \tag{3.8}$$

Here, the gas phase is taken as incompressible ($\lambda_g = 0$).

From the Lun et al. model [121], the solid bulk viscosity is

$$\lambda_s = \frac{4}{3} \alpha_s \rho_s d_s g_{0,ss} (1 + e_{ss}) \left(\frac{\theta_s}{\pi} \right)^{\frac{1}{2}} \tag{3.9}$$

The fluid phase viscosity (μ_g) is a combination of the normal viscosity (μ_{gn}) and the turbulent viscosity ($\mu_{t,g}$). The normal viscosity of the gas is defined as per the varying temperature, along the length of the computational domain. A two-equation $k - \varepsilon$ turbulence model is used to describe the turbulent viscosity ($\mu_{t,g}$).

The shear viscosity for the solid phase consists of two terms, i.e., a kinetic term and a collisional term, and is presented in eq. 3.10.

$$\mu_s = \mu_{s,kin} + \mu_{s,coll} \tag{3.10}$$

From the Syamlal et al. model [122],

$$\mu_{s,kin} = \frac{\alpha_s d_s \rho_s \sqrt{\theta_s \pi}}{6(3 - e_{ss})}\left[1 + \frac{2}{5}(1 + e_{ss})(3e_{ss} - 1)\alpha_s g_{0,ss}\right] \tag{3.11}$$

and

$$\mu_{s,coll} = \frac{4}{5}\alpha_s \rho_s d_s g_{0,ss}(1 + e_{ss})\left(\frac{\theta_s}{\pi}\right)^{\frac{1}{2}} \tag{3.12}$$

3.2.2.2 Solid pressure

The Lun et al. model [121] is used to calculate the solid pressure and is given in eq. 3.13.

$$\bar{p_s} = \alpha_s \rho_s \theta_s + 2\rho_s(1 + e_{ss})\alpha_s^2 g_{0,ss}\theta_s \tag{3.13}$$

where $g_{0,ss}$ is the radial distribution function.

The radial distribution function by the Lun et al. model [121] is

$$g_{0,ss} = \left(1 - \left(\frac{\alpha_s}{\alpha_{s,max}}\right)^{\frac{1}{3}}\right)^{-1} \tag{3.14}$$

where $\alpha_{s,max}$ is the maximum packing limit. The maximum packing limit is 0.63.

3.2.2.3 $k - \varepsilon$ Turbulence model

The standard $k - \varepsilon$ turbulence model (30 < wall y-plus > 300) [118] is selected, due to the ease of convergence, and it fast-tracks the solution process. Swain and Mohanty [123] noticed that the standard $k - \varepsilon$ turbulence model is preferred over the Reynolds stress model for smaller particles (99 μm in size), due to its less computational time. Moreover, several researchers [29,55,124,125] used the standard $k - \varepsilon$ turbulence model to study hydrodynamics and/or heat transfer analysis of gas-solid flows in different pipes. Therefore, it encourages the use of the standard $k - \varepsilon$ turbulence model in the present work.

This model includes two extra terms, for example, the turbulent kinetic energy for the gas phase (k_g) and the turbulent energy dissipation rate for the gas phase (ε_g) for the presence of solid particles in the preliminary gas phase.

In the gas phase, the turbulent kinetic energy (k_g) equation is

$$\frac{\partial}{\partial t}\left(\alpha_g \rho_g k_g\right) + \nabla.\left(\alpha_g \rho_g \vec{v}_g k_g\right) = \nabla.\left(\alpha_g \frac{\mu_{t,g}}{\sigma_k} \nabla k_g\right) + \alpha_g G_{k,g} - \alpha_g \rho_g \varepsilon_g + \alpha_g \rho_g \Pi_{k,g} \quad (3.15)$$

The turbulent energy dissipation rate (ε_g) equation is

$$\frac{\partial}{\partial t}\left(\alpha_g \rho_g \varepsilon_g\right) + \nabla.\left(\alpha_g \rho_g \vec{v}_g \varepsilon_g\right) = \nabla.\left(\alpha_g \frac{\mu_{t,g}}{\sigma_\varepsilon} \nabla \varepsilon_g\right) + \alpha_g \frac{\varepsilon_g}{k_g}\left(C_{1\varepsilon} G_{k,g} - C_{2\varepsilon} \rho_g \varepsilon_g\right) + \alpha_g \rho_g \Pi_{\varepsilon,g} \quad (3.16)$$

where $G_{k,g}$ is the generation of the turbulent kinetic energy, because of the velocity gradients, and $\Pi_{k,g}$ and $\Pi_{\varepsilon,g}$, the interactions between both phases, represent the turbulent generation, because of the average slip velocity between the phases.

$$\Pi_{k,g} = K_{gs}\left(\theta_s - 2k_g\right) \quad (3.17)$$

$\Pi_{\varepsilon,g}$ is derived from the Elgobashi and Abou-Arab model [126].

$$\Pi_{\varepsilon,g} = C_{3\varepsilon} \frac{\varepsilon_g}{k_g} \Pi_{k,g} \quad (3.18)$$

$$\mu_{t,g} = \rho_g C_\mu \frac{k_g^2}{\varepsilon_g} \quad (3.19)$$

The closure coefficients used in the present study are
$C_{1\varepsilon} = 1.44$, $C_{2\varepsilon} = 1.92$, $C_{3\varepsilon} = 1.3$, $C_\mu = 0.09$, $\sigma_k = 1$, and $\sigma_\varepsilon = 1.3$.

3.2.2.4 Granular temperature model

The kinetic energy in the random motion of the solid particles generates the granular temperature. In this study, the partial differential equation form of the granular temperature model is used for the solid phase [127] and is given in eq. 3.20.

$$\frac{3}{2}\left[\frac{\partial}{\partial t}(\rho_s \alpha_s \theta_s) + \nabla.\rho_s \alpha_s \vec{v}_s \theta_s\right] = \left(-\bar{\bar{p}}_s \bar{\bar{I}} + \bar{\bar{\tau}}_s\right) : \nabla \vec{v}_s + \nabla.(\kappa_{\theta s} \nabla \theta_s) - \gamma \theta_s + \phi_{gs} \tag{3.20}$$

Here, $\left(-\bar{\bar{p}}_s \bar{\bar{I}} + \bar{\bar{\tau}}_s\right) : \nabla \vec{v}_s$ means the energy generated by the solid stress tensor, $\nabla.(\kappa_{\theta s} \nabla \theta_s)$ means the diffusion of energy, $\gamma \theta_s$ means the collisional dissipation of energy, and ϕ_{gs} means the energy exchange between the phases, due to the random fluctuation in the particle velocity. In the diffusion of the energy term, $\kappa_{\theta s}$ is the diffusion coefficient. The interaction of the fluctuation energy must be included in the simulations, because of its importance [128].

The diffusion coefficient for the granular energy is modeled by the Syamlal et al. model [122] and is given in eq. 3.21.

$$\kappa_{\theta s} = \frac{15 d_s \rho_s \alpha_s \sqrt{\theta_s \pi}}{4(41 - 33\eta)}\left[1 + \frac{12}{5}\eta^2(4\eta - 3)\alpha_s g_{0,ss} + \frac{16}{15\pi}(41 - 33\eta)\eta \alpha_s g_{0,ss}\right] \tag{3.21}$$

Here, e_{ss} is the restitution coefficient for particle-particle collisions, and η is a coefficient, whose value depends on e_{ss}.

$$\eta = \frac{1}{2}(1 + e_{ss}) \tag{3.22}$$

$\gamma \theta_s$ and ϕ_{gs} are modeled by the expressions given by the Lun et al. model [121], and the Gidaspow et al. model [129] respectively.

$$\gamma \theta_s = \frac{12(1 - e_{ss}^2) g_{0,ss}}{d_s \sqrt{\pi}} \rho_s \alpha_s^2 \theta_s^{3/2} \tag{3.23}$$

$$\phi_{gs} = -3 K_{gs} \theta_s \tag{3.24}$$

3.2.2.5 Drag force model

The Gidaspow drag model [119] is used in this work. The Gidaspow drag model uses the Wen and Yu model [130] when $\alpha_g > 0.8$, and it uses the Ergun model [131] when $\alpha_g \leq 0.8$.

When $\alpha_g > 0.8$ [130],

$$K_{gs} = \frac{3}{4} C_D \frac{\alpha_s \alpha_g \rho_g |\vec{v}_g - \vec{v}_s|}{d_s} \alpha_g^{-2.65} \tag{3.25}$$

When $Re_s \leq 1000$,

$$C_D = \frac{24}{Re_s}[1 + 0.15(Re_s)^{0.687}] \tag{3.26}$$

When $Re_s > 1000$,

$$C_D = 0.44 \tag{3.27}$$

Here, Re_s is the particle Reynolds number and is expressed as

$$Re_s = \frac{\alpha_g \rho_g |\vec{v}_g - \vec{v}_s| d_s}{\mu_g} \tag{3.28}$$

When $\alpha_g \leq 0.8$ [131],

$$K_{gs} = 150 \frac{\alpha_s (1-\alpha_g) \mu_g}{\alpha_g d_s^2} + 1.75 \frac{\alpha_s \rho_g |\vec{v}_g - \vec{v}_s|}{d_s} \tag{3.29}$$

3.2.2.6 Lift force model

The lift force on solids with a lift coefficient of 0.2 is considered in horizontal flows [132]. The widely used correlation for the lift coefficient has been expressed by Mei and Klausner [133].

The lift force on solids in horizontal flows is [132]

$$F_{L,s} = -C_L \rho_g \alpha_s (\vec{v}_g - \vec{v}_s) \times (\nabla . \vec{v}_g) \tag{3.30}$$

For the gas phase, the lift force is, $F_{L,g} = -F_{L,s}$.

The lift force on vertical flows is neglected.

3.2.2.7 Constitutive equations for heat transfer

The HTC between phases (h_{sg}) is defined as

$$h_{sg} = \frac{6k_g\alpha_s\alpha_g Nu_s}{d_s^2} \tag{3.31}$$

The particle Nusselt number is defined by the Gunn model [134].

$$Nu_s = \left(7 - 10\alpha_g + 5\alpha_g^2\right)\left(1 + 0.7Re_s^{0.2}{Pr_g}^{1/3}\right) + \left(1.33 - 2.4\alpha_g + 1.2\alpha_g^2\right)Re_s^{0.7}{Pr_g}^{1/3} \tag{3.32}$$

The Prandtl number for the gas phase is

$$Pr_g = \frac{\mu_g C_{pg}}{k_g} \tag{3.33}$$

As per Fourier's law of heat conduction,

$$q_g = -\alpha_g k_g \nabla T_g \tag{3.34}$$

$$q_s = -\alpha_s k_s \nabla T_s \tag{3.35}$$

3.2.2.8 Properties of the gas

The properties of the gas vary with the temperature, due to heat exchange takes place from the hot gas to the solids. Therefore, the properties of the gas are defined with the temperature. The calculation of the gas properties with the temperature is given below.

The density of the gas is defined as per the incompressible, ideal gas conditions.

$$\rho_g = \frac{P_{op}}{R_A T_g} \tag{3.36}$$

where P_{op} is the operating pressure, which is 101325 Pa.

The normal dynamic viscosity of gas (μ_{gn}) is defined as a function of the temperature (piecewise-polynomial profile) [135].

$$\mu_{gn}(T_g) = A - BT_g + C{T_g}^2 - D{T_g}^3 + E{T_g}^4 - F{T_g}^5 + G{T_g}^6 - H{T_g}^7 \tag{3.37}$$

where A, B, C, D, E, F, G, and H are the coefficients, whose values are given in Table 3.1.

Table 3.1: Values of coefficient

Coefficient	Value
A	1161.482
B	2.368819
C	0.01485511
D	5.034909×10^{-05}
E	9.928569×10^{-08}
F	1.111097×10^{-10}
G	6.540196×10^{-14}
H	1.573588×10^{-17}

Two separate user-defined functions are provided to define the gas phase thermal conductivity and specific heat at constant pressure, according to Dixon [136], and are presented in eq. 3.38 and eq. 3.39 respectively.

$$k_g = 0.02624\left(\frac{T_g}{300}\right)^{0.8646} \tag{3.38}$$

$$C_{Pg} = 1002.5 + 275 \text{ x } 10^{-6}\left(T_g - 200\right)^2 \tag{3.39}$$

3.2.2.9 Calculation of average gas-solid Nusselt number (Nu_{avg})

In the present case, heat transfer takes place from the hot gas to the cold solids. Therefore, from the energy balance,

$$\dot{m}_g C_{pg}\left(T_{g,i} - T_{g,o}\right) + \dot{m}_s C_{ps}\left(T_{s,i} - T_{s,o}\right) = 0 \tag{3.40}$$

Here, the subscript 'i' refers to the inlet, and the subscript 'o' refers to the outlet.

The overall gas-solid HTC (U) is calculated as

$$\dot{m}_g C_{pg}\left(T_{g,i} - T_{g,o}\right) = UA_s(\text{LMTD}) \tag{3.41}$$

where A_s is the heat transfer area (total surface area of the solid particles in the pipe at any location) and LMTD is the logarithmic mean temperature difference.

The heat transfer area of the solid particles can be calculated as

$$A_s = 6M_s/(\rho_s . d_s) \tag{3.42}$$

Here, M_s is the solid holdup and can be calculated as

$$M_s = (\dot{m}_s . \Delta l)/\vec{v}_s \tag{3.43}$$

where $\dot{m}_s$ is the mass flow rate of the solid and Δl is the distance from the particle feeding point (inlet).

The LMTD is calculated as

$$LMTD = (\Delta T_i - \Delta T_o)/(\ln(\Delta T_i/\Delta T_o)) \tag{3.44}$$

$$\Delta T_i = T_{g,i} - T_{s,i} \tag{3.45}$$

$$\Delta T_o = T_{g,o} - T_{s,o} \tag{3.46}$$

The local gas-solid Nusselt number (Nu_l) is calculated as

$$Nu_l = UD/k_{eff} \tag{3.47}$$

where k_{eff} is the effective thermal conductivity of the gas. The effective thermal conductivity of the gas is the average thermal conductivity of the gas in the computational domain, considering the volume fraction of the solid particles.

The average gas-solid Nusselt number (Nu_{avg}) is

$$Nu_{avg} = \int_0^L Nu_l . dl/L \tag{3.48}$$

The above method of calculating the average gas-solid Nusselt number in gas-solid flows, subjected to an adiabatic wall, is also mentioned in the experimental modeling paper of Mokhtarifar et al. [117].

3.3 Initial and boundary conditions

A fully-developed velocity profile ($1/7^{th}$ power law) is used for the gas phase at the inlet as written in eq. 3.49.

$$\frac{\vec{v}_g}{\vec{v}_{gc}} = \left(1 - \frac{r}{R}\right)^{1/7} \tag{3.49}$$

However, a uniform axial velocity boundary condition is used for the solid phase at the inlet. The velocity of both phases is assumed as equal since the solid phase is dispersed in the gas phase (dilute flow). Similarly, an outflow boundary condition is used for both phases at the outlet. At the wall, a no-slip wall boundary condition is used for the gas phase, whereas, a partial-slip wall boundary condition is used for the solid phase, according to Johnson and Jackson [137].

Moreover, the gas temperature (443.15K), the turbulent intensity (equals $0.16\mathrm{Re}_g^{1/8}$), and the hydraulic diameter (0.058 m) values are provided at the inlet, for the gas phase. However, for the solid phase, the solid temperature (308.15K), the granular temperature (equals $0.004\vec{v}_s^2$), and the SVF values are provided at the inlet. The value of the SVF is calculated from the value of the SLR. The SLR is defined as the ratio of the mass flow rate of the solid to the mass flow rate of the gas. The relation between the SLR and SVF is

$$\mathrm{SLR} = \frac{(\mathrm{SVF})\rho_s\vec{v}_s}{(1 - \mathrm{SVF})\rho_g\vec{v}_g} \tag{3.50}$$

The pipe wall is at an adiabatic condition. The numerical simulation values are initialized from the values at the inlet.

3.4 Numerical procedure

The commercial software package ANSYS 15.0 of National Institute of Technology Warangal is used for the numerical work. First, the geometry (a horizontal and a vertical pipe of internal diameter 0.058 m and length 6 m) is created by the ANSYS design modeler, and the meshing is done with the help of the ANSYS meshing tool. The diameter of the pipe is taken as 0.058 m, because the validation is done with respect to the benchmark experimental data having a pipe of diameter 0.058 m. The details of the geometry along with the meshing are shown in the respective chapters. The pipe length is taken more than 100 times the pipe diameter (6 m) to assume fully-developed flow at the outlet.

Then, the grid and time-step independence tests are conducted, for proper selection of grid and time-step. Further, the numerical sensitivity studies are conducted, considering different drag models and varying the values of the particle-particle and particle-wall collisions and specularity coefficient (SC). The details of the grid and time-step independence tests and numerical sensitivity studies are shown in the respective chapters.

Air is used as the gas phase, and three solid particles such as sand, plastic pellets, and glass are used as the solid phase. The inlet gas temperature is 443.15 K (170 ºC), and the inlet solid temperature is 308.15 K (35 ºC). The properties of the gas and solids used at the inlet of the pipe are shown in Table 3.2. The inlet air properties are calculated according to the inlet air temperature of 443.15 K.

Table 3.2: Properties of gas and solids used at the pipe entrance

Properties	**Value**			
	Gas (air)	**Solids**		
		Plastic	**Sand**	**Glass**
Density, kg/m^3	0.7967	1000	1500	2600
Specific heat, J/kg-K	1020	1255	800	735
Thermal conductivity, W/m-K	0.03677	0.2	0.8	1
Viscosity, kg/m-s	2.457×10^{-5}	-	-	-

The transient simulations are carried out in ANSYS FLUENT 15.0 software, which is based on the finite volume approach. The double-precision option is chosen for higher accuracy. The solver is pressure-based, and the formulation is implicit. For the pressure and velocity coupling, the phase-coupled semi-implicit method for pressure-linked equations (PC-SIMPLE) algorithm, which was developed by Vasquez and Ivanov [138], is used. A second-order upwind scheme is used for the momentum and energy equations, and the quadratic upstream interpolation for convective kinetics (QUICK) scheme is used for the volume fraction equations. A first-order upwind scheme is used for the turbulent kinetic energy, turbulent energy dissipation rate, and granular temperature equations. Other simulation parameters used in the simulation are tabulated in Table 3.3.

Table 3.3: Simulation parameters

Description	Value
SLR at the entrance	0.1–1
Gas velocity at the entrance of the pipe	15–24 m/s
Particle size	100–400 μm
Particle-particle restitution coefficient	0.9
Particle-wall restitution coefficient	0.95
Lift coefficient	Horizontal pipe: 0.2
	Vertical pipe: 0
SC	Horizontal pipe: 0.08
	Vertical pipe: 0.05

The simulation parameters such as particle-particle and particle-wall restitution coefficients, lift coefficient, and specularity coefficient (SC) as described in Table 3.3 are chosen with respect to the validation with the benchmark experimental data. The inlet SLR is in the range 0.1–1 due to the focus of the present study to very dilute flow. The inlet gas velocity is in the range 15–24 m/s due to the assumption of suspension flow and to avoid blockage. The particle size is in the range 100–400 μm due to its wide applicability in various industries.

A convergence criterion of 10^{-3} is used for all the quantities. The simulations are carried out in an Intel (R) Xeon (R) E5-2630 CPU workstation with 32 GB of RAM. The simulations are run up to 60 seconds, where the steady-state or statistical steady-state condition is reached in both phases. To examine this, some flow variables such as air temperature, solid temperature, air velocity, and solid velocity are monitored at the outlet of the pipe. Moreover, to confirm the accuracy of the results, the inlet and outlet fluxes are checked for overall mass, momentum, and heat balances. It is noticed that the net imbalance is less than 0.1% of the net flux through the domain, which is acceptable as suggested by Fluent Inc. [139]. The whole solution process is computationally rigorous, and each simulation requires one week of computational time.

3.5 Closure

The mathematical model of the gas-solid flow problem is presented in the present chapter. The governing and the constitutive equations related to the flow problem are written. Moreover, the calculation of the average gas-solid Nusselt number is explained. The initial and boundary conditions and simulation procedure are also given in the present chapter.

Chapter 4

Heat Transfer and Pressure Drop Studies of Gas-Solid Flow through a Horizontal, Adiabatic Pipe

4.1 Introduction

Horizontal pipes are found in numerous industrial applications such as pneumatic conveying, drying and preheating, and fluidized beds in chemical, process, pharmaceutical, agricultural industries, and many others. The knowledge of heat transfer and pressure drop is very essential in these systems. In this chapter, the heat transfer and pressure drop studies of gas-solid flow through a horizontal, adiabatic pipe are discussed. First, the geometry of the horizontal pipe is modeled, followed by the meshing of the pipe. Then, the grid and time-step independence studies are conducted, and after that, the numerical sensitivity studies are discussed. Finally, the effects of flow variables such as SLR, particle size, and gas velocity on heat transfer and pressure drop are presented.

4.2 Pipe geometry

The computational domain of the horizontal, adiabatic pipe is presented in Figure 4.1. The computational domain is created in ANSYS 15.0 design modeler. The internal diameter of the horizontal pipe is 0.058 m, whereas the pipe length is 6 m. The pipe has three sections such as inlet, outlet, and wall. The wall is at an adiabatic condition. The flow takes place from the inlet to the outlet. The X and Y axes are placed along the radial directions, whereas the Z-axis is placed along the length of the pipe.

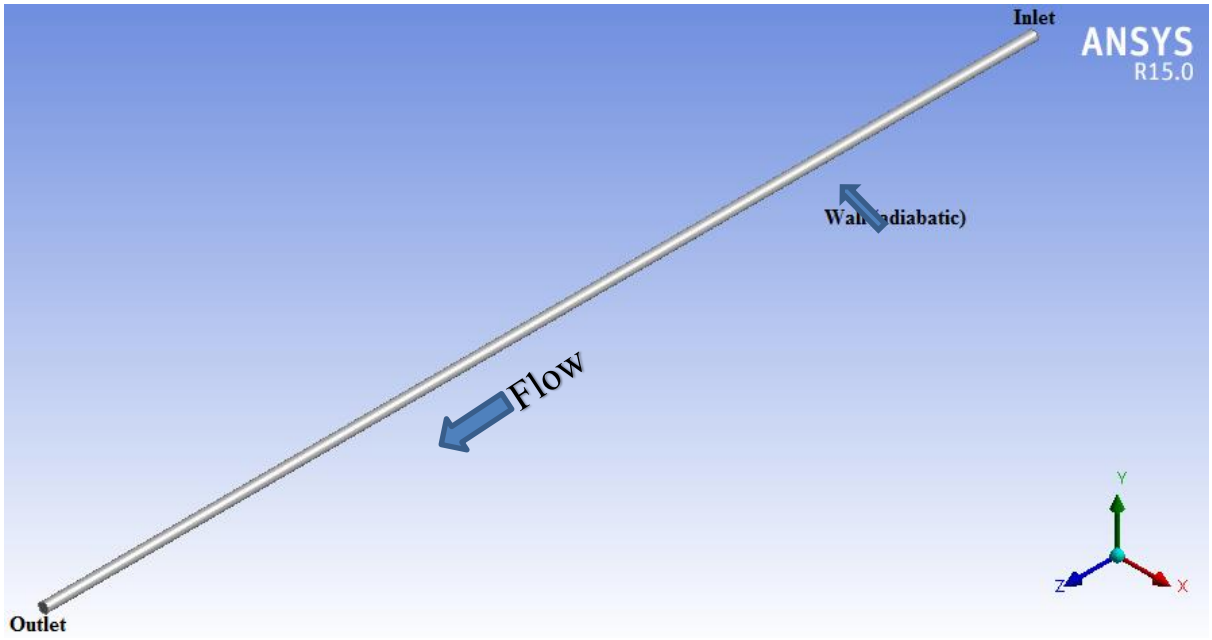

Figure 4.1: Computational domain of the horizontal pipe

4.3 Pipe meshing

After creating the computational domain, the mesh of the pipe is created in ANSYS 15.0 meshing tool. The mesh of the pipe at an enlarged view is shown in Figure 4.2. The type of mesh is tetrahedrons in nature. The final mesh consists of 252000 cells.

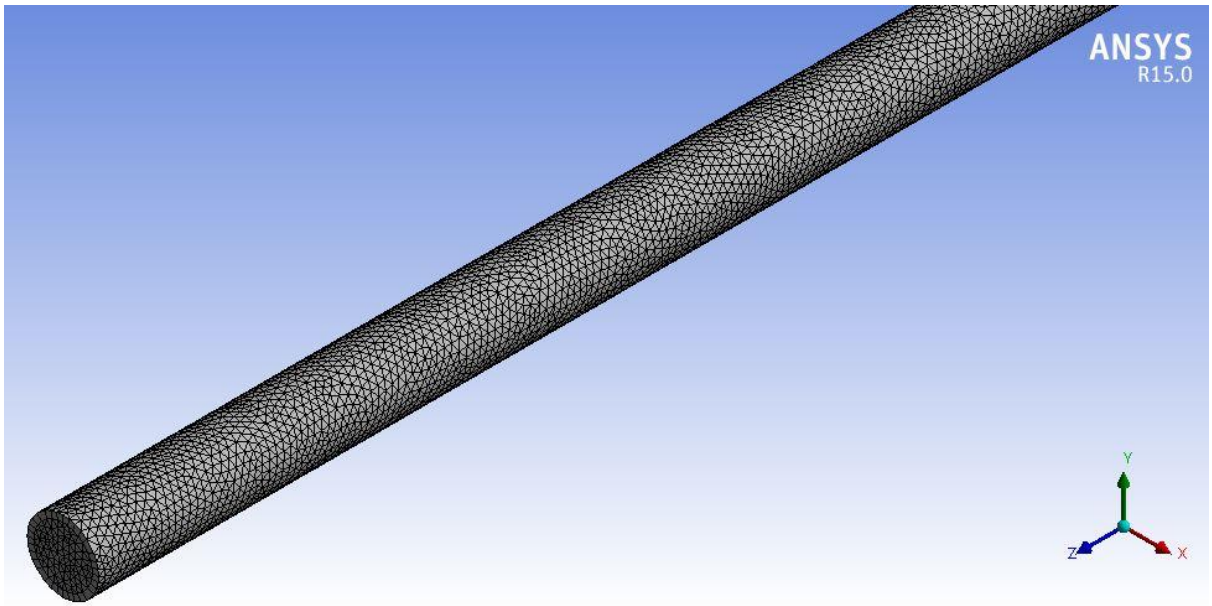

Figure 4.2: Computational mesh of the horizontal pipe

4.4 Grid and time-step independence studies

Grid and time-step play significant roles in the accuracy of the solution. Increasing the grid size and time-step size increase the accuracy of the solution; however, simultaneously, they increase the time required to achieve the converged solution. Therefore, the grid and time-step independence tests are conducted for optimum selection of grid and time-step sizes. Grid independence tests are conducted considering three grid sizes such as 114000 cells, 252000 cells, and 504000 cells, keeping all other parameters constant, and are shown in Figures 4.3–4.5.

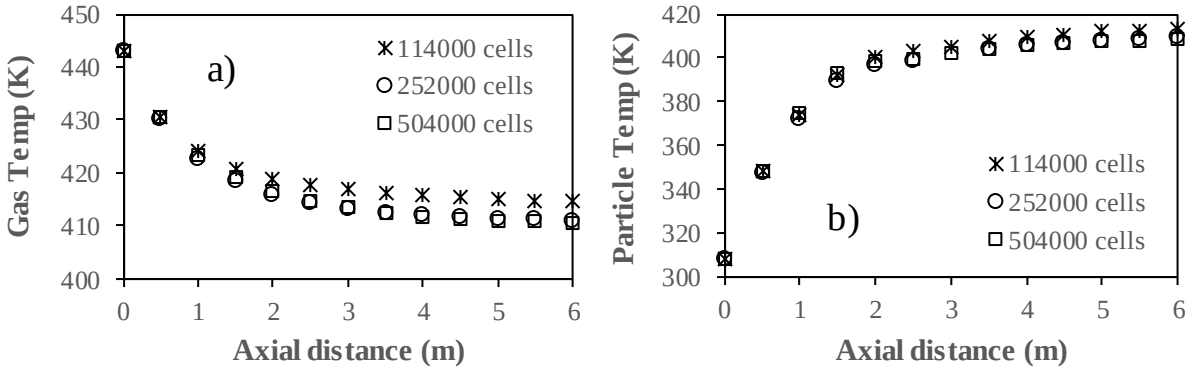

(Gas velocity = 18.5 m/s; average SLR = 0.413; particle diameter = 253 μm)

Figure 4.3: Grid independence studies for gas temperature and particle temperature

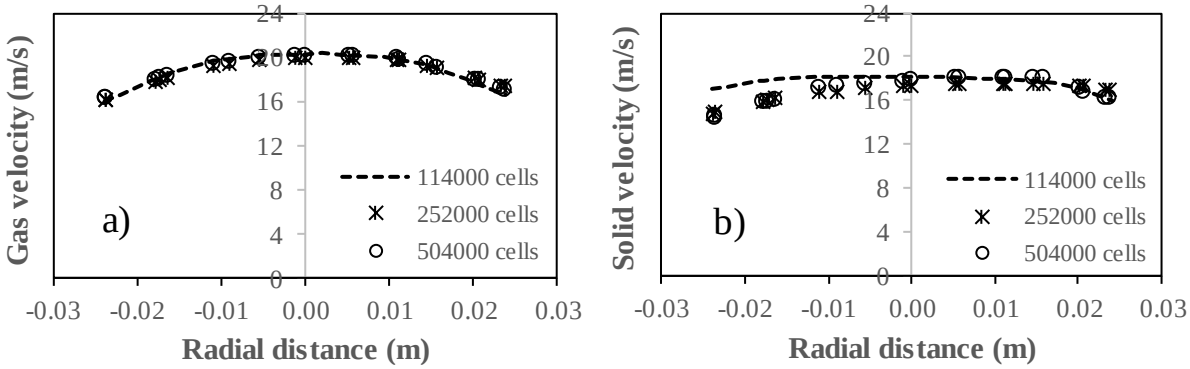

(Gas velocity = 18.5 m/s; average SLR = 0.413; particle diameter = 253 μm)

Figure 4.4: Grid independence studies for gas velocity and particle velocity

It is noticed from Figures 4.3–4.5 that, by changing the grid size from 252000 cells to 504000 cells, the results of gas temperature and particle temperature, gas velocity and particle velocity, and axial pressure are insignificantly affected. Therefore, the final grid size consisting of 252000 cells is considered in the rest of the simulation, to save computational time.

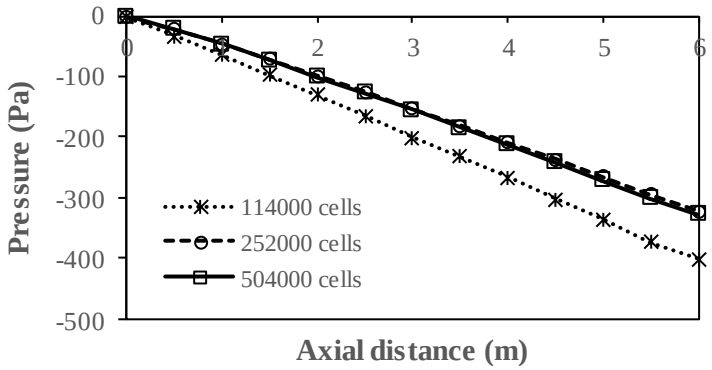

(Gas velocity = 18.5 m/s; average SLR = 0.413; particle diameter = 253 μm)

Figure 4.5: Grid independence studies for pressure

Similarly, time-step independence tests are conducted considering three time-step sizes such as 0.01s, 0.001s, and 0.0001s, keeping all other parameters constant, and are shown in Figures 4.6–4.8.

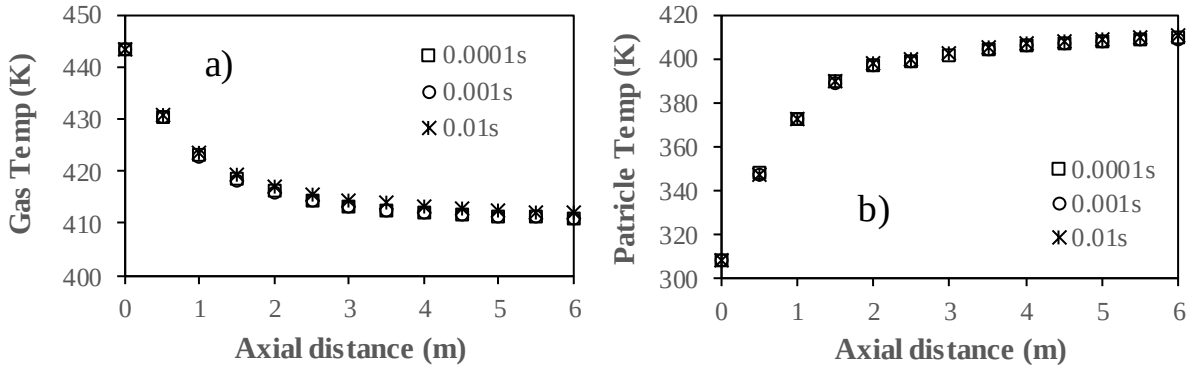

(Gas velocity = 18.5 m/s; average SLR = 0.413; particle diameter = 253 μm)

Figure 4.6: Time-step independence studies for gas temperature and particle temperature

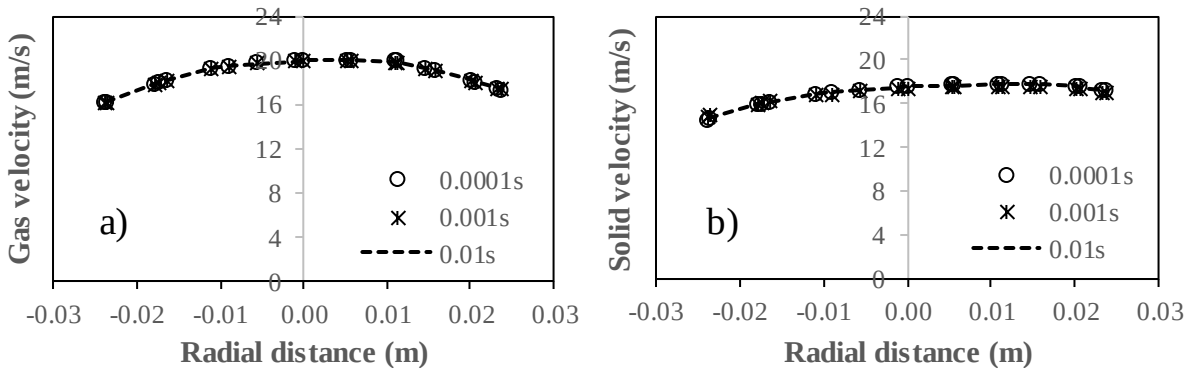

(Gas velocity = 18.5 m/s; average SLR = 0.413; particle diameter = 253 μm)

Figure 4.7: Time-step independence studies for gas velocity and particle velocity

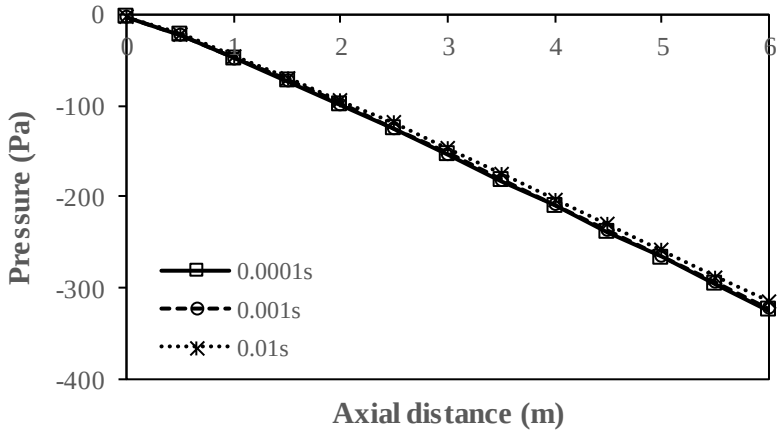

(Gas velocity = 18.5 m/s; average SLR = 0.413; particle diameter = 253 μm)

Figure 4.8: Time-step independence studies for pressure

It is noticed from Figures 4.6–4.8 that, by changing the time-step size from 0.001s to 0.0001s, the results of gas temperature and particle temperature, gas velocity and particle velocity, and axial pressure are insignificantly affected. Therefore, the final time-step size of 0.001s is considered in the rest of the simulation, to save computational time.

4.5 Validation studies

In numerical works, the numerical deviations are reported with respect to the experimental work. The present model is validated with the experimental results of Mokhtarifar et al. [117]. Figure 4.9(a) compares the average SLR by the simulation results with the experimental

results of Mokhtarifar et al. [117]. Figure 4.9(a) shows that the simulation outcomes satisfactorily agree with the experimental results of Mokhtarifar et al. [117].

Moreover, the numerical gas-solid Nusselt number is compared with the experimental results of Mokhtarifar et al. [117] and is shown in Figure 4.9(b). The numerical gas-solid Nusselt number shows a maximum deviation of -9% with the experimental gas-solid Nusselt number by Mokhtarifar et al. [117]. Therefore, the present numerical model agrees satisfactorily with the experimental work of Mokhtarifar et al. [117].

Figure 4.9(c) depicts the comparison of numerical gas temperature values with the experimental gas temperature values by Mokhtarifar et al. [117], calculated at a distance of 70 mm from the particle feeder (inlet). Figure 4.9(c) points that the numerical gas temperature values satisfactorily agree with the experimental gas temperature values by Mokhtarifar et al. [117].

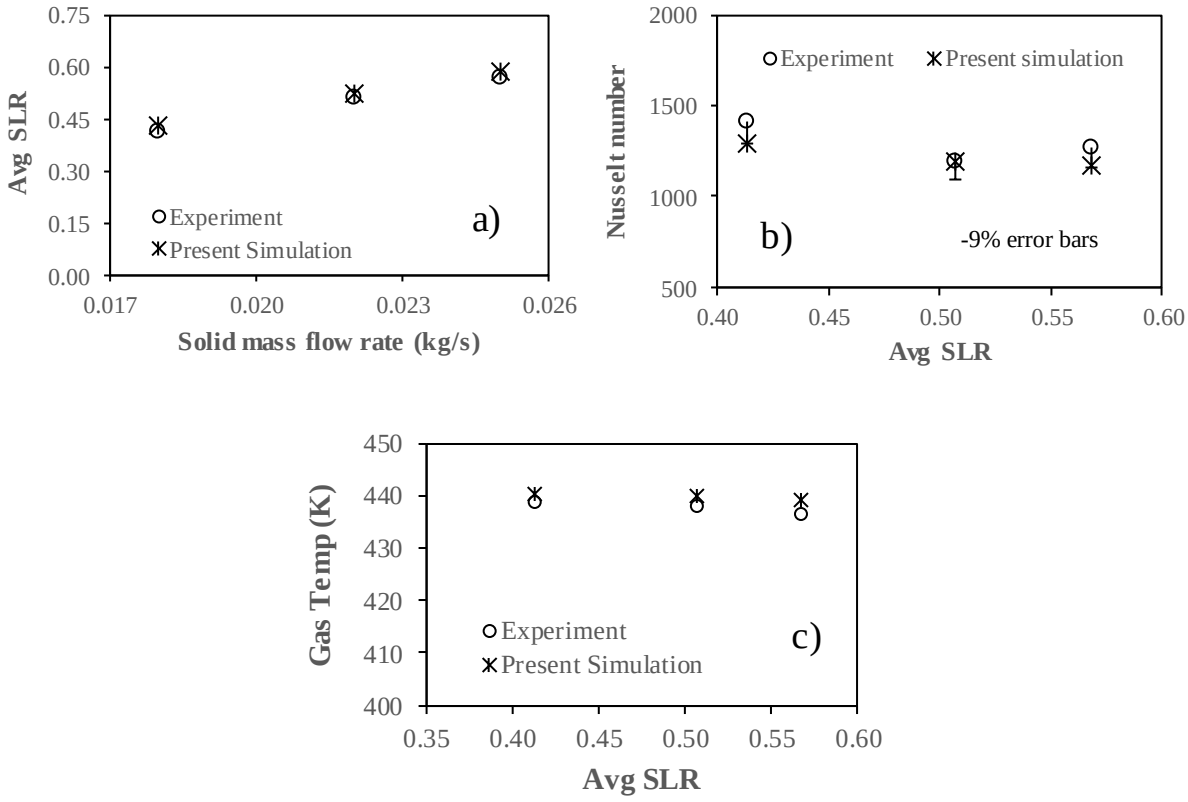

Figure 4.9: Validation studies of heat transfer using the variable gas properties model

To find the influence of the variable gas properties model, the comparison of Nusselt number with respect to the average SLR between the variable and constant gas properties is shown in

Figure 4.10. The constant gas properties are: density = 0.7967 kg/m^3, viscosity = 2.457×10^{-5} kg/ms, thermal conductivity = 0.03677 W/mK, and specific heat = 1020 j/kgK. The gas-solid Nusselt number with the constant gas properties model underpredicts by a maximum value of 8% with respect to the variable gas properties model (Figure 4.10).

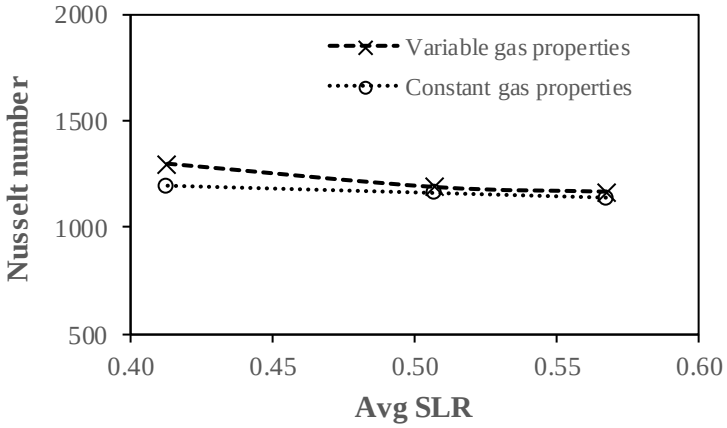

Figure 4.10: Comparison of heat transfer results between the variable gas properties model and constant gas properties model

For the hydrodynamics validation, the numerical pressure drop is compared with the experimental results of Tsuji and Morikawa [140], using a glass wall and plastic pellets of density 1000 kg/m^3, for an isothermal gas-solid flow, and is shown in Figure 4.11. It is noticed from Figure 4.11 that the numerical pressure drop shows a maximum deviation of ±9%, with the experimental pressure drop by Tsuji and Morikawa [140].

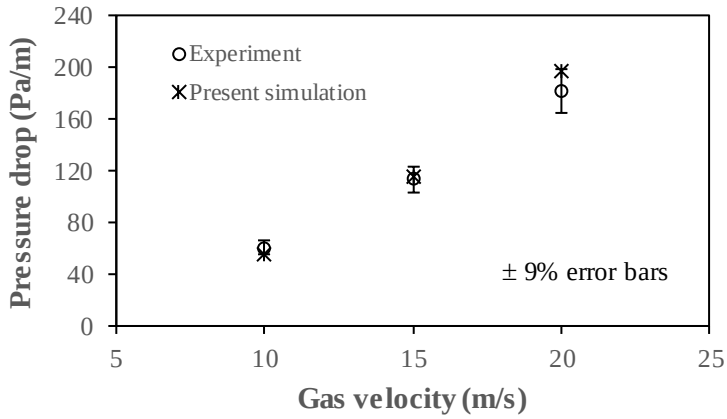

Figure 4.11: Numerical pressure drop vs experimental pressure drop

Again, the pressure drop results considering the variable gas properties and constant gas properties with respect to the average SLR at a gas velocity of 18.5 m/s and a particle diameter of 253 μm are picturized in Figure 4.12. It is seen from Figure 4.12 that there is a major difference between the two results, and the significance of the variable gas properties is noticed. The constant gas properties model overpredicts the pressure drop by 13% to 21% compared to the variable gas properties model. Therefore, the variable gas properties model is used in the present work.

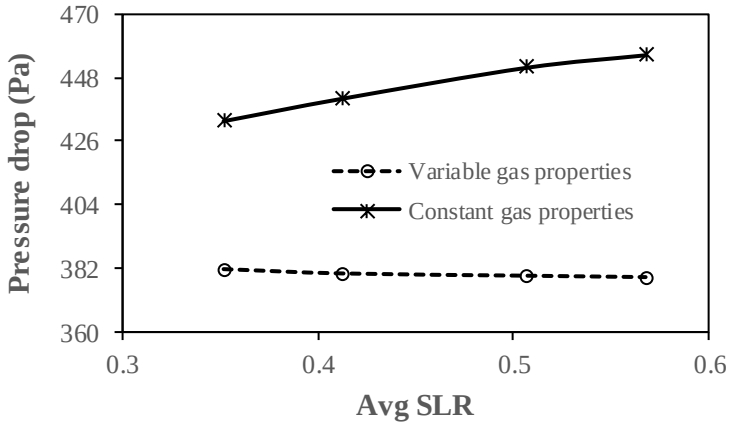

Figure 4.12: Comparison of pressure drop between the variable gas properties model and constant gas properties model

The numerical non-dimensional temperature for plastic, sand, and glass particles is compared with the theoretical values in Figure 4.13. The properties of plastic, sand, and glass particles have already been given in Table 3.2 of chapter 3. The calculation of non-dimensional temperature is given below. From the energy balance, the non-dimensional temperature is

$$\left(T_{g,i} - T_{g,o}\right)/\left(T_{s,o} - T_{s,i}\right) = m(C_{p,s}/C_{p,g}) \tag{4.1}$$

where m is the SLR.

The right side of eq. 4.1 represents the theoretical value. The numerical non-dimensional temperature values well agree with the theoretical values, as noticed from Figure 4.13. The solid particles such as plastic, sand, and glass are considered for validation, because the thermo-hydrodynamic characteristics of gas-solid flows using the aforementioned solid particles are studied later.

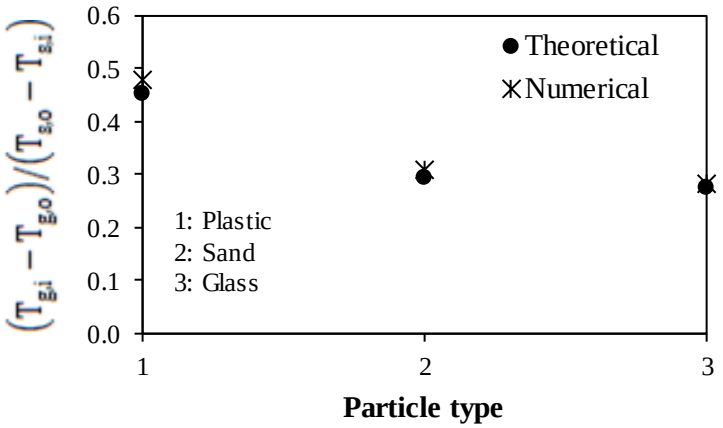

Figure 4.13: Comparison of non-dimensional temperature between the numerical values and theoretical values ($\vec{v}_g$ = 21 m/s; inlet SLR = 0.4; d_s= 200 µm)

4.6 Numerical sensitivity studies

The numerical sensitivity studies have been conducted considering different drag models (Gidaspow model [119], Wen and Yu model [130], and Syamlal model [141]), particle-particle restitution coefficients (e_{ss}), particle-wall restitution coefficients (e_{sw}), and SCs. These are shown in Figures 4.14–4.17. It is noticed from Figures 4.14–4.17 that the results of temperature difference (gas temperature minus solid temperature) and pressure variation are insignificantly affected by changing the values of e_{ss}, e_{sw}, and SC as well as by changing the drag models. The Gidaspow drag model [119] is used for further simulations. The value of other model parameters used in the present work are given in Table 3.3.

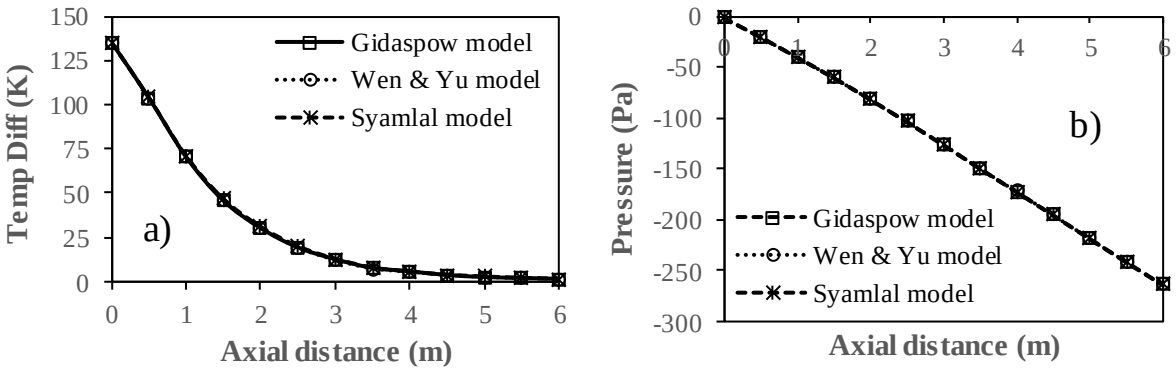

(Gas velocity = 15 m/s; inlet SLR = 0.1; particle diameter = 400 µm)

Figure 4.14: Numerical sensitivity studies using different drag models

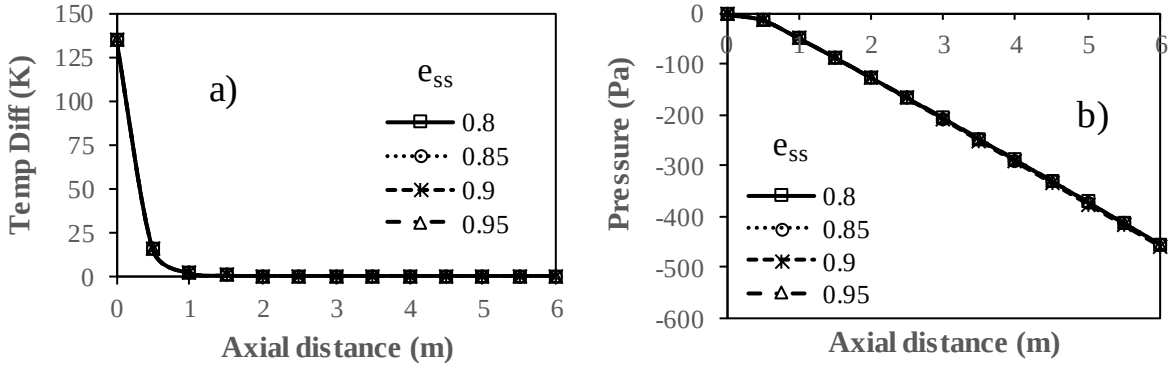

(Gas velocity = 21 m/s; inlet SLR = 0.4; particle diameter = 100 μm)

Figure 4.15: Numerical sensitivity studies using different e_{ss} values

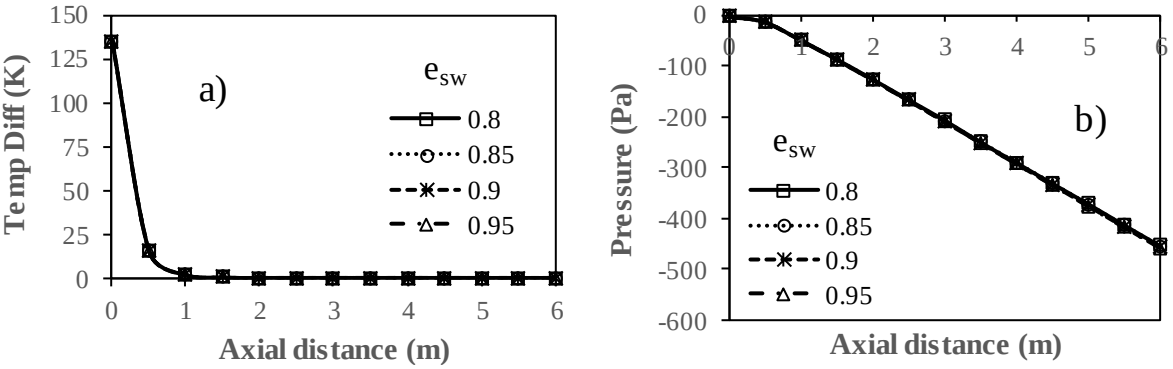

(Gas velocity = 21 m/s; inlet SLR = 0.4; particle diameter = 100 μm)

Figure 4.16: Numerical sensitivity studies using different e_{sw} values

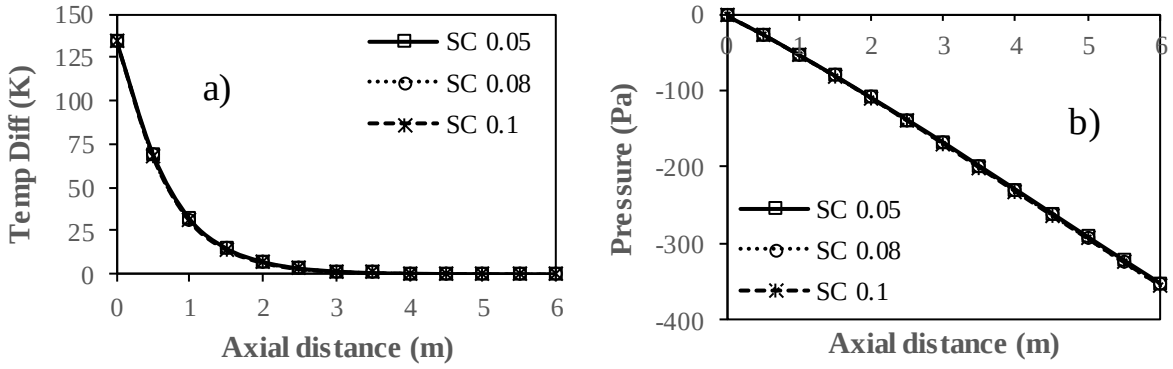

(Gas velocity = 18 m/s; inlet SLR = 0.1; particle diameter = 200 μm)

Figure 4.17: Numerical sensitivity studies using different SC values

4.7 Results and discussions

4.7.1 Effect of flow parameters on gas-solid Nusselt number and pressure drop using sand particles

In industrial applications, poor handling of solid particles may result in poor system performance. Therefore, it is necessary to effectively design the system based on various factors such as type of material, SLR, particle size, inlet gas velocity, and many other factors. The effect of different flow parameters, i.e., particle diameter, SLR, and gas Reynolds number on gas-solid Nusselt number and overall pressure drop is studied in this subsection. The Nusselt number is the average Nusselt number over the whole length of the pipe and it is calculated as per eq. 3.48. The overall pressure drop is calculated as the inlet pressure drop minus the outlet pressure drop in the computational domain.

In horizontal flows, the overall pressure drop is

$$\Delta p_{overall} = \Delta p_{acceleration} + \Delta p_{friction} \tag{4.2}$$

The acceleration pressure drop is

$$\Delta p_{acceleration} = A\left(\frac{\rho_g \vec{v}_g^{\,2}}{2} + \frac{\rho_s \vec{v}_s^{\,2}}{2}\right) \tag{4.3}$$

where A is a constant and is a function of flow conditions and particle properties.
The frictional pressure drop is (using Darcy's equation)

$$\Delta p_{friction} = \frac{f_g \rho_g \vec{v}_g^{\,2}(1-\alpha_s)L}{2D} + \frac{f_s \rho_s \vec{v}_s^{\,2}\alpha_s L}{2D} \tag{4.4}$$

where f_g and f_s are the friction factor of the gas phase and solid phase respectively.
Eq. 4.4 can be rewritten as

$$\Delta p_{friction} = K\left(\frac{\rho_g \vec{v}_g^{\,2}}{2} + \frac{\rho_s \vec{v}_s^{\,2}}{2}\right) \tag{4.5}$$

where K is a constant and is a function of particle properties and flow conditions.

4.7.1.1 Effect of particle diameter on gas-solid Nusselt number and pressure drop

The effect of particle diameter on gas-solid Nusselt number at different solid feed rates is shown in Figure 4.18(a). It is seen from Figure 4.18(a) that the Nusselt number decreases with an increase in the particle diameter. This type of behavior is as a result of the turbulence suppression by the fine particles.

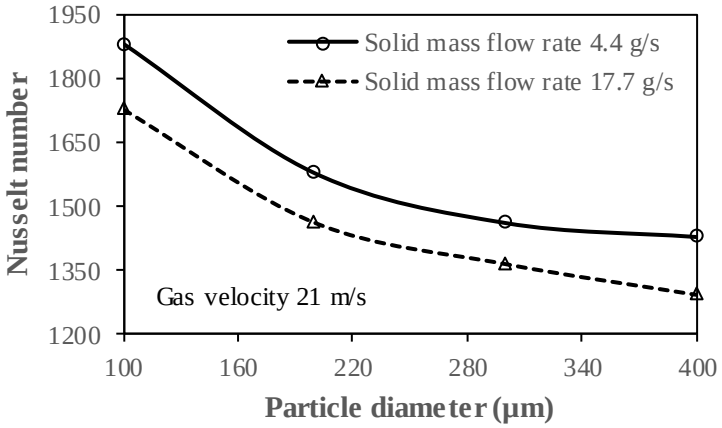

Figure 4.18(a): Effect of particle diameter on Nusselt number

The effect of particle diameter on gas turbulent Reynolds number at different solid feed rates is shown in Figure 4.18(b). It is seen from Figure 4.18(b) that increasing the particle diameter decreases the gas Reynolds number. Thus, the Nusselt number decreases with an increase in the particle diameter.

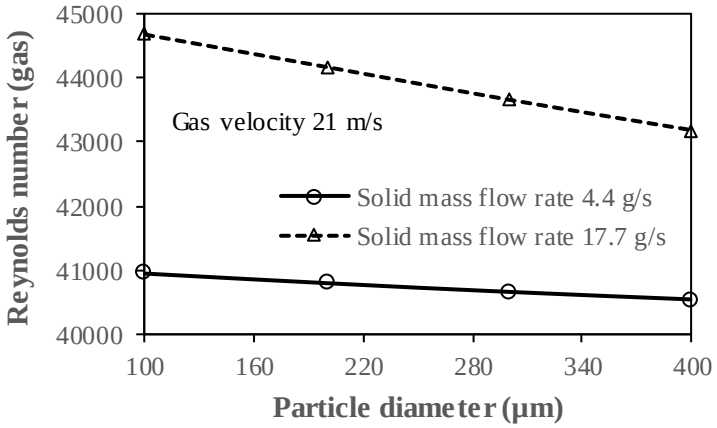

Figure 4.18(b): Effect of particle diameter on gas turbulent Reynolds number

The effect of particle diameter on pressure drop at different solid feed rates is shown in Figure 4.19. It is noticed from Figure 4.19 that the pressure drop increases with increasing the particle diameter. An increase in the particle diameter increases the slip velocity between the gas and solid. This leads to an increase in the drag force, and hence, the pressure drop increases.

The difference of pressure drop between the solid mass flow rates is higher for larger particle size due to the dominant nature of the increased collisions (increased drag force) and increased effective density of the gas.

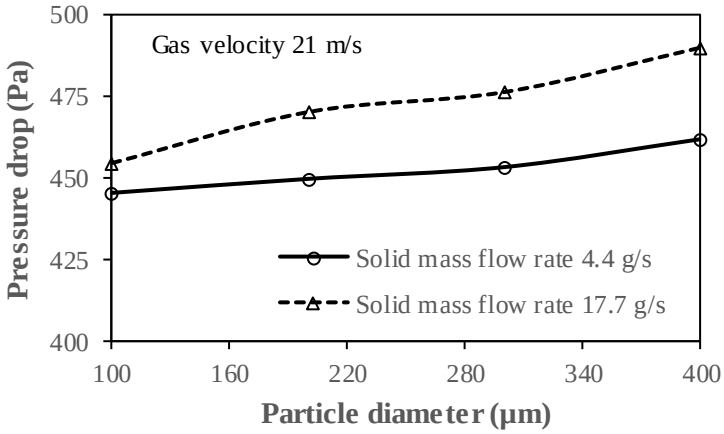

Figure 4.19: Effect of particle size on pressure drop

4.7.1.2 Effect of SLR on gas-solid Nusselt number and pressure drop

The effect of SLR on Nusselt number at different particle diameters is plotted in Figure 4.20. It is observed from Figure 4.20 that the Nusselt number decreases with an increase in the SLR at a particle diameter of 100 µm. Nevertheless, the Nusselt number first decreases up an SLR of 0.63 and then increases at a particle diameter of 200 µm. Two important factors, which affect the heat transfer, are the heat capacity-density ratio ($\rho_s C_{ps}/\rho_g C_{pg}$) and effective thermal conductivity of the gas. Increasing the heat capacity-density ratio increases the heat transfer. However, increasing the effective thermal conductivity of the gas reduces the heat transfer (from eq. 47 and 48). Increasing the SLR decreases the heat capacity-density ratio and effective thermal conductivity of the gas. At a lower particle diameter of 100 µm, the effect of the reduction in the heat capacity-density ratio is dominant. Hence, the Nusselt number decreases with increasing the SLR at a particle diameter of 100 µm. Similarly, due to

the above reason, the Nusselt number decreases up to an SLR of 0.63 at a particle diameter of 200 µm. However, at a particle diameter of 200 µm and an SLR of 0.88, the effect of the reduction in the effective thermal conductivity of the gas is significant, due to which the Nusselt number increases.

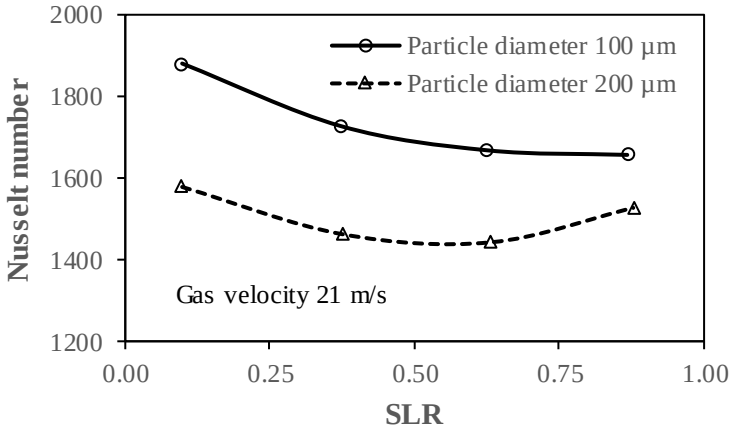

Figure 4.20: Effect of SLR on Nusselt number

The effect of SLR on pressure drop at different gas velocities and particle diameters is shown in Figure 4.21(a) and Figure 4.21(b). It is noticed from Figure 4.21(a) that the pressure drop first increases, and after that, it decreases at a gas velocity of 21 m/s. But, at a gas velocity of 15 m/s, the pressure drop continuously falls at a particle diameter of 100 µm and shows negligible effect at a particle diameter of 300 µm, as observed from Figure 4.21(b). As the SLR increases, more solids are introduced which increases the intersolid and solid-wall collisions. The intersolid and solid-wall collisions increase the pressure drop. Nevertheless, at the same time, increasing the SLR changes the effective properties of the gas (increases the effective density and decreases the effective viscosity of the gas). The effective property of the gas is the average value of the property in the computational domain. For instance, the effective density of the gas is defined as the average values of the density of the gas in the computational domain. At the inlet of the pipe, the density of the gas is defined as a function of the gas temperature. Once the particles are introduced, the temperature of the gas is varied. As a result, the effective density of the gas comes into play. Similarly, the effective viscosity of the gas can be defined. The gas velocity also affects the lateral dispersion of particles. Therefore, the SLR shows different behavior on pressure drop.

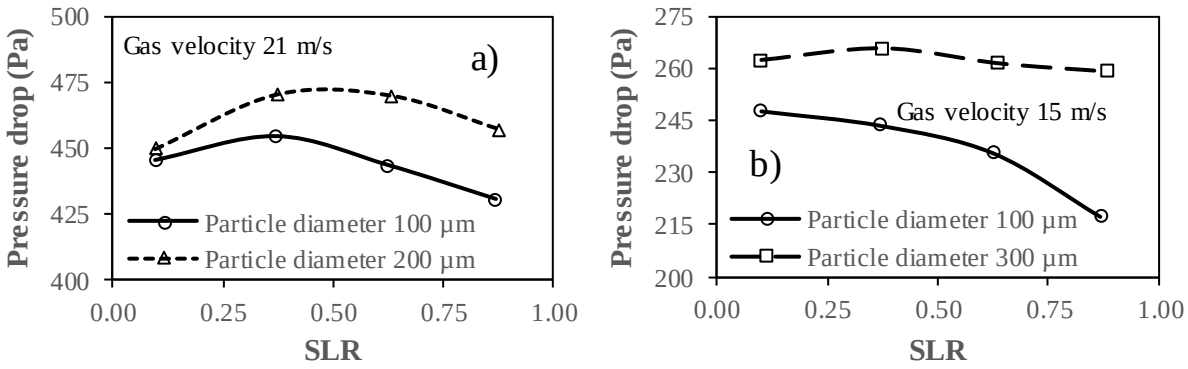

Figure 4.21: Effect of SLR on pressure drop

It is noticed from Figures 4.20 and 4.21(a) that the lowest Nusselt number and highest pressure drop occur for 200 µm particles at an SLR of 0.63. The lowest Nusselt number occurs due to the dominant nature of the reduction in the heat capacity-density ratio. However, the highest pressure drop occurs due to the combined effects of the increased collisions (intersolid and solid-wall collisions) and increased effective density of the gas.

4.7.1.3 Effect of inlet gas velocity on gas-solid Nusselt number and pressure drop

The effect of gas Reynolds number on Nusselt number at two SLRs (0.1 and 0.87) is shown in Figure 4.22. Four gas velocities such as 15 m/s, 18 m/s, 21 m/s, and 24 m/s are considered in the present work. The gas Reynolds number is calculated as

$$\mathrm{Re_g} = \frac{\rho_{\mathrm{eff}} \vec{v}_g D}{\mu_{\mathrm{eff}}} \tag{4.6}$$

Here, ρ_{eff} and μ_{eff} are the effective density and effective viscosity of the gas, which are the average values in the computational domain. It is observed from Figure 4.22 that the Nusselt number increases when the gas Reynolds number increases. Increasing the gas velocity increases the convection heat transfer which increases the Nusselt number.

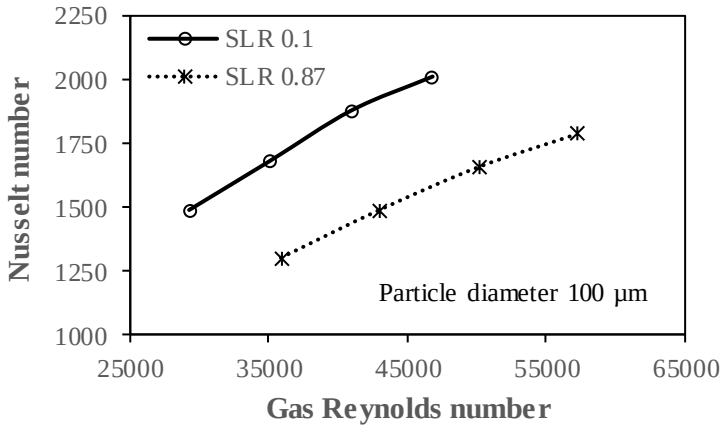

Figure 4.22: Effect of gas Reynolds number on Nusselt number

The effect of gas Reynolds number on pressure drop at different SLRs is plotted in Figure 4.23. It is observed from Figure 4.23 that the pressure drop rises in its value when the gas Reynolds number increases. The pressure drop increases owing to an increment in the drag force, which acts on the solid particles.

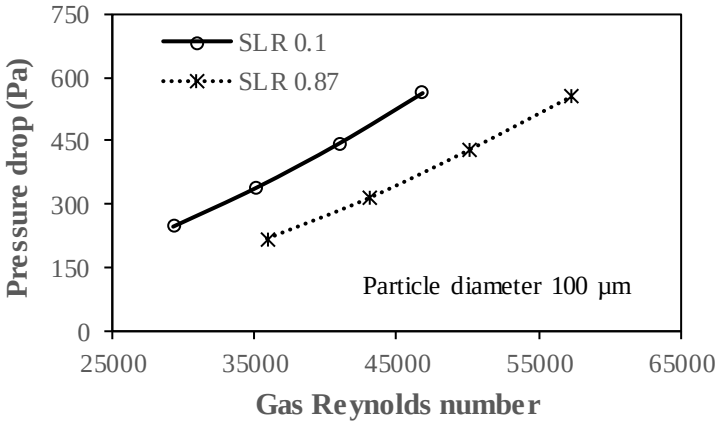

Figure 4.23: Effect of gas Reynolds number on pressure drop

4.7.2 Gas Prandtl number variation

The gas Prandtl number variation with respect to the particle diameter, SLR, and gas velocity is exposed in Figure 4.24(a), Figure 4.24(b), and Figure 4.24(c) respectively. The gas Prandtl number is calculated using the effective properties of the gas (i.e., the average gas properties in the computational domain), and is written in the following equation.

$$Pr_g = \mu_{eff} C_{p,eff} / k_{eff} \quad (4.7)$$

It is noticed from Figures 4.24(a)–(c) that the gas phase Prandtl number variation is not affected by the flow parameters such as the particle diameter, SLR, and gas velocity, although the gas properties change with respect to the temperature. The change in the particle diameter and SLR affect the effective properties of the gas. However, the change in the gas velocity does not affect the effective properties of the gas. Increasing the particle diameter increases the effective viscosity of the gas, increases the effective thermal conductivity of the gas, and slightly increases the effective specific heat of the gas. Increasing the SLR decreases the effective viscosity of the gas, decreases the effective thermal conductivity of the gas, and slightly decreases the effective specific heat of the gas. However, the net effect of the effective properties of the gas on gas Prandtl number is insignificant.

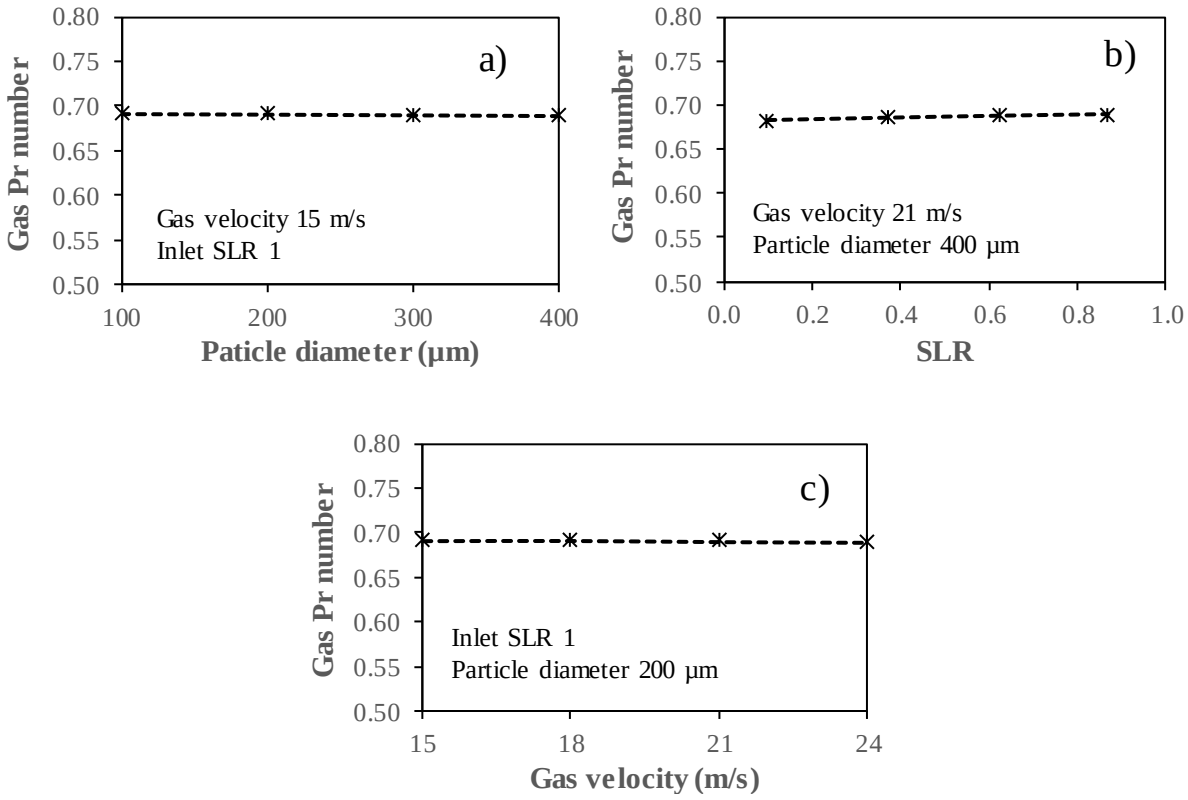

Figure 4.24: Gas Prandtl number variation

4.7.3 A correlation of gas-solid Nusselt number

A total 64 number of simulations have been conducted to predict the gas-solid Nusselt number in the horizontal pipe, for the below-mentioned operating conditions.

$15\ \mathrm{m/s} \leq \vec{v}_g \leq 24\ \mathrm{m/s}$ ($29000 \leq \mathrm{Re}_g \leq 57300$), $100\ \mu\mathrm{m} \leq d_s \leq 400\ \mu\mathrm{m}$, $0.1 \leq m \leq 1$.

A nonlinear regression analysis has been carried out to generate a correlation, to calculate the gas-solid Nusselt number in the following form.

$$\mathrm{Nu}_{avg} = a_1 \left(\frac{d_s}{D}\right)^{a_2} \times \left(\mathrm{Re}_g\right)^{a_3} \times (m)^{a_4} \tag{4.8}$$

The optimized regression parameters are:

a_1 = 1.485; a_2 = -0.172; a_3 = 0.548; a_4 = -0.083.

The above correlation predicts the gas-solid Nusselt number within ±9% deviation, as noticed from Figure 4.25.

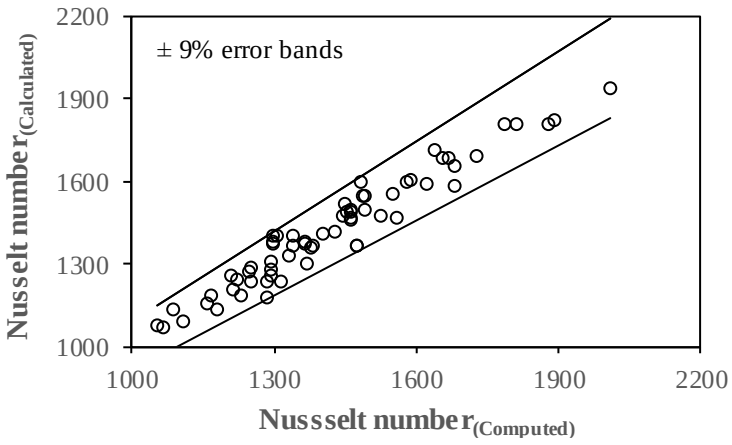

Figure 4.25: Calculated values vs computed values of Nusselt number

4.7.4 Studies of local heat transfer characteristics using sand particles

To ensure reliable thermal designs, local heat transfer studies are necessary in several industrial applications of gas-solid flows in horizontal pipes, for example, pneumatic conveying, circulating fluidized beds, and powder handling. Therefore, in this subsection, the

local heat transfer characteristics of dilute gas-solid flows through an adiabatic, horizontal pipe are studied.

4.7.4.1 Temperature profiles

The variation of the axial temperature profiles of the gas and solid is shown in Figure 4.26. It is observed from Figure 4.26 that, for both SLRs (0.43 and 0.59), the gas temperature gradually decreases, and in the meantime, the solid temperature gradually increases, along the length of the pipe. Moreover, at any location, the solid temperature is lower than the gas temperature, which obeys the heat exchanger law. The temperature difference between the gas and solid is more at the inlet of the pipe and gradually decreases towards the outlet of the pipe, due to the heat transfer from the gas to the solid. The gas phase gets cooled, and the solid phase gets heated. The temperature difference between the gas and solid is very small towards the end of the pipe, especially at the last one meter of the pipe. Therefore, this is similar to a direct contact type parallel flow heat exchanger.

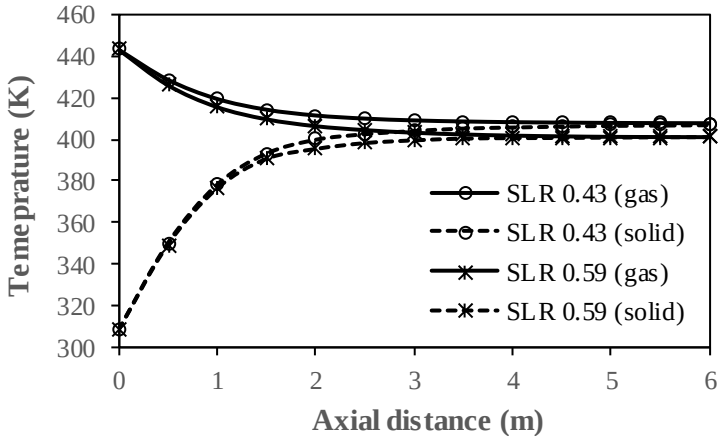

Figure 4.26: Variation of axial temperature profiles of the gas and solid at a gas velocity of 18.5 m/s and a particle diameter of 253 μm

The variation of the solid temperature (also known as the particle temperature) along the circumference (5 mm from the wall) and at the center is shown in Figure 4.27 and Figure 4.28 at different axial locations. The bottom wall is the bottom line having coordinates X = 0, Y = –0.029 m, L = 0–6 m, and let $\theta = 0$ for this bottom line. Similarly, $\theta = \pi/2$ for right, $\theta = \pi$ for top, and $\theta = 3\pi/2$ for left can be defined along the wall.

At an inlet gas velocity of 15 m/s (an inlet gas Reynolds number of 28210), an inlet SLR of 1, and a particle diameter of 400 µm, the maximum solid temperature is found near the top and bottom walls (Figure 4.27(a)). However, at an inlet gas velocity of 24 m/s (an inlet gas Reynolds number of 45135), an inlet SLR of 1, and a particle diameter of 400 µm, the maximum solid temperature is found near the bottom wall (Figure 4.27(b)). This is by reason of the presence of fewer solid particles, which quickly heats the particles due to the less heat transfer area. However, for both cases, the minimum solid temperature is found at the center. This is by reason of the presence of several particles at the center.

However, at an inlet gas velocity of 24 m/s, an inlet SLR of 0.1, and a particle diameter of 100 µm (Figure 4.28), the solid temperature is nearly equal at all positions (along the circumference of 5 mm from the wall and at the center). This is because of the full suspension flow due to which the particles are uniformly distributed and heated. In this case, the heat transfer from the gas to the particles is uniform. It is noticed from Figure 4.27 and Figure 4.28 that the inlet gas velocity along with the inlet SLR and particle diameter plays a major role in the positioning of the solid particles.

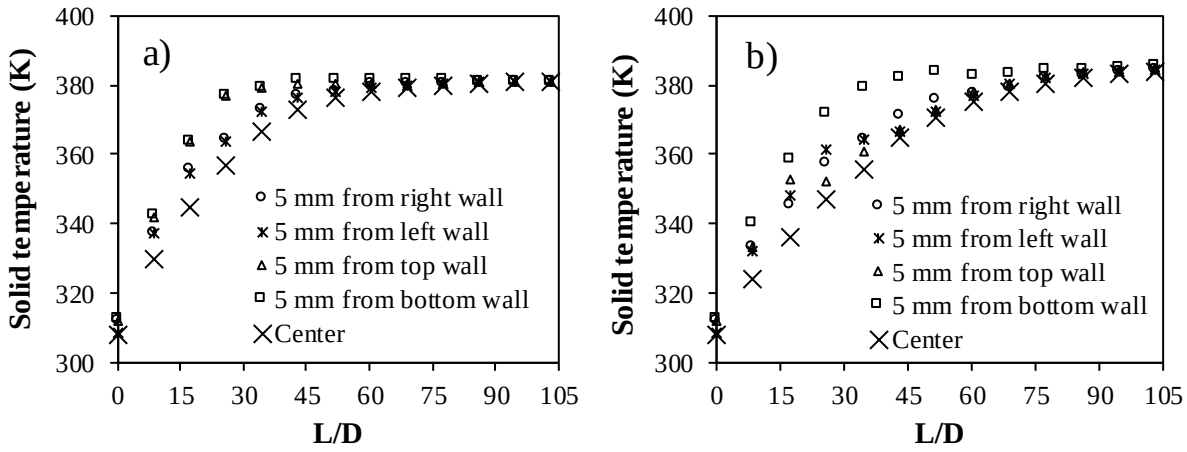

Inlet gas velocity 15 m/s Inlet gas velocity 24 m/s

Figure 4.27: Variation of solid temperature at an inlet SLR of 1 and a particle diameter of 400 µm

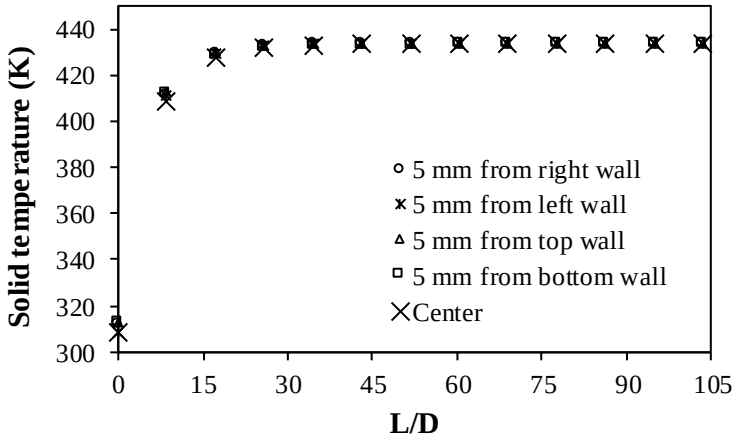

Figure 4.28: Variation of solid temperature at an inlet gas velocity of 24 m/s, an inlet SLR of 0.1, and a particle diameter of 100 µm

The contour plots of gas temperature and solid temperature at different locations at a gas velocity of 15 m/s, an inlet SLR of 1, and a particle diameter of 200 µm are shown in Figures 4.29(a) and 4.29(b) respectively.

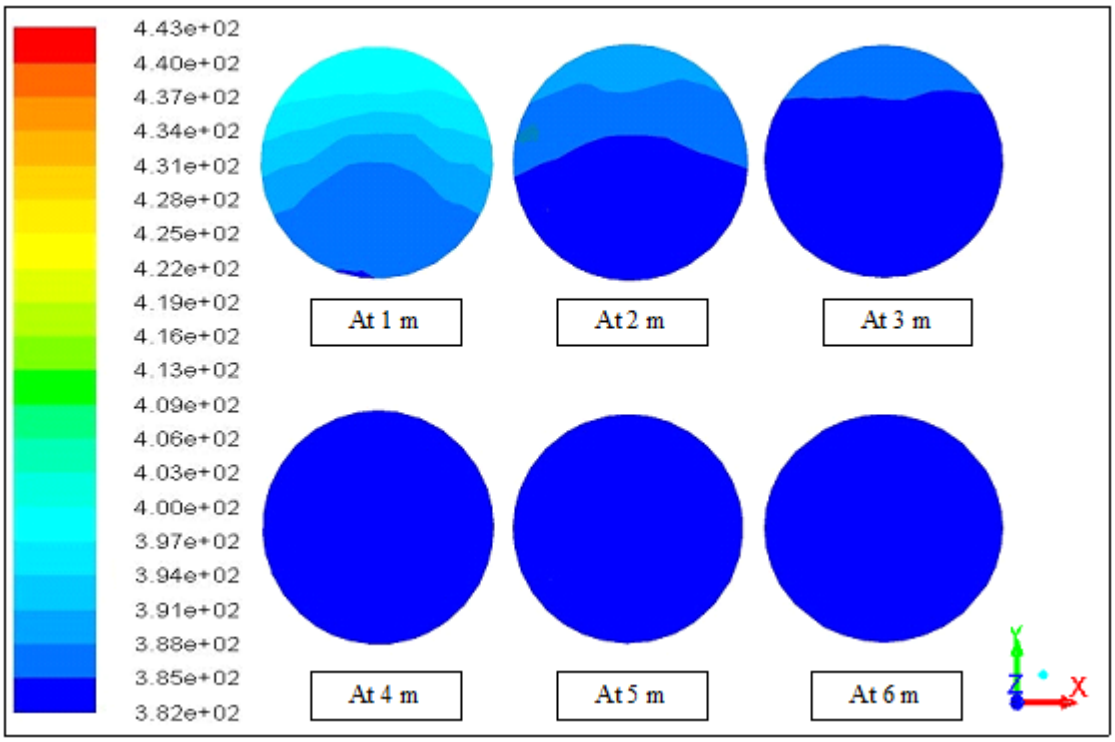

Figure 4.29(a): Contour plots of gas temperature at different locations

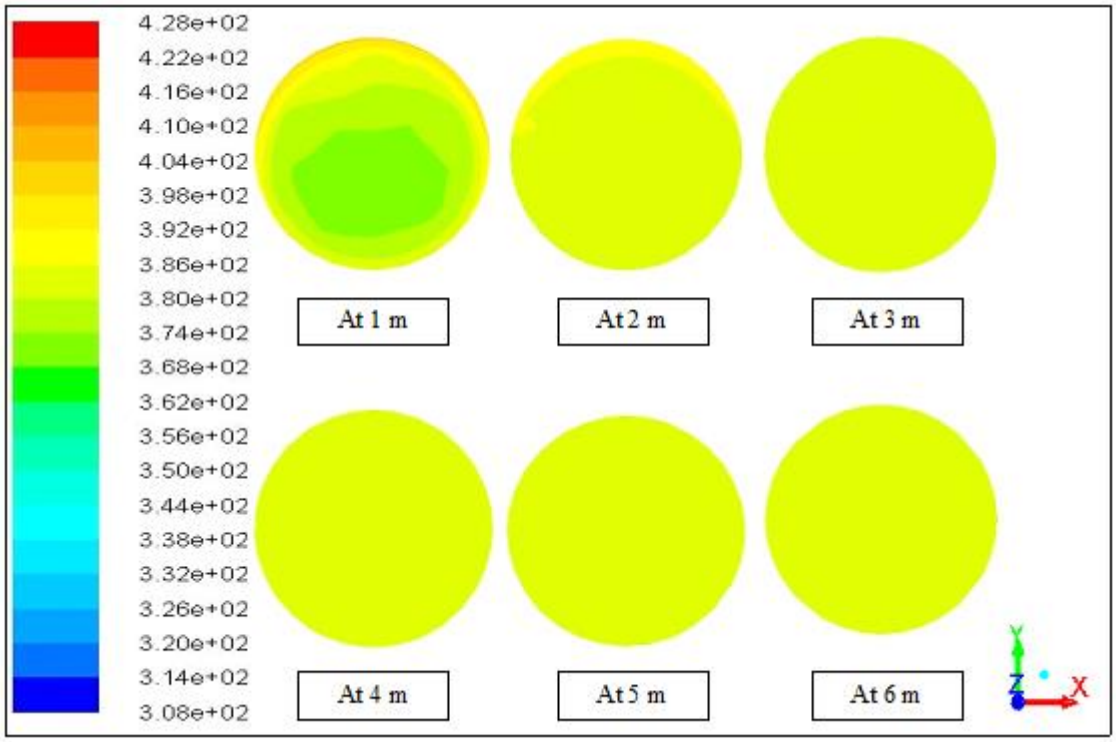

Figure 4.29(b): Contour plots of solid temperature at different locations

The gas temperature and solid temperature are lower at the lower half of the pipe up to the thermal equilibrium length, as noticed from Figures 4.29(a) and 4.29(b) respectively. This is due to the presence of more particles at the lower half of the pipe. Due to the presence of more particles, more heat is extracted from the gas, so the gas temperature is lower. At the same time, more particles increase the area of particles, which divides the heat, so the solid temperature is lower. At or after the thermal equilibrium length, the gas temperature and the solid temperature are unchanged. In the present case, the thermal equilibrium occurs at the length of 4 m from the inlet.

The effect of particle diameter, SLR, and inlet gas velocity on gas and solid temperatures is shown in Figures 4.30–4.33. The gas and solid temperatures are taken at the location of 100 mm from the inlet (area weighted average). Figure 4.30(a) and Figure 4.30(b) show the effect of particle diameter on gas and solid temperatures at a gas velocity of 15 m/s, considering inlet SLRs of 0.1 and 1 respectively. It is observed from Figure 4.30(a) and Figure 4.30(b) that increasing the particle diameter increases the gas temperature and decreases the solid temperature at the location (100 mm). Increasing the particle diameter decreases the heat transfer area of particles (with the same SLR), and the heat energy from the gas is absorbed

by the solid particles having less surface area. Again, the particle residence time decreases with increasing the particle diameter, due to the less number of particles. The gas temperature increases due to a decrease in both heat transfer area and particle resident time. However, the solid temperature decreases due to the decreased particle resident time, despite a decrease in the heat transfer area.

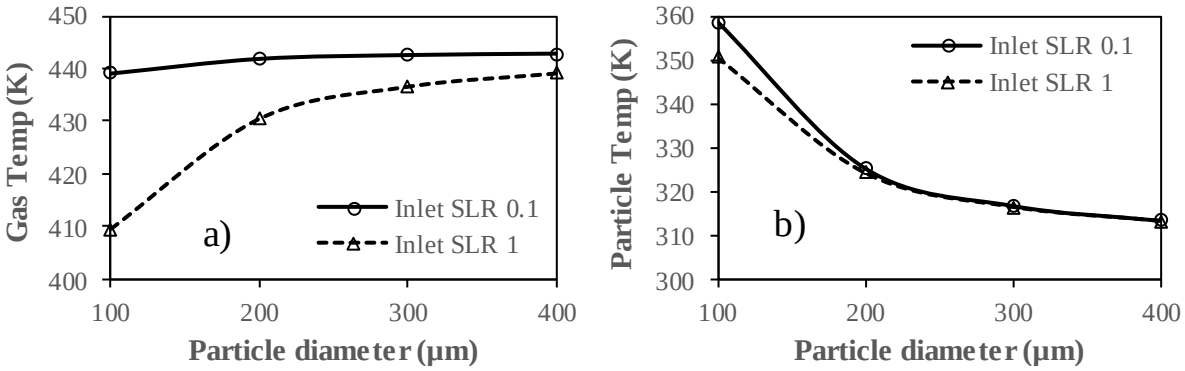

Figure 4.30: Effect of particle diameter on gas and solid temperatures at a gas velocity of 15 m/s

Figure 4.31(a) and Figure 4.31(b) show the effect of SLR on gas and solid temperatures at the location (100 mm) at a gas velocity of 21 m/s, for particle diameters of 100 µm and 400 µm respectively. It is noticed from Figure 4.31(a) and Figure 4.31(b) that, at the location (100 mm), increasing the SLR decreases the gas temperature, and decreases the solid temperature at a particle diameter of 100 µm, and marginally decreases the solid temperature at a particle diameter of 400 µm. Increasing the SLR increases the heat transfer area due to the introduction of several particles and increases the particle resident time. Due to the increased heat transfer area and particle residence time, more heat is taken from the gas, as a result, the gas temperature decreases. Due to the increased heat transfer area, the solid temperature decreases, and due to the increased particle resident time, the solid temperature increases. However, the effect of the increased heat transfer area is more than the effect of the increased particle resident time. Therefore, the solid temperature decreases at a lower particle diameter of 100 µm. At a higher particle diameter of 400 µm, both the effects are nearly equal, and therefore, the solid temperature marginally decreases.

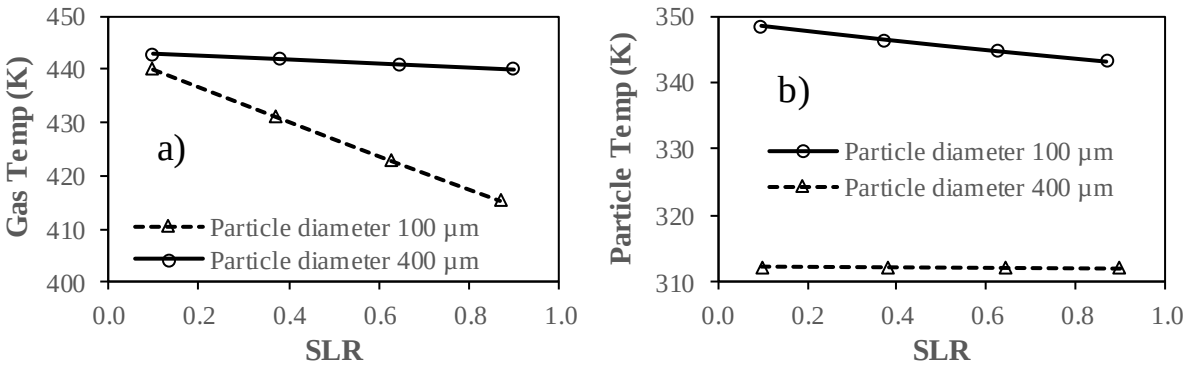

Figure 4.31: Effect of SLR on gas and solid temperatures at a gas velocity of 21 m/s

Figure 4.32 and Figure 4.33 show the effect of inlet gas velocity on gas and solid temperatures at the location (100 mm) at different particle diameters and inlet SLRs. Four types of inlet gas velocity, i.e., 15 m/s, 18 m/s, 21 m/s, and 24 m/s are used. The corresponding inlet gas Reynolds numbers are presented in Table 4.1.

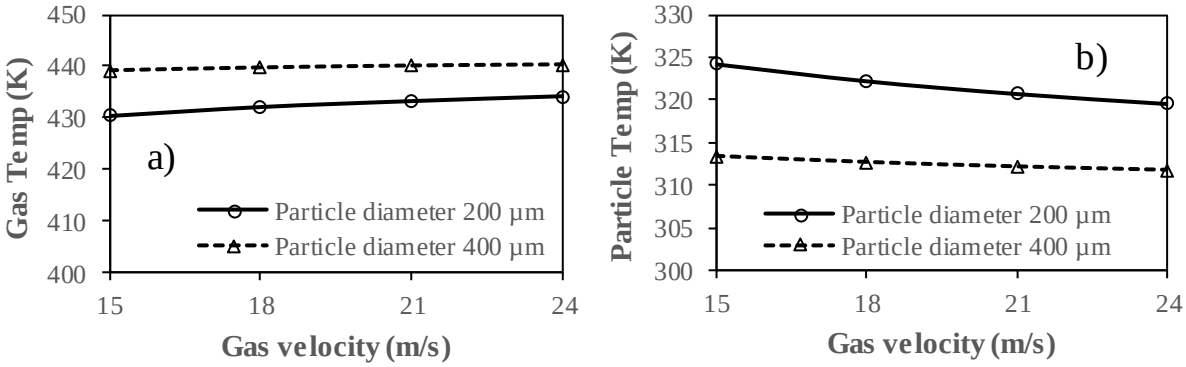

Figure 4.32: Effect of inlet gas velocity on gas and solid temperatures at an inlet SLR of 1

Table 4.1: Inlet gas Reynolds numbers for inlet gas velocity

Inlet gas velocity	Inlet gas Reynolds number
15 m/s	28210
18 m/s	33850
21 m/s	39495
24 m/s	45135

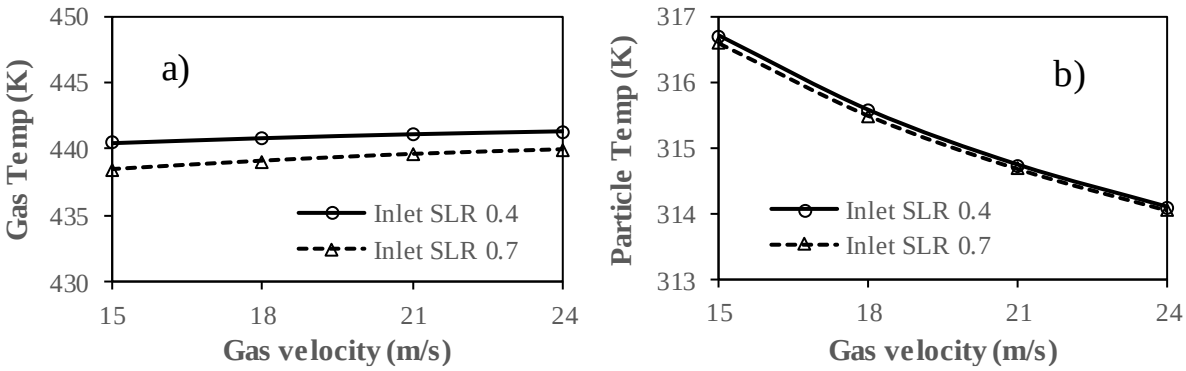

Figure 4.33: Effect of inlet gas velocity on gas and solid temperatures at a particle diameter of 300 µm

It is noticed from Figure 4.32 and Figure 4.33 that the gas temperature increases and the solid temperature decreases at the location (100 mm) with increasing the inlet gas velocity. This is due to the decreased particle resident time with increasing the inlet gas velocity.

4.7.4.2 Solid volume fraction (SVF) profiles

The radial distribution of SVF contours at different locations of the pipe at an SLR of 0.43 and 0.59 are shown in Figure 4.34(a) and Figure 4.34(b) respectively. In the horizontal pipe, the Z-axis is along the length.

It is observed from Figure 4.34(a) and Figure 4.34(b) that the SVFs are more towards the bottom of the pipe and least towards the top of the pipe. The particles begin to settle down at the bottom of the pipe because of gravity. The bulk gas velocity significantly influences the SVF profiles in horizontal gas-solid flows. Here, the bulk gas velocity is 18.5 m/s. Further, the SVF profiles change from location to location, due to a change in the density of the gas, which is due to a change in the temperature of the gas.

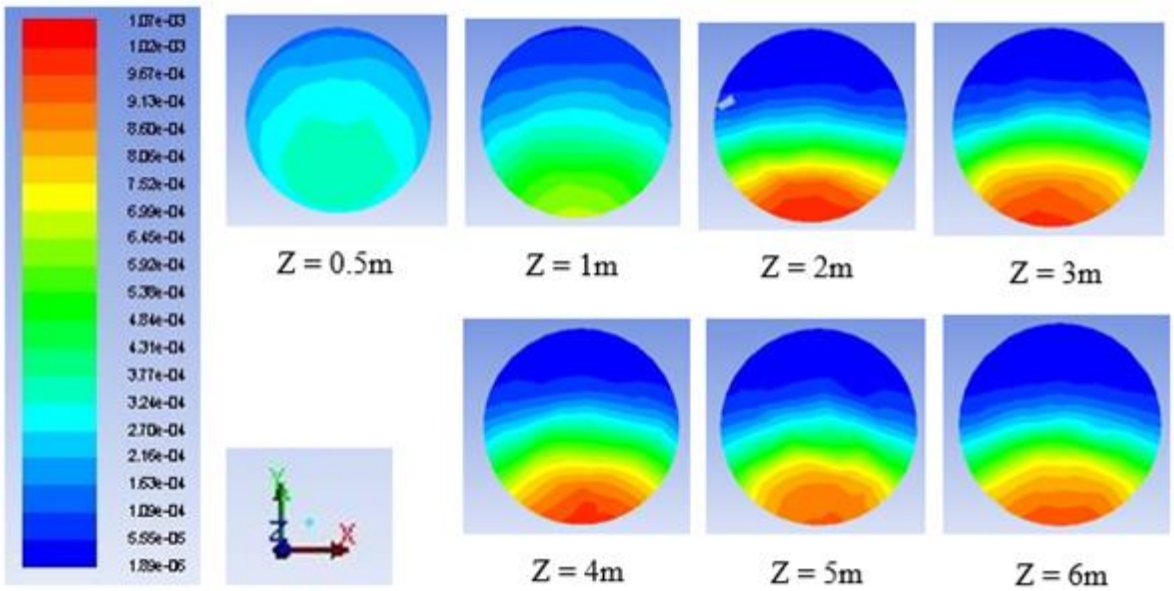

Figure 4.34(a): SVF contours at different locations along the pipe (at an SLR of 0.43 and a particle diameter of 253 µm)

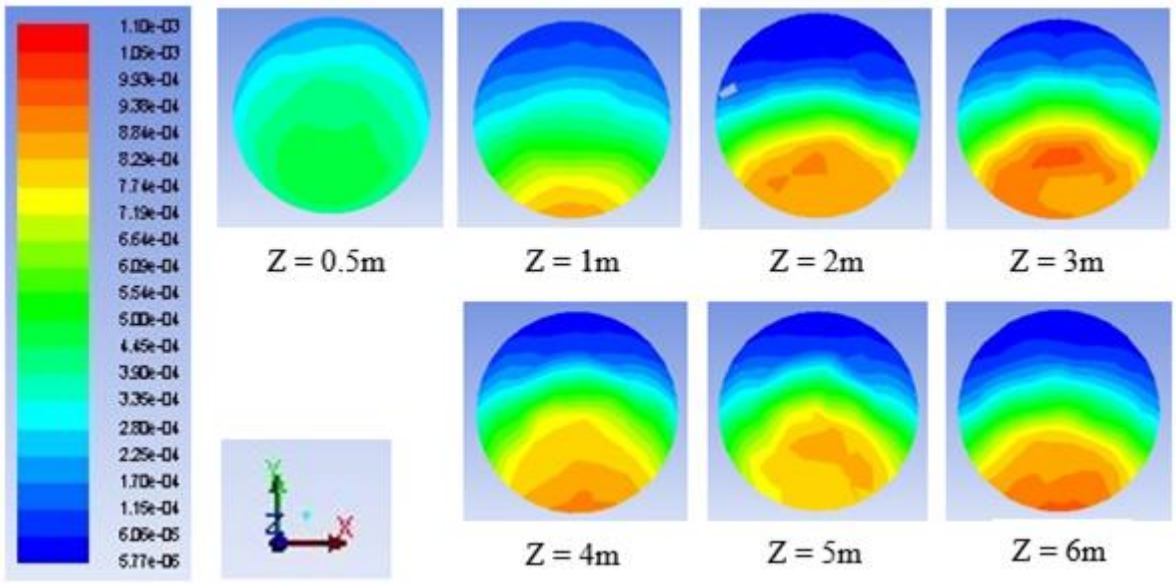

Figure 4.34(b): SVF contours at different locations along the pipe (at an SLR of 0.59 and a particle diameter of 253 µm)

4.7.4.3 Local logarithmic mean temperature difference (LMTD) profiles

The local LMTD (at a position of 100 mm from the inlet) is calculated as per eq. 3.44, and the local LMTD profiles are shown in Figures 4.35–4.38. Figure 4.35 shows the effect of particle diameter on LMTD at a gas velocity of 15 m/s, for inlet SLRs of 0.1 and 1. It is noticed from Figure 4.35 that increasing the particle diameter increases the LMTD. With increasing the particle diameter, the gas temperature at the location (100 mm) increases, and the solid temperature at the location (100 mm) decreases. Therefore, the temperature difference between the gas and solid at the location (100 mm) increases, which increases the LMTD.

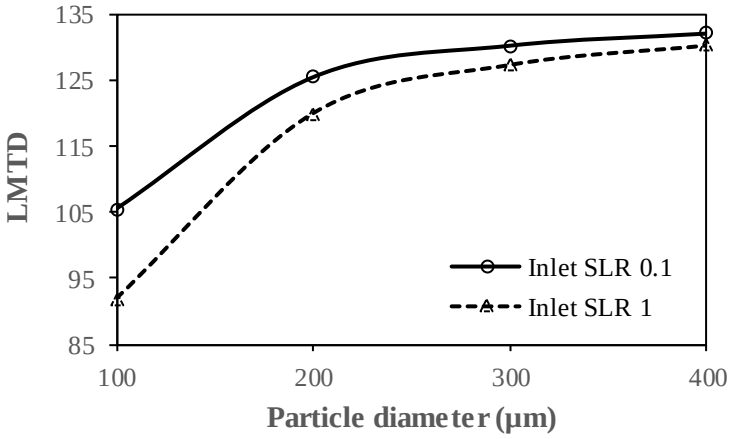

Figure 4.35: Effect of particle diameter on local LMTD at a gas velocity of 15 m/s

Figure 4.36 shows the effect of SLR on LMTD at the location (100 mm) at a gas velocity of 21 m/s, for particle diameters of 100 µm and 400 µm. It is noticed from Figure 4.36 that increasing the SLR decreases the LMTD. By increasing the SLR, both the gas and solid temperatures decrease at the location (100 mm). However, the effect of the decreased gas temperature is more than the effect of the decreased solid temperature, which reduces the temperature difference between the gas and solid. Therefore, the LMTD decreases with the increase of the SLR.

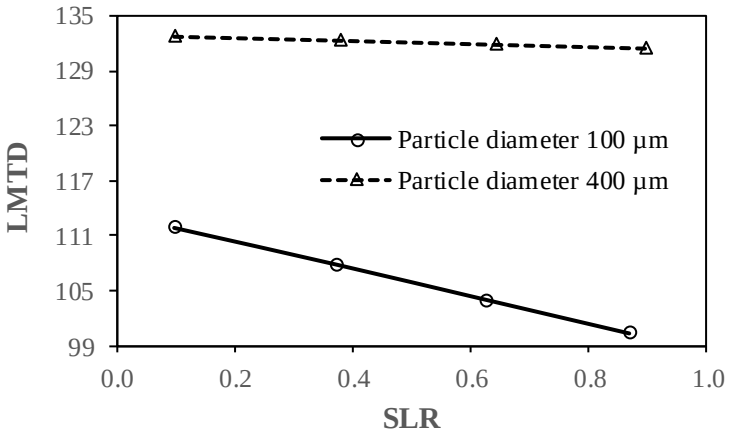

Figure 4.36: Effect of SLR on local LMTD at a gas velocity of 21 m/s

Figure 4.37 shows the effect of inlet gas velocity on LMTD at the location (100 mm) at an inlet SLR of 1, for particle diameters of 200 µm and 400 µm. Likewise, Figure 4.38 depicts the influence of inlet gas velocity on LMTD at the location (100 mm) at a particle diameter of 300 µm, for inlet SLRs of 0.4 and 0.7. It is noticed from Figures 4.37 and 4.38 that the LMTD increases with increasing the inlet gas velocity. Increasing the inlet gas velocity increases the gas temperature and decreases the solid temperature at the location (100 mm), which increases the temperature difference between the gas and solid. Therefore, the LMTD increases with the increase of the inlet gas velocity.

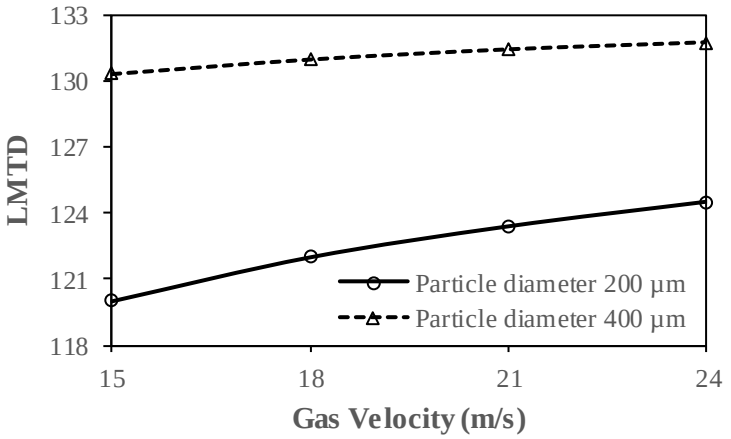

Figure 4.37: Effect of inlet gas velocity on local LMTD at an inlet SLR of 1

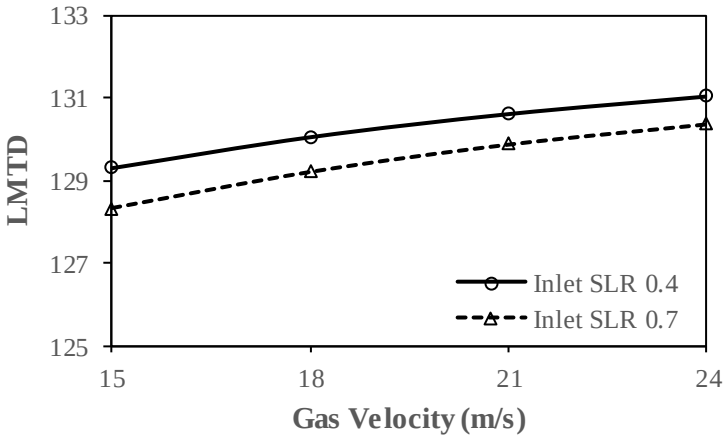

Figure 4.38: Effect of inlet gas velocity on local LMTD at a particle diameter of 300 µm

4.7.4.4 Local gas-solid Nusselt number profiles

The variation of local gas-solid Nusselt number along the pipe at SLRs of 0.43 and 0.59 is shown in Figure 4.39. The local gas-solid Nusselt number is calculated as per eq. 3.47.

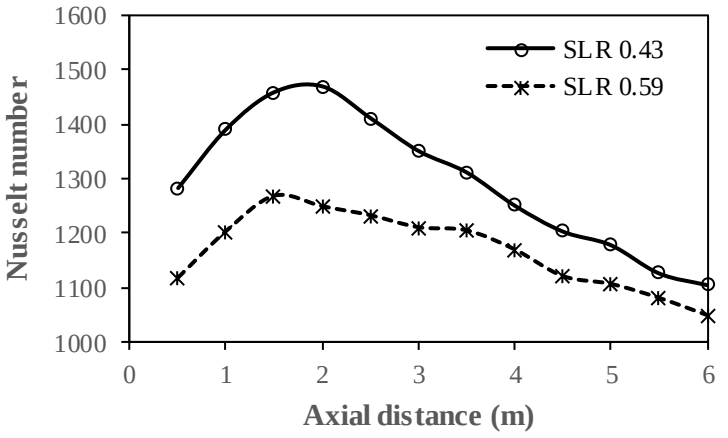

Figure 4.39: Variation of local gas-solid Nusselt number at a gas velocity of 18.5 m/s and a particle diameter of 253 µm

It is observed from Figure 4.39 that the local gas-solid Nusselt number first increases up to a certain distance, and then, it starts decreasing. This is the distance up to which heat transfer takes place rapidly from the gas to the solids, due to an increase in the overall heat transfer coefficient. The temperature profiles of the gas and solid affect the overall heat transfer coefficient. This distance is different for different SLRs. For an SLR of 0.43, the local Nusselt number increases up to an L/D of 35, and then, it gradually decreases. However, for an SLR

of 0.59, the local Nusselt number increases up to an L/D of 26, and then, it gradually decreases.

The local Nusselt number is calculated at a position of 100 mm from the inlet. Figure 4.40 shows the effect of particle diameter on gas-solid Nusselt number at the location (100 mm) at a gas velocity of 15 m/s, for inlet SLRs of 0.1 and 1. The Nusselt number decreases with increasing the particle diameter, as seen from Figure 4.40. Increasing the particle diameter decreases the turbulent gas Reynolds number, which is also known as turbulent suppression. Therefore, the Nusselt number decreases due to the turbulent suppression.

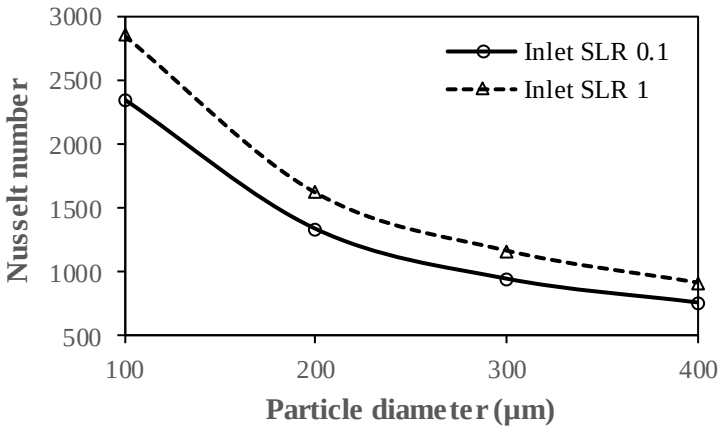

Figure 4.40: Effect of particle diameter on local gas-solid Nusselt number at a gas velocity of 15 m/s

Figure 4.41 shows the effect of SLR on gas-solid Nusselt number at the location (100 mm) at a gas velocity of 21 m/s, for particle diameters of 100 µm and 400 µm. The Nusselt number increases with increasing the SLR, as seen from Figure 4.41. Increasing the SLR increases the turbulent gas Reynolds number; therefore, the Nusselt number increases.

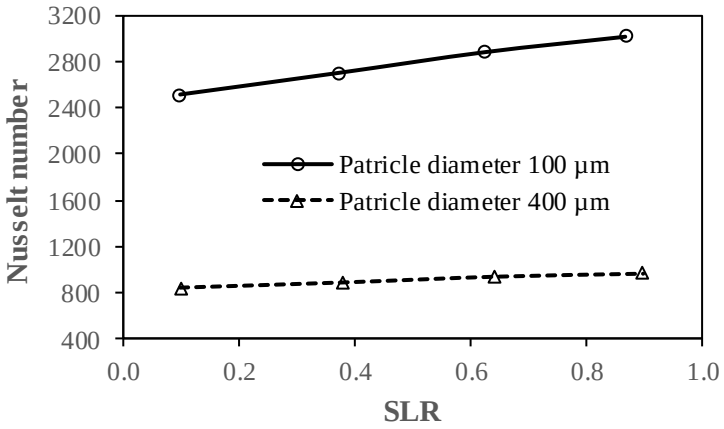

Figure 4.41: Effect of SLR on local gas-solid Nusselt number at a gas velocity of 21 m/s

Figure 4.42 shows the effect of inlet gas velocity on gas-solid Nusselt number at the location (100 mm) at an inlet SLR of 1, for particle diameters of 200 µm and 400 µm. Likewise, Figure 4.43 shows the influence of inlet gas velocity on gas-solid Nusselt number at a particle diameter of 300 µm, for inlet SLRs of 0.4 and 0.7. It is noticed from Figures 4.42 and 4.43 that the Nusselt number increases with increasing the inlet gas velocity. This is due to the increased convection heat transfer from the gas to the particles with increasing the inlet gas velocity.

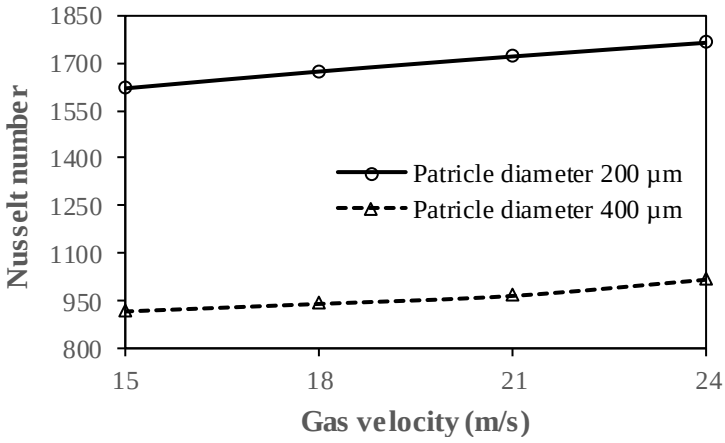

Figure 4.42: Effect of inlet gas velocity on local gas-solid Nusselt number at an inlet SLR of 1

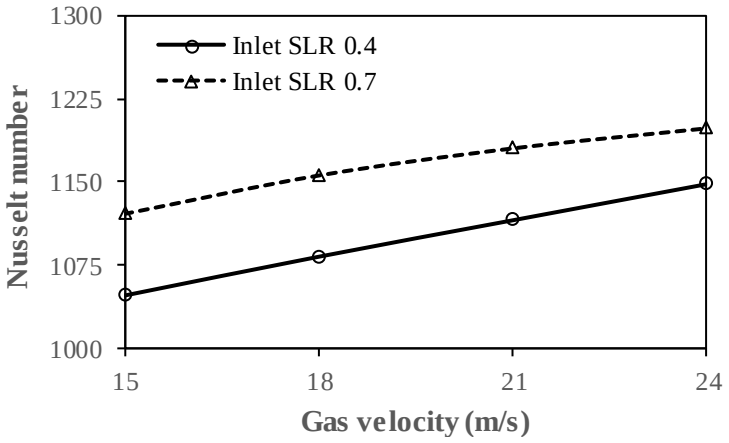

Figure 4.43: Effect of inlet gas velocity on local gas-solid Nusselt number at a particle diameter of 300 µm

4.7.4.5 Thermal effectiveness of the gas and solid

The thermal effectiveness of a phase (gas or solid) is defined as the mean temperature change of the phase to the maximum possible temperature change of two phases. Hence, at any location (n), the thermal effectiveness of the gas is

$$S_{g,n} = (T_{g,i} - T_{g,n})/(T_{g,i} - T_{s,i}) \quad (4.9)$$

and the thermal effectiveness of the solid is

$$S_{s,n} = (T_{s,n} - T_{s,i})/(T_{g,i} - T_{s,i}) \quad (4.10)$$

The thermal effectiveness of the gas and solid at a position of 100 mm from the inlet is shown in Figures 4.44–4.47. Figure 4.44 shows the effect of particle diameter on thermal effectiveness of the gas and solid at the location (100 mm) at a gas velocity of 15 m/s, for inlet SLRs of 0.1 (Figure 4.44(a)) and 1 (Figure 4.44(b)). It is observed from Figure 4.44(a) and Figure 4.44(b) that the thermal effectiveness of the gas and solid decreases with increasing the particle diameter. This is due to a decrease in the mean temperature change of the phase, as the maximum possible temperature change is constant. With increasing the particle diameter, the gas temperature increases and the solid temperature decreases at the location (100 mm), which in turn decreases the mean temperature change of both the gas and solid phases.

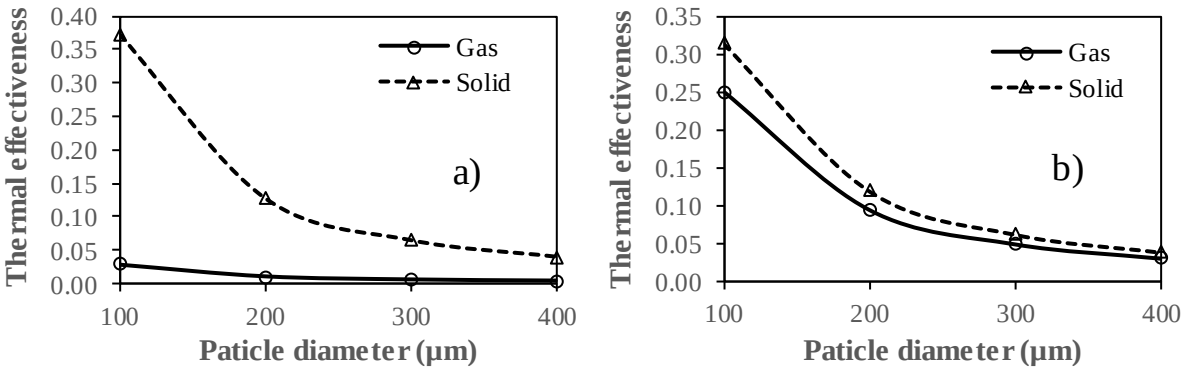

Inlet SLR 0.1 Inlet SLR 1

Figure 4.44: Effect of particle diameter on thermal effectiveness of the gas and solid at a gas velocity of 15 m/s

Figure 4.45 shows the effect of inlet SLR on thermal effectiveness of the gas and solid at the location (100 mm) at a gas velocity of 21 m/s, for particle diameters of 100 µm (Figure 4.45(a)) and 400 µm (Figure 4.45(b)). It is observed from Figure 4.45(a) and Figure 4.45(b) that, with increasing the SLR, the thermal effectiveness of the gas increases; however, the thermal effectiveness of the solid decreases at a particle diameter of 100 µm, and a marginal decrease in the thermal effectiveness of the solid at a particle diameter of 400 µm. The thermal effectiveness of the gas increases at particle diameters of 100 µm and 400 µm, due to an increase in the mean temperature change of the gas. Increasing the inlet SLR decreases the gas temperature at the location (100 mm), which increases the mean temperature change of the gas. At a particle diameter of 100 µm, the thermal effectiveness of the solid decreases due to a decrease in the mean temperature change of the solid. The mean temperature change of the solid decreases due to a decrease in the solid temperature at the location (100 mm) with increasing the inlet SLR at a particle diameter of 100 µm. However, at a particle diameter of 400 µm, there is a marginal decrease in the thermal effectiveness of the solid, due to a negligible variation in the mean temperature change of the solid phase. At a particle diameter of 400 µm with an increase of the inlet SLR, the mean temperature change of the solid is negligible, due to a negligible change in the solid temperature.

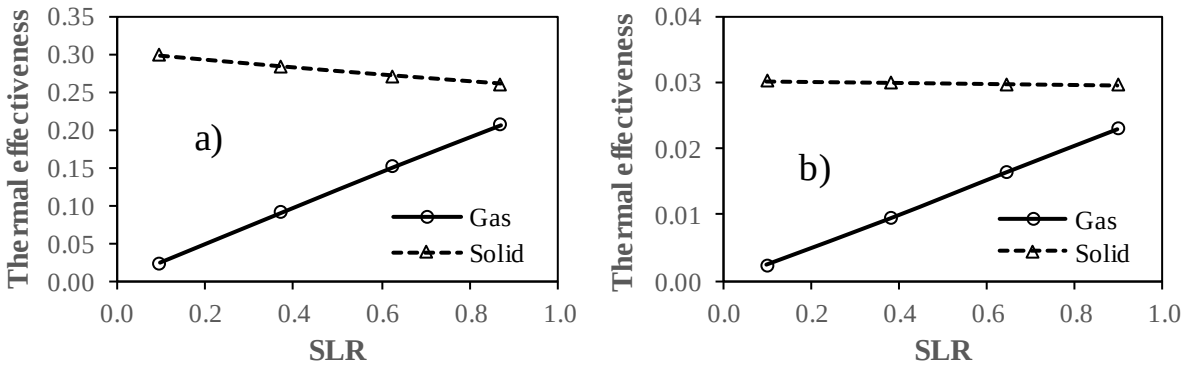

Particle diameter 100 µm Particle diameter 400 µm

Figure 4.45: Effect of SLR on thermal effectiveness of the gas and solid at a gas velocity of 21 m/s

Figure 4.46 shows the effect of inlet gas velocity on thermal effectiveness of the gas and solid at the location (100 mm) at an inlet SLR of 1, for particle diameters of 200 µm (Figure 4.46(a)) and 400 µm (Figure 4.46(b)). Likewise, Figure 4.47 shows the effect of inlet gas velocity on thermal effectiveness of the gas and solid at a particle diameter of 300 µm, for inlet SLRs of 0.4 (Figure 4.47(a)) and 0.7 (Figure 4.47(b)).

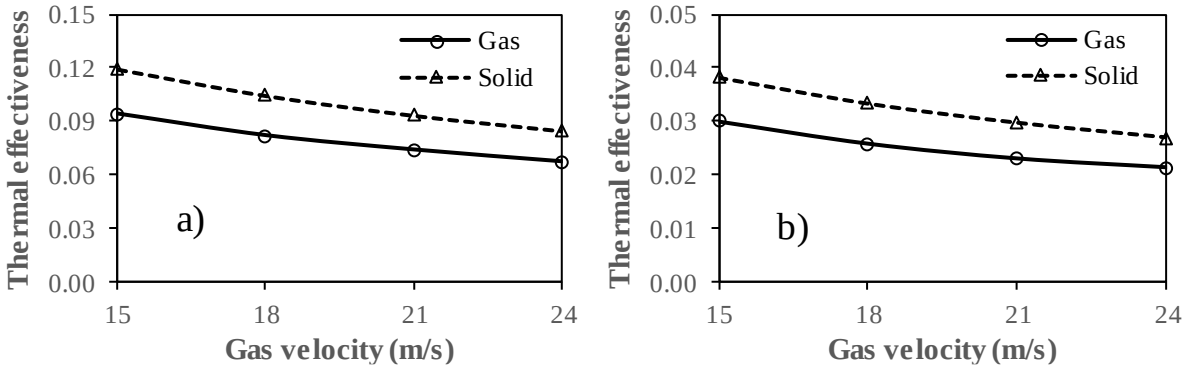

Particle diameter 200 µm Particle diameter 400 µm

Figure 4.46: Effect of inlet gas velocity on thermal effectiveness of the gas and solid at an inlet SLR of 1

It is observed from Figure 4.46 and Figure 4.47 that, with increasing the inlet gas velocity, the thermal effectiveness of the gas and solid decreases. This is due to a decrease in the mean temperature change of the individual phase. Increasing the inlet gas velocity increases the gas

temperature and decreases the solid temperature at the location (100 mm), which in turn decreases the mean temperature change of both gas and solid phases.

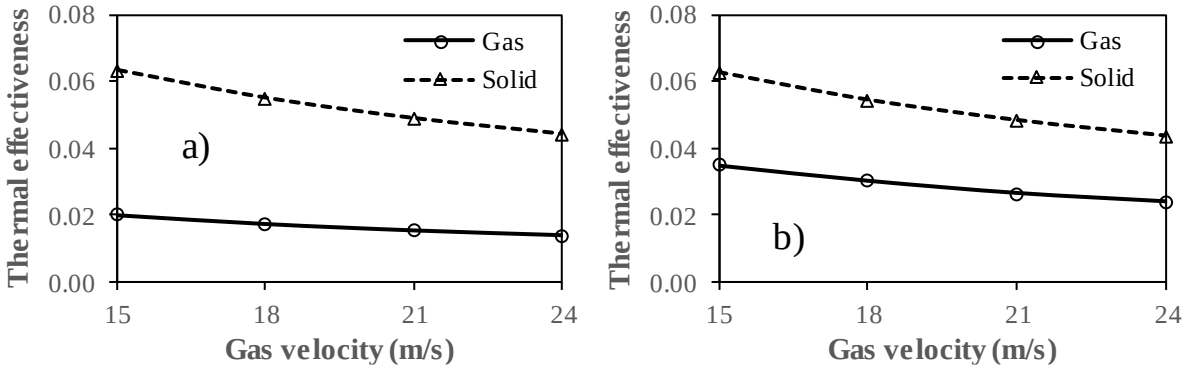

Inlet SLR 0.4 Inlet SLR 0.7

Figure 4.47: Effect of inlet gas velocity on thermal effectiveness of the gas and solid at a particle diameter of 300 μm

4.7.5 Comparison of heat transfer and pressure drop results using plastic, sand, and glass particles

Three solid particles such as plastic, sand, and glass are used to compare the heat transfer and pressure drop results of dilute gas-solid flows in the horizontal, adiabatic pipe. The selection of these three solid materials is due to their wide industrial applications. The properties of plastic, sand, and glass particles have already been given in Table 3.2 of chapter 3.

4.7.5.1 Comparison of temperature profiles among the flows using plastic, sand, and glass particles

The comparison of gas temperature profiles among the flows using plastic, sand, and glass particles along the axis is exposed in Figure 4.48. It is noticed from Figure 4.48 that the gas temperature is higher for air-glass flow and lower for air-plastic flow along with the axial distance.

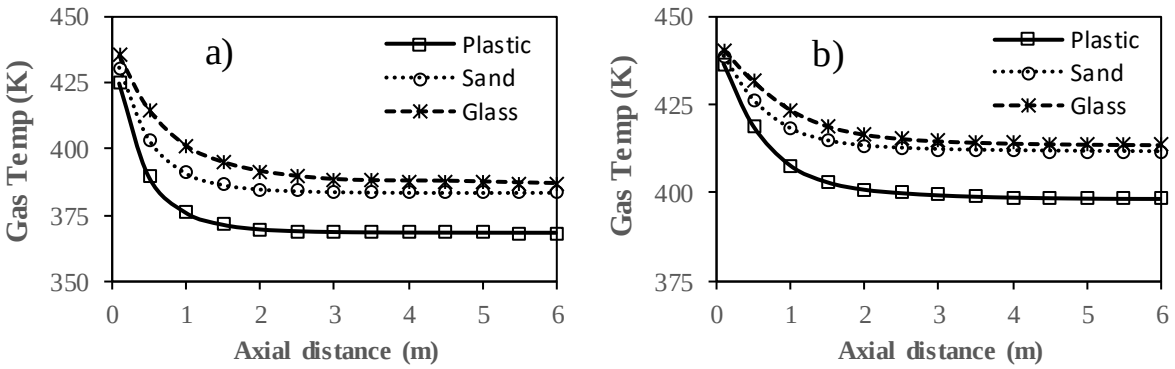

Figure 4.48: Comparison of gas temperature profiles among the flows using plastic, sand, and glass particles for, (a) $\vec{v}_g$=15 m/s, inlet SLR=1, d_s=200 µm; (b) $\vec{v}_g$=18 m/s, inlet SLR=0.4, d_s=200 µm

To find out the reason behind this, a new concept in gas-solid flows, which is called the heat properties ratio, is defined in the present study. The heat properties ratio is defined as the ratio of the multiplication of the density, specific heat, and thermal conductivity of the solid to the gas ($(\rho C_p k)_{solid}$ / $(\rho C_p k)_{gas}$). The heat properties ratio is useful when different solids having different properties are used. For the gas, the effective properties (average values) are used. Due to the higher heat properties ratio of air-glass flow and lower heat properties ratio of air-plastic flow, the gas temperature is higher for air-glass flow and lower for air-plastic flow along with the axial distance. The heat properties ratio corresponding to Figure 4.48(a) and Figure 4.48(b) is shown in Table 4.2 and Table 4.3 respectively. It is noticed from Table 4.2 and Table 4.3 that the heat properties ratio of air-glass flow is higher and the heat properties ratio of air-plastic flow is lower.

Table 4.2: Heat properties ratio of various flows (for $\vec{v}_g$=15 m/s; inlet SLR=1; d_s=200 µm)

Flow type	**Heat properties ratio**
Air-plastic flow	8268.1
Air-sand flow	31753.1
Air-glass flow	63283.7

Table 4.3: Heat properties ratio of various flows (for $\vec{v}_g$=18 m/s; inlet SLR=0.4; d_s=200 µm)

Flow type	Heat properties ratio
Air-plastic flow	8333.8
Air-sand flow	31962.5
Air-glass flow	63661.5

The comparison of particle temperature profiles among the flows using plastic, sand, and glass particles along the axis is exposed in Figure 4.49. It is seen from Figure 4.49 that the particle temperature rises rapidly up to a certain distance known as the initial length, and after that, it remains constant where the equilibrium temperature exists between the phases. The particle temperature is higher for air-glass flow and lower for air-plastic flow in the equilibrium temperature region. This is mainly due to the higher heat properties ratio of air-glass flow and lower heat properties ratio of air-plastic flow. However, up to a part of the initial length, the particle temperature is higher for air-sand flow and lower for air-glass flow. This depends upon the value of the heat capacity-density ratio and a lower value yields a higher temperature. The heat capacity-density ratio is defined as the ratio of the multiplication of the density and specific heat of the solid to the gas. This value is lower for sand particles and higher for glass particles.

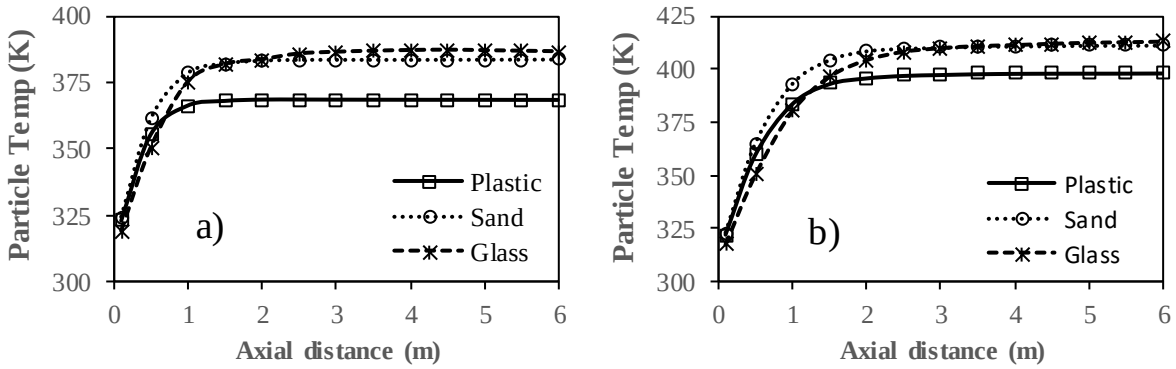

Figure 4.49: Comparison of particle temperature profiles among the flows using plastic, sand, and glass particles for, (a) $\vec{v}_g$=15 m/s, inlet SLR=1, d_s=200 µm; (b) for $\vec{v}_g$=18 m/s, inlet SLR=0.4, d_s=200 µm

4.7.5.2 Comparison of heat transfer results among the flows using plastic, sand, and glass particles

The influence of particle diameter on Nusselt number at a gas velocity of 15 m/s and an inlet SLR of 0.4 for plastic, sand, and glass particles is depicted in Figure 4.50. It is observed from Figure 4.50 that the Nusselt number decreases as the particle diameter increases for the three particles, where the turbulence suppression by the fine particles is the reason.

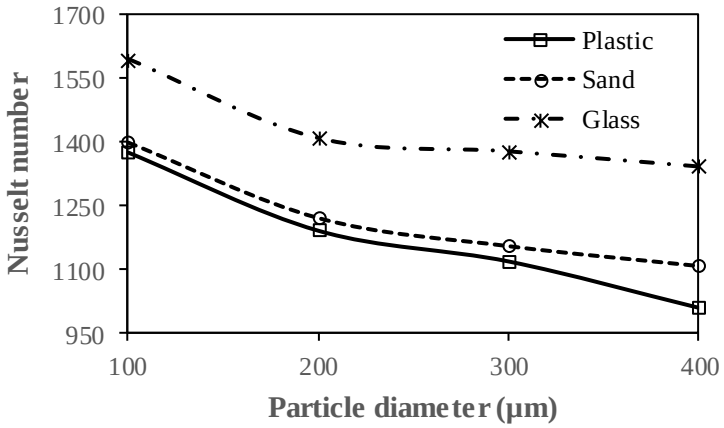

Figure 4.50: Comparison of Nusselt number among the flows using plastic, sand, and glass particles with respect to the particle diameter ($\vec{v}_g$=15 m/s; inlet SLR=0.4)

The Nusselt number is higher for glass particles and lower for plastic particles. This is due to the higher heat properties ratio of glass particles and lower heat properties ratio of plastic particles.

The influence of inlet SLR on the Nusselt number at a gas velocity of 15 m/s and a particle diameter of 200 µm for plastic, sand, and glass particles is depicted in Figure 4.51. It is seen from Figure 4.51 that the Nusselt number first decreases, goes to a bottom, and after that, it increases as the inlet SLR increases for the three particles. Increasing the inlet SLR decreases the heat capacity-density ratio and effective thermal conductivity of the gas. Decreasing the heat capacity-density ratio decreases the heat transfer, and decreasing the effective thermal conductivity of the gas increases the heat transfer. At lower inlet SLRs (0.1 and 0.4), the effect of the reduction in the heat capacity-density ratio is dominant. However, at higher inlet SLRs (0.7 and 1), the effect of the reduction in the effective thermal conductivity of the gas is significant due to which the Nusselt number increases.

The Nusselt number is higher for glass particles due to the higher heat properties ratio and higher heat capacity-density ratio of glass particles. However, the Nusselt number is lower for plastic particles at lower inlet SLRs (0.1 and 0.4) and lower for sand particles at higher inlet SLRs (0.7 and 1). The heat properties ratio of sand particles is higher than plastic particles; however, the heat capacity-density ratio of sand particles is lower than plastic particles. Hence, at lower inlet SLRs, the effect of the heat properties ratio is dominant due to which the Nusselt number is lower for plastic particles. However, at higher inlet SLRs, the effect of the heat capacity-density ratio is dominant due to which the Nusselt number is lower for sand particles.

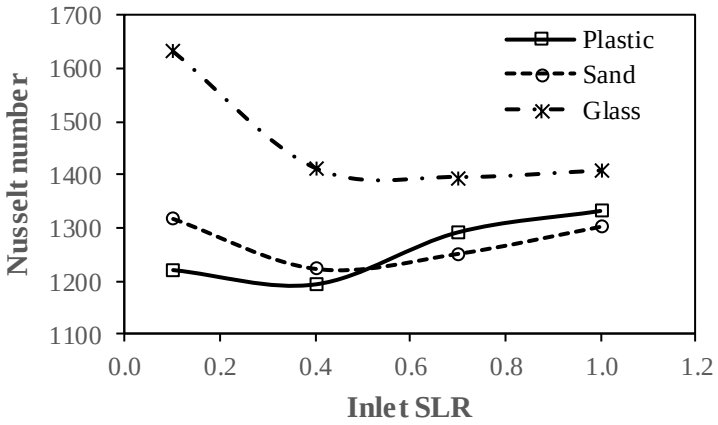

Figure 4.51: Comparison of Nusselt number among the flows using plastic, sand, and glass particles with respect to the inlet SLR ($\vec{v}_g$=15 m/s; d_s=200 µm)

The influence of inlet gas velocity on Nusselt number at an inlet SLR of 0.4 and a particle diameter of 200 µm for plastic, sand, and glass particles is exposed in Figure 4.52. It is seen from Figure 4.52 that the Nusselt number increases as the gas velocity increases for the three particles. This is because of the increase in the convection heat transfer with increasing the gas velocity.

The Nusselt number is higher for glass particles due to the higher heat properties ratio and higher heat capacity-density ratio of glass particles. However, the Nusselt number is lower for sand particles at lower inlet gas velocities (15 and 18 m/s) and lower for plastic particles at higher inlet gas velocities (21 and 24 m/s). At lower inlet gas velocities, the effect of the heat capacity-density ratio is dominant due to which the Nusselt number is lower for sand particles

(sand particles have a lower heat capacity-density ratio than plastic particles). However, at higher inlet gas velocities, the effect of the heat properties ratio is dominant due to which the Nusselt number is lower for plastic particles (plastic particles have a lower heat properties ratio than sand particles).

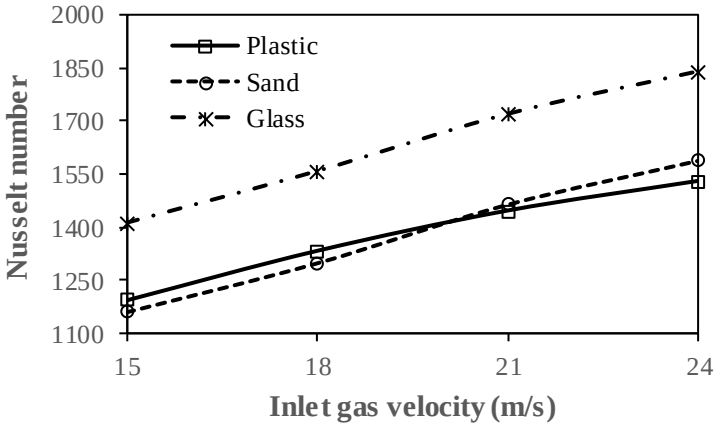

Figure 4.52: Comparison of Nusselt number among the flows using plastic, sand, and glass particles with respect to the inlet gas velocity (inlet SLR=0.4; d_s=200 µm)

4.7.5.3 Comparison of pressure drop results among the flows using plastic, sand, and glass particles

The influence of particle diameter on pressure drop at a gas velocity of 15 m/s and an inlet SLR of 0.4 for plastic, sand, and glass particles is shown in Figure 4.53. It is noticed from Figure 4.53 that the pressure drop increases as the particle diameter increases for the three particles. An increase in the particle diameter increases the slip velocity between two phases, which causes an increment in the drag force. Therefore, the pressure drop increases with increasing the particle diameter.

The pressure drop is higher for glass particles and lower for plastic particles. This is due to the higher density of glass particles and lower density of plastic particles.

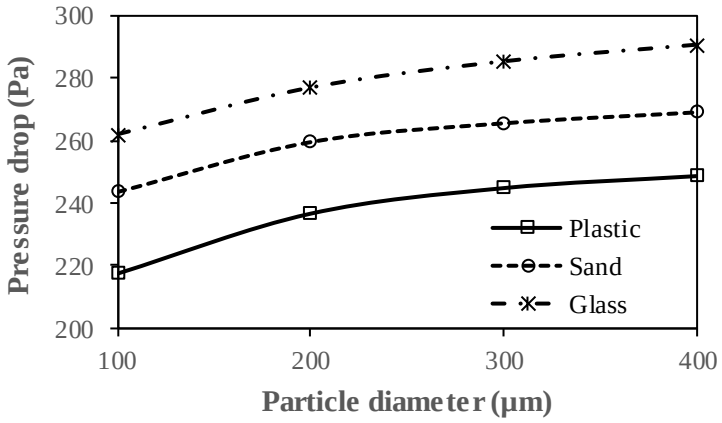

Figure 4.53: Comparison of pressure drop among the flows using plastic, sand, and glass particles with respect to the particle diameter ($\vec{v}_g$=15 m/s; inlet SLR=0.4)

The influence of inlet SLR on pressure drop at a gas velocity of 15 m/s and a particle diameter of 200 µm for plastic, sand, and glass particles is shown in Figure 4.54. It is noticed from Figure 4.54 that the pressure decreases as the inlet SLR increases for plastic particles. For sand particles, it first increases, goes to a maximum value, and after that, it decreases; however, for glass particles, it first increases, and after that, it shows insignificant effects. As the inlet SLR increases, more particles are introduced, and it increases the interparticle and particle-wall collisions. The collisions increase the pressure drop. Nevertheless, at the same time, increasing the inlet SLR modifies the effective properties of the gas (increases the effective density and decreases the effective viscosity of the gas). An increase in the effective density of the gas increases the pressure drop, and a decrease in the effective viscosity of the gas decreases the pressure drop. For plastic particles, the effect of the decreased effective viscosity of the gas is dominant, and as a result, the pressure drop continuously decreases.

The pressure drop is higher for glass particles and lower for plastic particles. This is due to the higher density of glass particles and lower density of plastic particles.

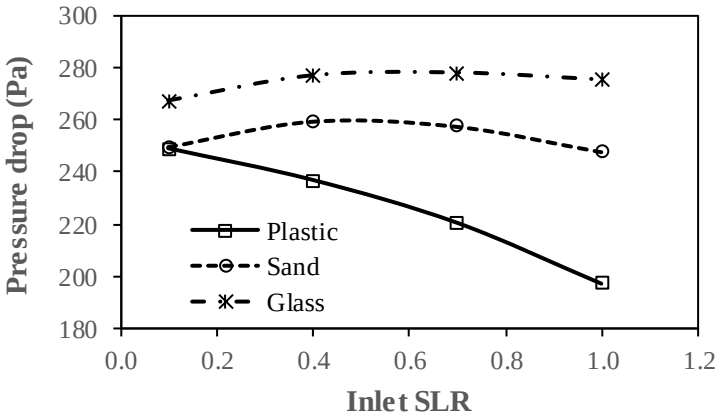

Figure 4.54: Comparison of pressure drop among the flows using plastic, sand, and glass particles with respect to the inlet SLR ($\vec{v}_g$=15 m/s; d_s=200 µm)

The influence of inlet gas velocity on pressure drop at an inlet SLR of 0.4 and a particle diameter of 200 µm for plastic, sand, and glass particles is shown in Figure 4.55. It is seen from Figure 4.55 that the pressure drop increases as the inlet gas velocity increases for the three particles. This is due to an increase in the drag force on the solid particles with increasing the gas velocity.

The pressure drop is higher for glass particles and lower for plastic particles. This is due to the higher density of glass particles and lower density of plastic particles.

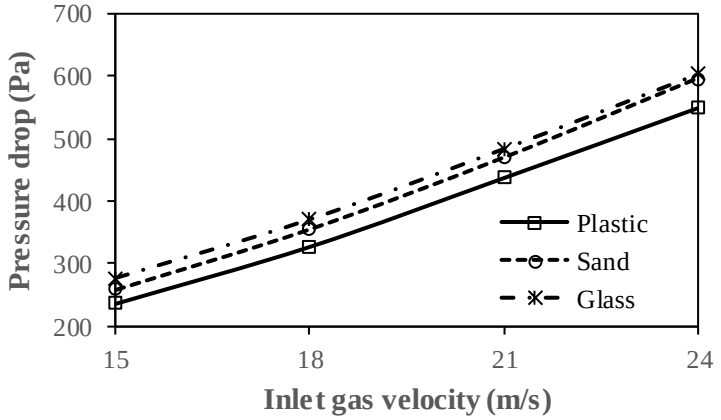

Figure 4.55: Comparison of pressure drop among the flows using plastic, sand, and glass particles with respect to the inlet gas velocity (inlet SLR=0.4; d_s=200 µm)

4.8 Closure

The heat transfer and pressure drop studies of dilute gas-solid flows through a horizontal, adiabatic pipe of internal diameter 0.058 m are studied in the present chapter. First, the pipe geometry is modeled in ANSYS 15.0 design modeler, and then, the pipe mesh is created in ANSYS 15.0 meshing tool. Moreover, the grid and time-step independence tests are conducted. The numerical model is successfully validated with the experimental results available in the literature and other theoretical data. Then, the numerical sensitivity studies are conducted, considering different drag models and different values of restitution coefficient and SC.

The effect of different flow variables such as SLR, particle diameter, and inlet gas velocity on average gas-solid Nusselt number, gas Prandtl number, and pressure drop is studied. A correlation is developed to predict the average gas-solid Nusselt number in the horizontal pipe. Further, the local heat transfer characteristics such as the temperature profiles of the gas and solid, SVF profiles, local LMTD profiles, local gas-solid Nusselt number profiles, and local thermal effectiveness profiles of the gas and solid are studied. Finally, the comparative studies of heat transfer and pressure drop are carried out, using three particles such as plastic, sand, and glass.

Chapter 5

Heat Transfer and Pressure Drop Studies of Gas-Solid Flow through a Vertical, Adiabatic Pipe

5.1 Introduction

Vertical pipes are found in numerous industrial applications such as pneumatic conveying, drying and preheating, and circulating fluidized beds in chemical, process, pharmaceutical, agricultural industries, and many others. The knowledge of heat transfer as well as the pressure drop is very important in these systems. In this chapter, the heat transfer and pressure drop studies of gas-solid flow through a vertical, adiabatic pipe are discussed. Initially, the geometry of the vertical pipe is modeled, followed by the meshing. Then, the grid and time-step independence studies are conducted, and after that, the numerical sensitivity studies are discussed. Finally, the effects of flow variables such as SLR, particle size, and gas velocity on heat transfer and pressure drop are presented.

5.2 Pipe geometry

The computational domain of the vertical, adiabatic pipe is depicted in Figure 5.1. The computational domain is created in ANSYS 15.0 design modeler. The internal diameter of the vertical pipe is 0.058 m, whereas the pipe length is 6 m. The pipe has three sections such as inlet, outlet, and wall. The wall is at an adiabatic condition. The flow takes place from the inlet to the outlet, i.e., upward concurrent flow.

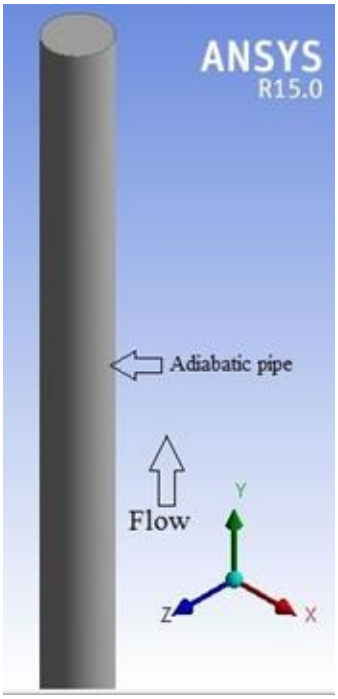

Figure 5.1: Computational domain of the vertical pipe

5.3 Pipe meshing

After creating the computational domain of the vertical pipe, the mesh of the pipe is created in ANSYS 15.0 meshing tool. The mesh of the pipe is shown in Figure 5.2. The type of mesh is tetrahedrons in nature. The final computational mesh consists of 252000 cells.

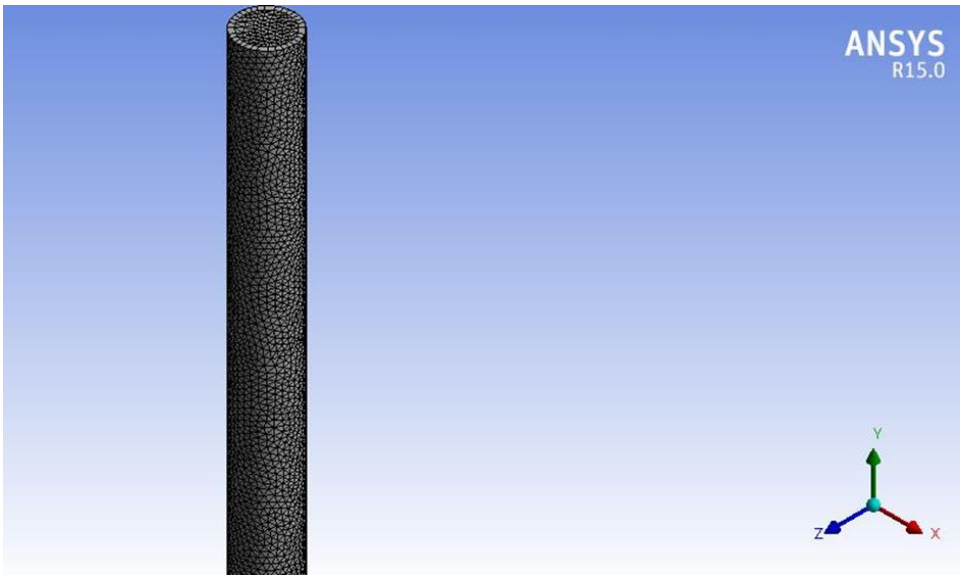

Figure 5.2: Computational mesh of the vertical pipe

5.4 Grid and time-step independence studies

Like the horizontal pipe case, the grid independence tests for the vertical pipe case are conducted, considering three grid sizes such as 114000 cells, 252000 cells, and 504000 cells, keeping all other parameters constant. This is shown in Figures 5.3–5.5. It is noticed from Figures 5.3–5.5 that, by changing the grid size from 252000 cells to 504000 cells, the results of gas temperature and particle temperature, gas velocity and particle velocity, and axial pressure are less affected. Therefore, the final grid size of 252000 cells is considered in the rest of the simulation, to save simulation time.

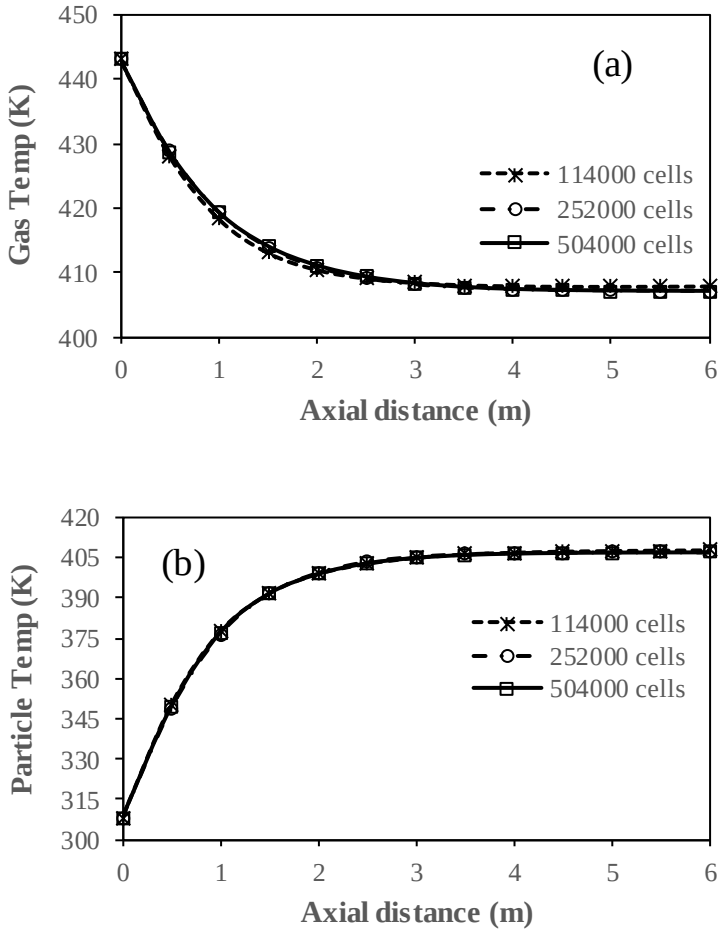

Figure 5.3: Grid independence studies for gas temperature and particle temperature

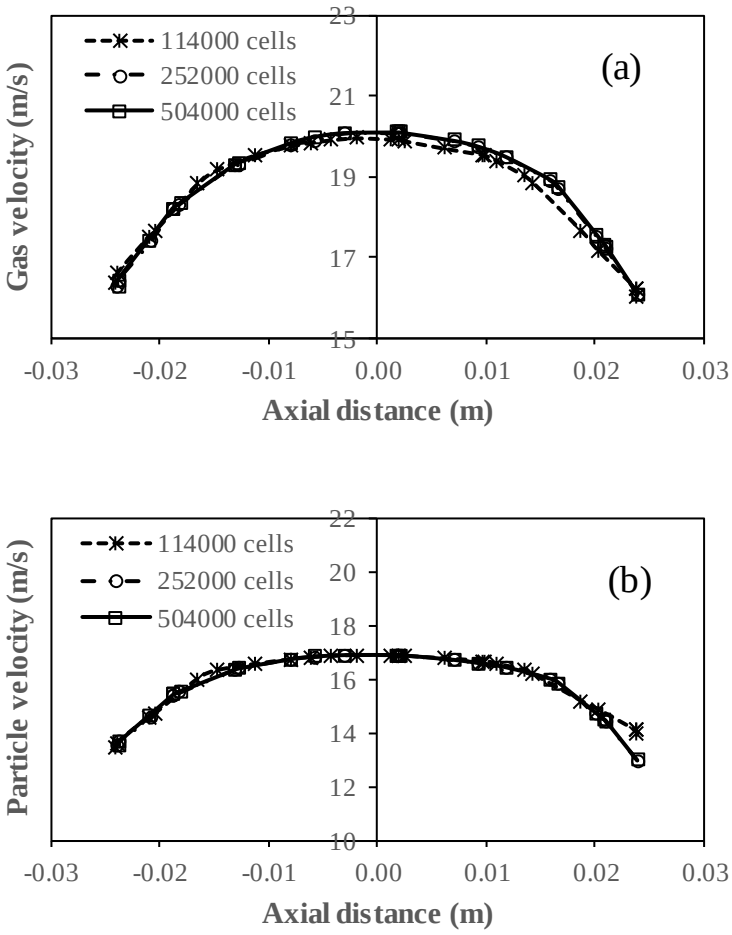

Figure 5.4: Grid independence studies for gas velocity and particle velocity

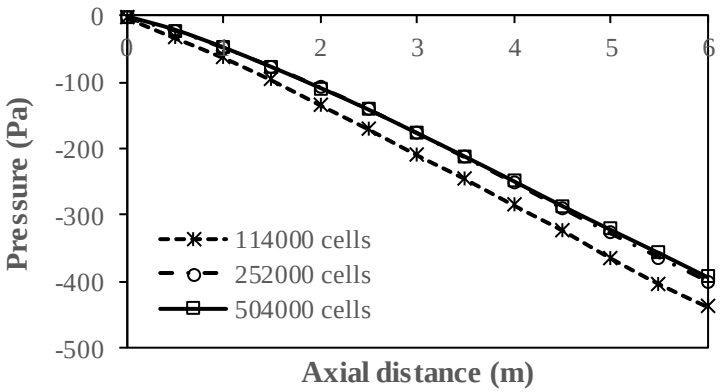

Figure 5.5: Grid independence studies for pressure

Similarly, the time-step independence tests are conducted considering three-time step sizes such as 0.01s, 0.001s, and 0.0001s, keeping all other parameters constant. This is shown in Figures 5.6–5.8. It is noticed from Figures 5.6–5.8 that, by changing the time-step size from

0.001s to 0.0001s, the results of gas temperature and particle temperature, gas velocity and particle velocity, and axial pressure are less affected. Therefore, the final time-step size of 0.001s is considered in the rest of the simulation, to save simulation time.

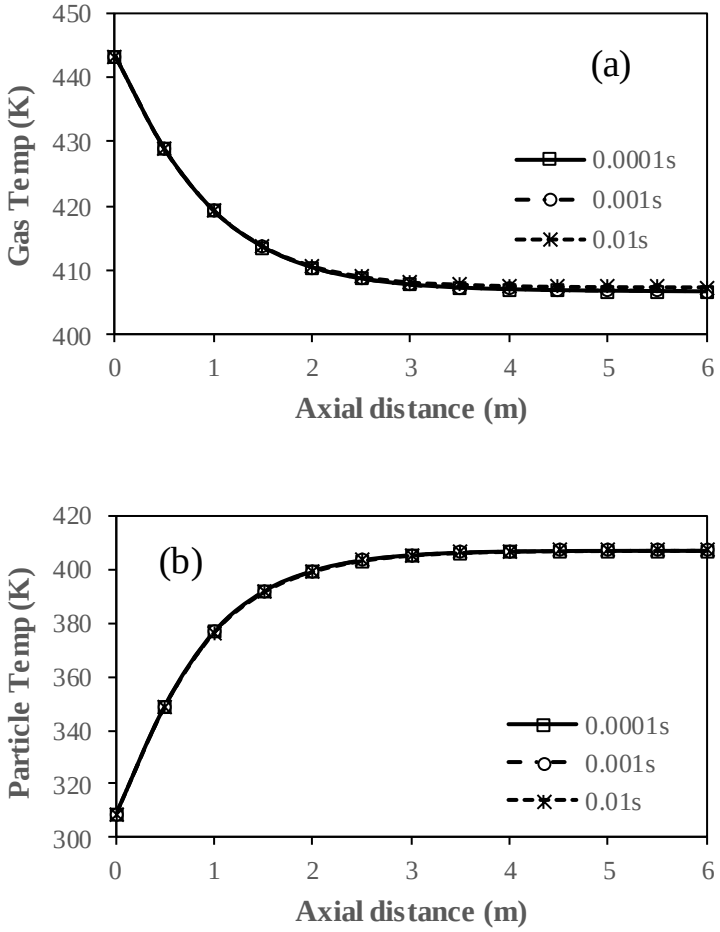

Figure 5.6: Time-step independence studies for gas temperature and particle temperature

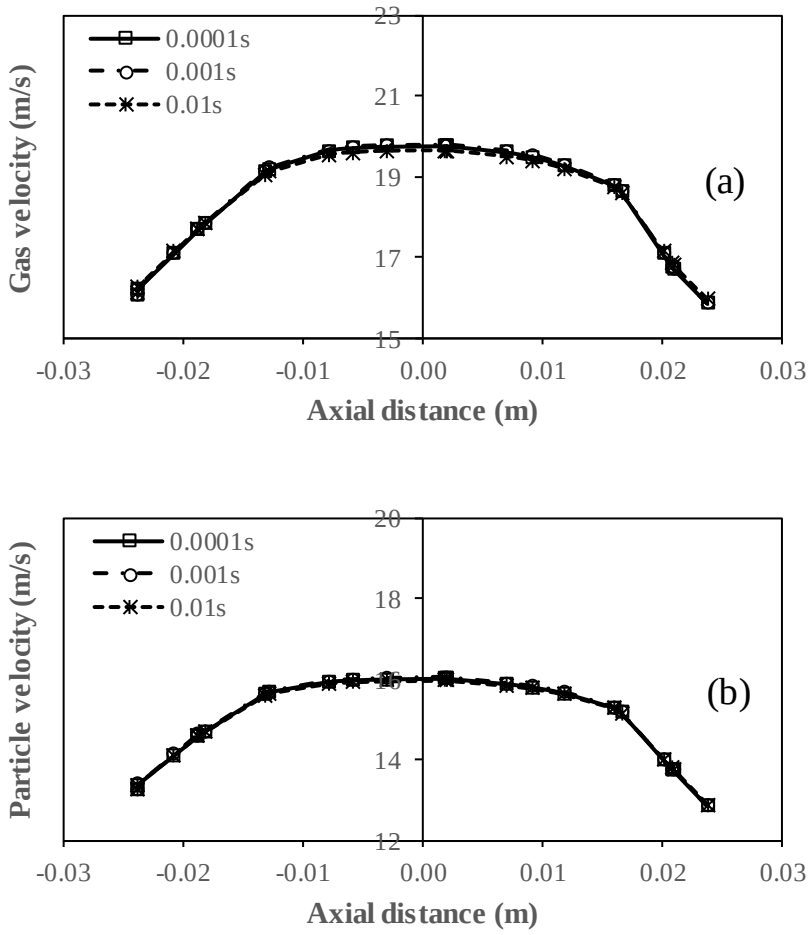

Figure 5.7: Time-step independence studies for gas velocity and particle velocity

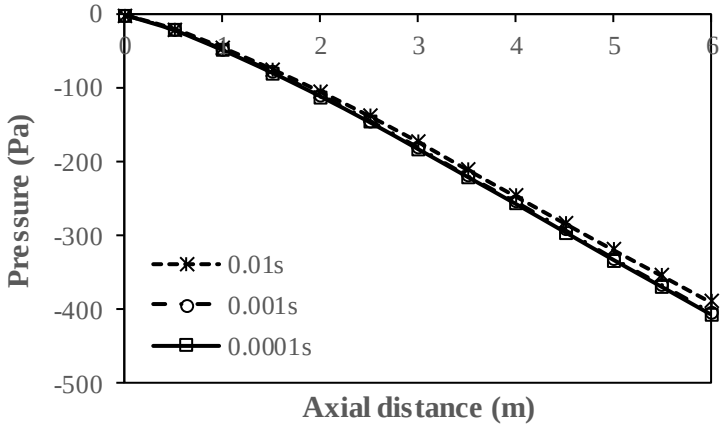

Figure 5.8: Time-step independence studies for pressure

5.5 Validation studies

First, the validation of the numerical model is carried out with respect to the experimental data of Mokhtarifar et al. [117] for heat transfer, and is shown in Figures 5.9(a) and 5.9(b). Figure 5.9(a) compares the average SLR from the simulation results with the experimental results of Mokhtarifar et al. [117]. It is observed from Figure 5.9(a) that the simulation results satisfactorily agree with the experimental results of Mokhtarifar et al. [117]. Moreover, the gas-solid Nusselt number is compared between the simulation results and experimental results of Mokhtarifar et al. [117] in Figure 5.9(b). The numerical gas-solid Nusselt number shows a maximum deviation of 6% with the experimental gas-solid Nusselt number, as noticed from Figure 5.9(b). Hence, the present model agrees satisfactorily with the experimental work of Mokhtarifar et al. [117].

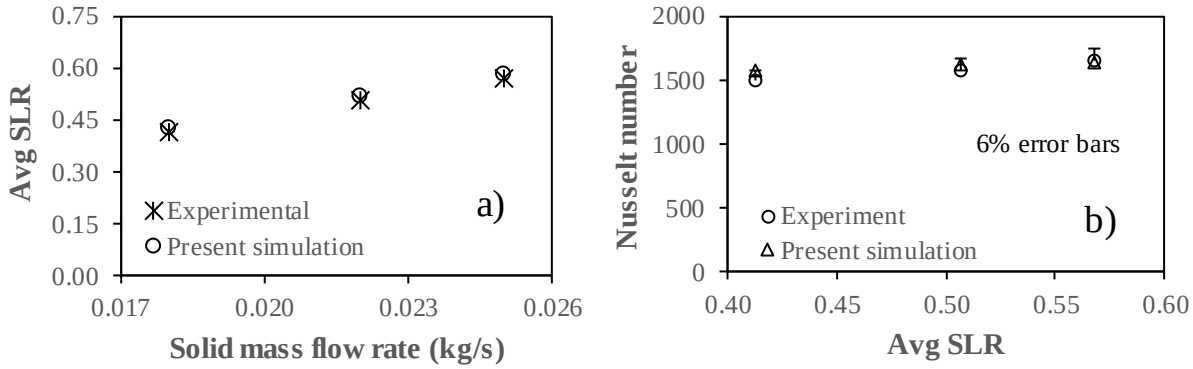

Figure 5.9: Validation studies of heat transfer using the variable gas properties model

The comparison of gas-solid Nusselt number with respect to the SLR between the variable gas properties and constant gas properties is shown in Figure 5.10. The constant gas properties are: density = 0.7967 kg/m^3, viscosity = 2.457×10^{-5} kg/ms, thermal conductivity = 0.03677 W/mK, and specific heat = 1020 j/kgK. The gas-solid Nusselt number with the constant gas properties model underpredicts by a maximum value of 3% with respect to the variable gas properties model, as noticed from Figure 5.10.

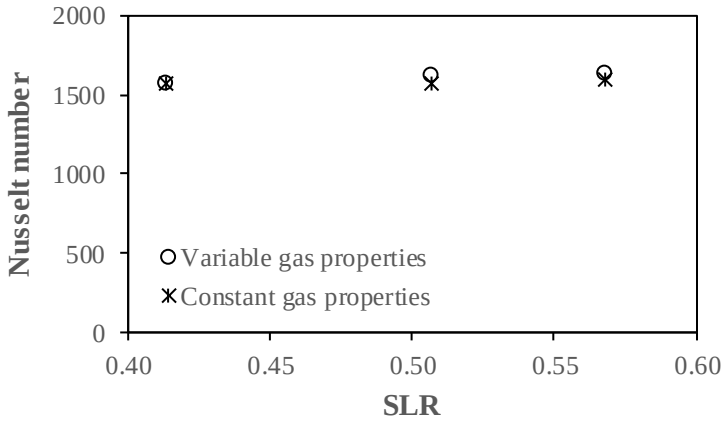

Figure 5.10: Comparison of heat transfer results between the variable gas properties model and constant gas properties model

The numerical velocity profile of the gas and particle is compared with the experimental results of Tsuji et al. [142] for an isothermal gas-solid flow, and is depicted in Figure 5.11. It is observed from Figure 5.11 that the numerical velocity profiles satisfactorily agree with the experimental velocity profiles.

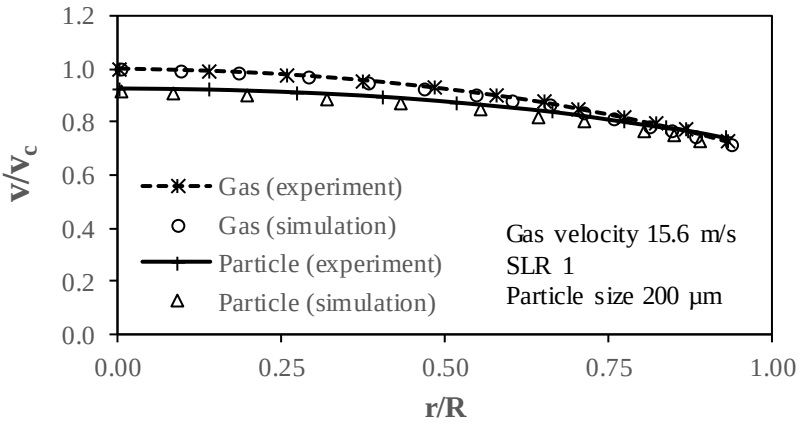

Figure 5.11: Validation of velocity profiles

Further, the pressure drop results considering the variable gas properties and constant gas properties with respect to the SLR at a gas velocity of 18.5 m/s and a particle size of 253 µm are depicted in Figure 5.12. It is noticed from Figure 5.12 that there is a major difference between the results of the variable gas properties and constant gas properties, and the significance of the variable gas properties is noticed. The pressure drop with the constant gas

properties overpredicts the pressure drop with the variable gas properties by 13% to 17%. Therefore, the variable gas properties model is used in the present work.

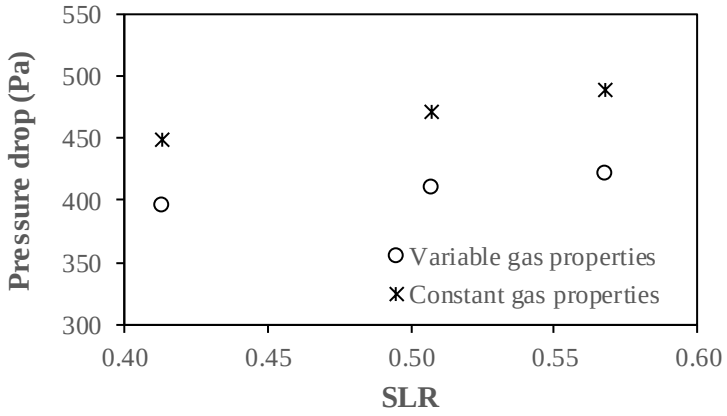

Figure 5.12: Comparison of pressure drop between the variable gas properties model and constant gas properties model

The numerical non-dimensional temperature for plastic, sand, and glass particles is compared with the theoretical values in Figure 5.13. The properties of plastic, sand, and glass particles have already been tabulated in Table 3.2 of chapter 3. The calculation of non-dimensional temperature has already been given in eq. 4.1 (chapter 4).

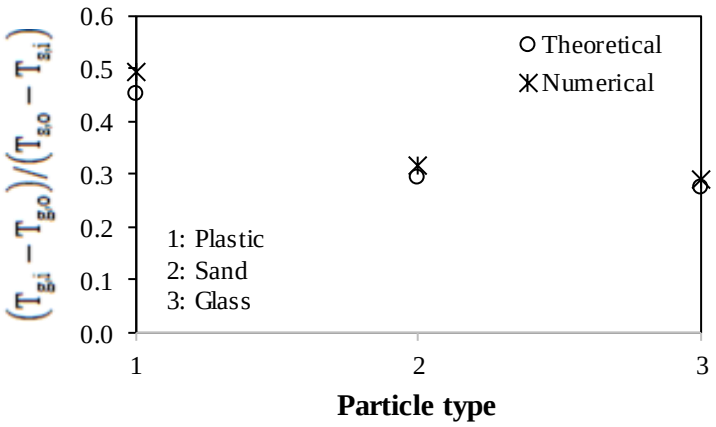

Figure 5.13: Comparison of the non-dimensional temperature between the numerical and theoretical values ($\vec{v}_g$=21 m/s; inlet SLR=0.4; d_s=200 µm)

The numerical non-dimensional temperature values well agree with the theoretical values, as noticed from Figure 5.13. Again, the above solid particles are considered for validation

because the thermo-hydrodynamic characteristics of gas-solid flows using the aforementioned solid particles are studied later.

5.6 Numerical sensitivity studies

The numerical sensitivity studies are conducted, considering different drag models (Gidaspow model [119], Wen and Yu model [130], and Syamlal model [141]) and different values of restitution coefficient (for particle-particle collisions and particle-wall collisions) and SC, and are shown in Figures 5.14–5.17.

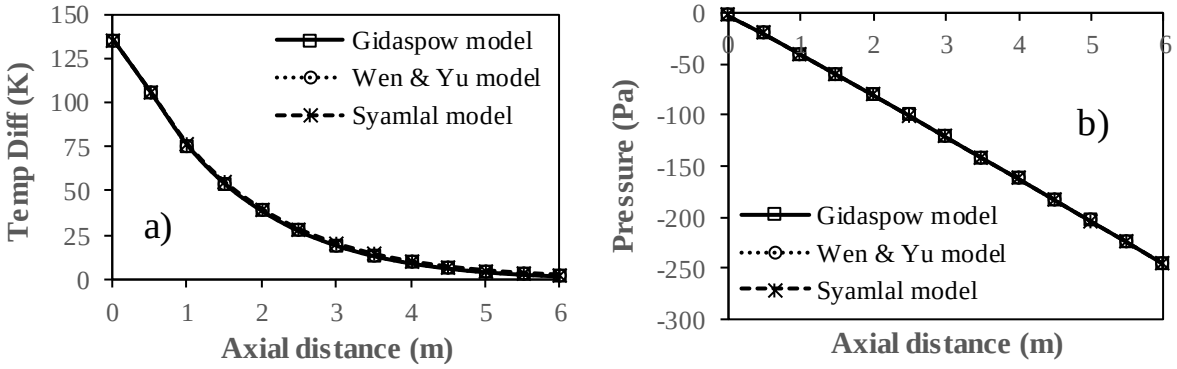

(Gas velocity = 15 m/s; inlet SLR = 0.1; particle diameter = 400 μm)

Figure 5.14: Numerical sensitivity studies using different drag models

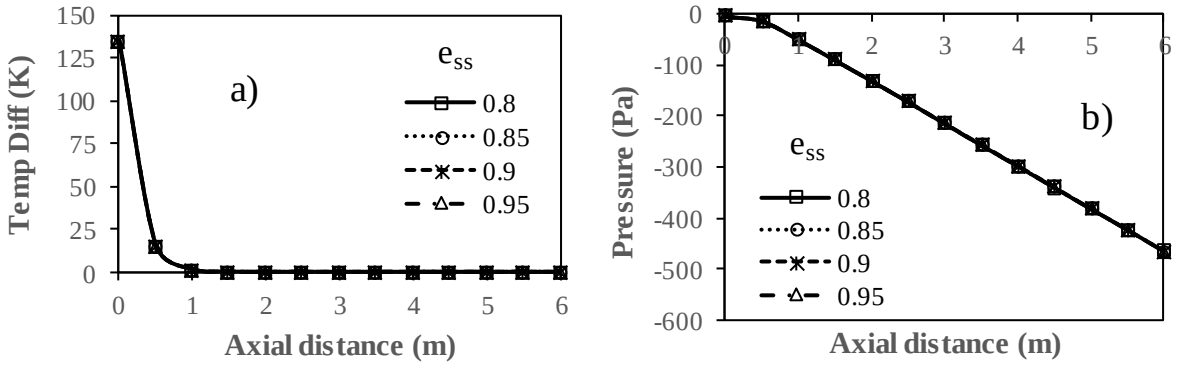

(Gas velocity = 21 m/s; inlet SLR = 0.4; particle diameter = 100 μm)

Figure 5.15: Numerical sensitivity studies using different e_{ss} values

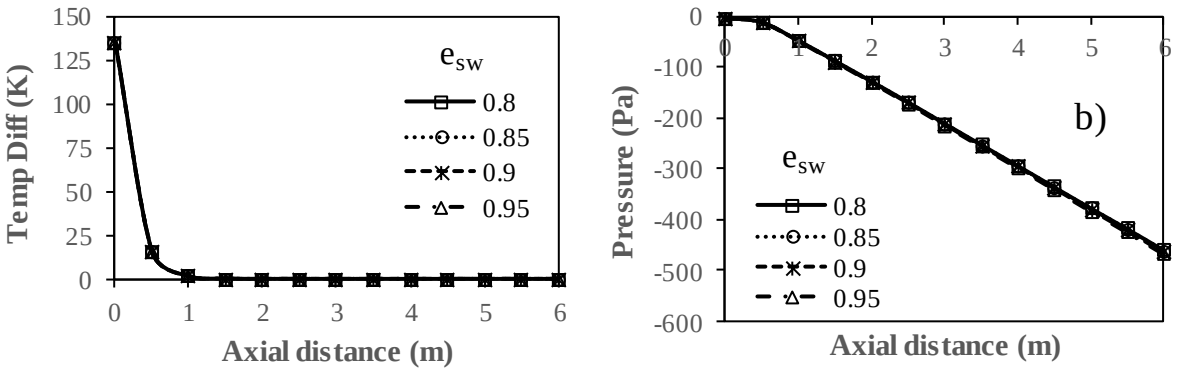

(Gas velocity = 21 m/s; inlet SLR = 0.4; particle diameter = 100 μm)

Figure 5.16: Numerical sensitivity studies using different e_{sw} values

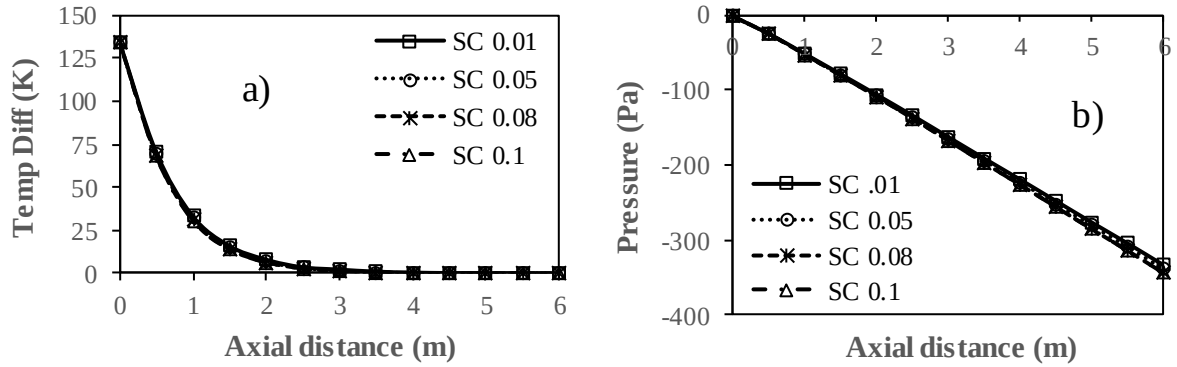

(Gas velocity = 18 m/s; inlet SLR = 0.1; particle diameter = 200 μm)

Figure 5.17: Numerical sensitivity studies using different SC values

It is observed from Figures 5.14–5.17 that the results of temperature difference (gas temperature minus solid temperature) and pressure variation are less affected by changing different drag models and the values of restitution coefficient and SC.

5.7 Results and discussions

5.7.1 Effect of flow parameters on gas-solid Nusselt number and pressure drop using sand particles

The effect of different flow parameters, i.e., particle diameter, SLR, and gas Reynolds number on gas-solid Nusselt number and overall pressure drop is studied in this subsection. The gas-

solid Nusselt number is calculated using eq. 3.48. The overall pressure drop is calculated as the inlet pressure drop minus the outlet pressure drop in the computational domain.

In vertical flows, the overall pressure drop is

$$\Delta p_{overall} = \Delta p_{gravitational} + \Delta p_{acceleration} + \Delta p_{friction} \quad (5.1)$$

In vertical flows, the gravitational pressure drop comes into play due to gravity (pipe elevation).

$$\Delta p_{gravitational} = \rho_g(1-\alpha_s)\vec{g}L + \rho_s\alpha_s\vec{g}L \quad (5.2)$$

5.7.1.1 Effect of particle diameter on gas-solid Nusselt number and pressure drop

The effect of particle diameter on gas-solid Nusselt number at different solid mass flow rates is picturized in Figure 5.18(a). It is noticed from Figure 5.18(a) that the Nusselt number continuously decreases with respect to the particle diameter. This is due to the turbulent suppression by the fine particles.

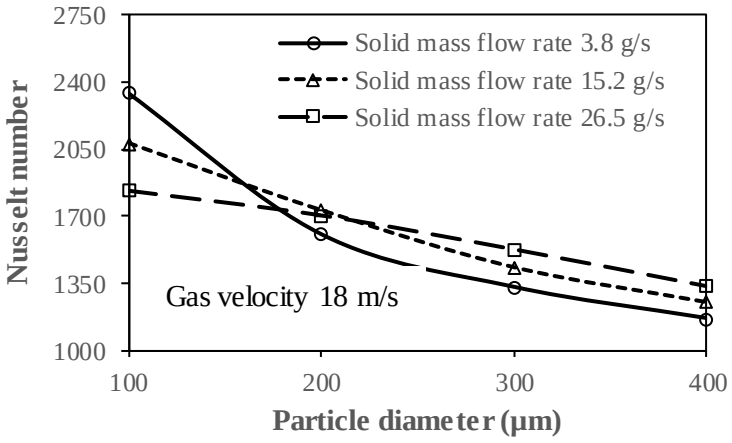

Figure 5.18(a): Effect of particle diameter on Nusselt number

The effect of particle size on gas turbulent Reynolds number at different solid mass flow rates is shown in Figure 5.18(b). It is noticed from Figure 5.18(b) that increasing the particle diameter decreases the gas Reynolds number. So, the Nusselt number decreases with an increase in the particle diameter.

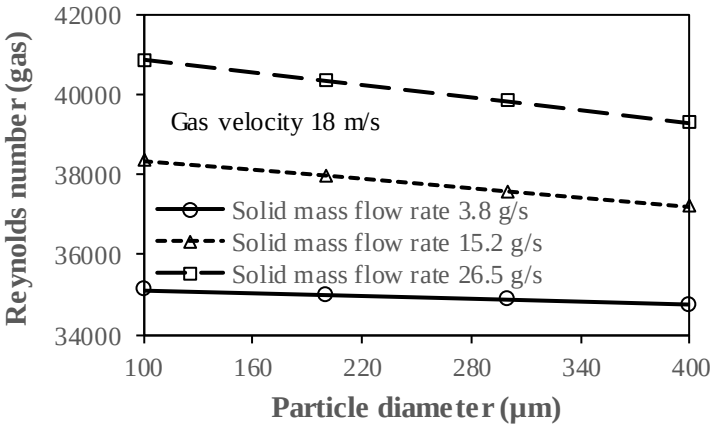

Figure 5.18(b): Effect of particle diameter on gas turbulent Reynolds number

The effect of particle size on pressure drop is picturized in Fig. 5.19, which illustrates that the pressure drop shows different behavior concerning the particle diameter increase, at different solid mass flow rates.

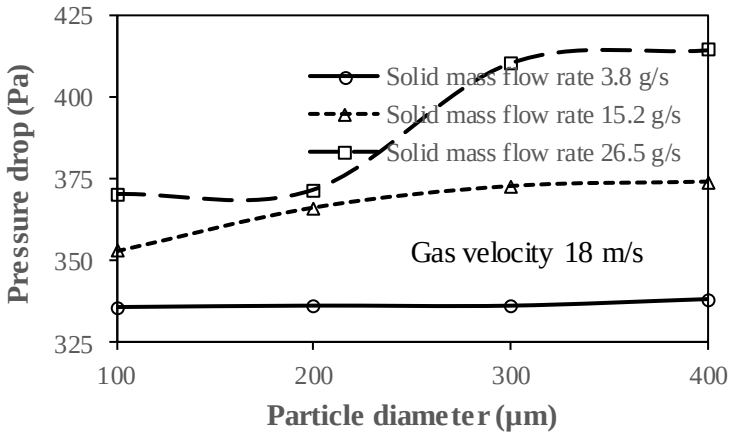

Figure 5.19: Effect of the particle diameter on the pressure drop

This different behavior is due to the change in the effective gas properties with increasing the particle diameter. An increased particle diameter increases the drag force, which increases the pressure drop. Simultaneously, it alters the effective properties of the gas. Increasing the particle diameter decreases the effective density of the gas and increases the effective viscosity of the gas. A decreased effective density of the gas lowers the pressure drop, while an increased effective viscosity of the gas results in a higher pressure drop. The dominant nature of the combined effect of the drag force and increased effective viscosity of the gas or

a decreased effective density of the gas results in a higher or a lower pressure drop. The pressure drop shows insignificant variation when both the effects are approximately equal.

5.7.1.2 Effect of SLR on gas-solid Nusselt number and pressure drop

The effect of SLR on Nusselt number is picturized in Figure 5.20. It is noticed from Figure 5.20 that the Nusselt number declines concerning the SLR increase at 100 µm particle size. Nevertheless, the Nusselt number initially increases, reaches a maximum, and afterward, it decreases with the SLR increase at 400 µm particle size. An increase in the SLR decreases both the heat capacity-density ratio and effective thermal conductivity of the gas. A decrease in the value of the effective thermal conductivity of the gas increases the heat transfer, whereas a decrease in the heat capacity-density ratio decreases the heat transfer. At a lower particle size (100 µm), the result of diminution in the heat capacity-density ratio prevails than the decreased effective thermal conductivity of the gas, which tends to decrease the Nusselt number. However, at a higher particle size (400 µm), the Nusselt number initially increases up to a specific SLR (0.64) due to the prevailing nature of the reduced effective thermal conductivity of the gas, and after that, the trend reverses. The trend reversal is due to again the dominance of the decreased heat capacity-density ratio.

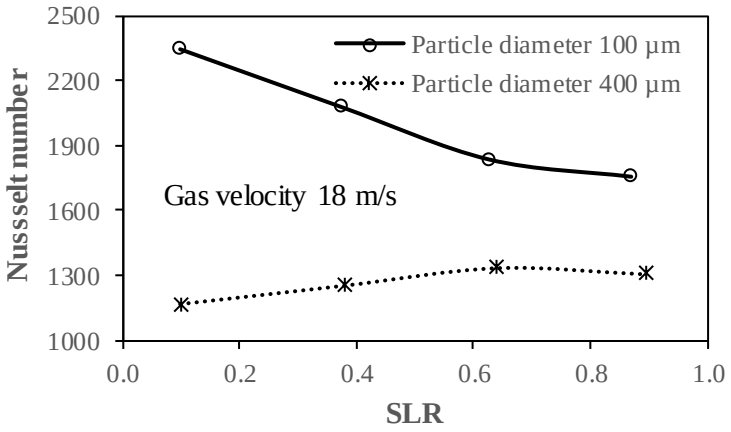

Figure 5.20: Effect of SLR on Nusselt number

The effect of SLR on pressure drop is picturized in Figure 5.21. It is noticed from Figure 5.21 that the pressure drop continuously increases with respect to the SLR increase at a particle diameter of 100 µm. However, the pressure drop initially increases, reaches a maximum, and later decreases with respect to the SLR increase at a particle diameter of 400 µm. Increasing

the SLR increases the effective density of the gas, and at the same time, it decreases the effective viscosity of the gas. An increase in the effective density of the gas increases the pressure drop, whereas a decrease in the effective viscosity of the gas decreases the pressure drop. Besides, the interparticle and particle-wall collisions increase with increasing the SLR, and the collisions increase the pressure drop. At a particle size of 100 μm, the combined effect of the increased effective density of the gas and collisional behavior is dominant than the decreased effective viscosity of the gas, as a result, the pressure drop increases. However, at a particle size of 400 μm, the pressure drop increases up to an SLR of 0.64, due to the dominance of the combined effect of the increased effective density of the gas and collisional behavior, and a further increase in the SLR reduces the pressure drop because of the prevailing nature of the decreased effective viscosity of the gas.

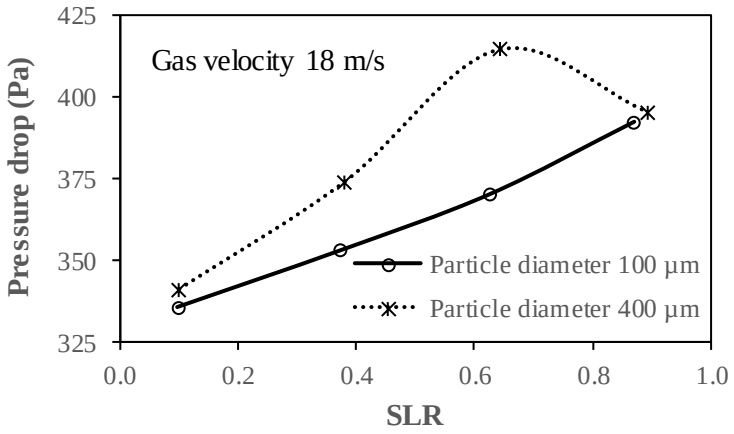

Figure 5.21: Effect of SLR on pressure drop

5.7.1.3 Effect of inlet gas velocity on gas-solid Nusselt number and pressure drop

The effect of gas Reynolds number (by changing the inlet gas velocity) on Nusselt number at different SLRs is shown in Figure 5.22. It is observed from Figure 5.22 that the Nusselt number increases when the gas Reynolds number increases. Increasing the gas velocity increases the convection heat transfer which increases the Nusselt number.

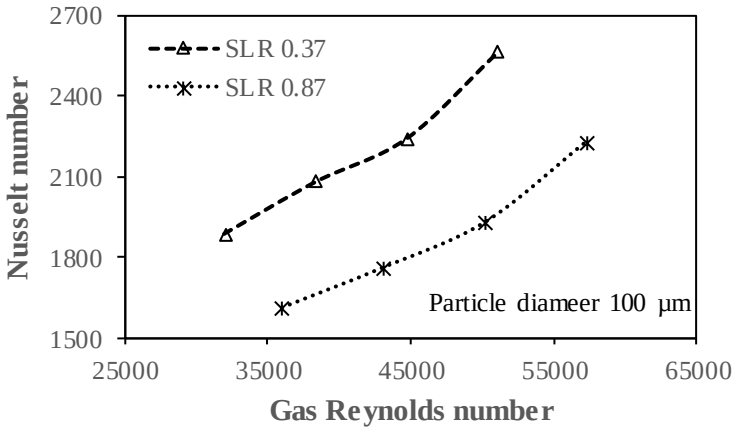

Figure 5.22: Effect of gas-phase Reynolds number on Nusselt number

The effect of gas Reynolds number (by changing the inlet gas velocity) on pressure drop at different SLRs is plotted in Figure 5.23. It is observed from Figure 5.23 that the pressure drop increases when the gas Reynolds number increases. The pressure drop increases due to an increment in the drag force, which acts on the solid particles during transportation.

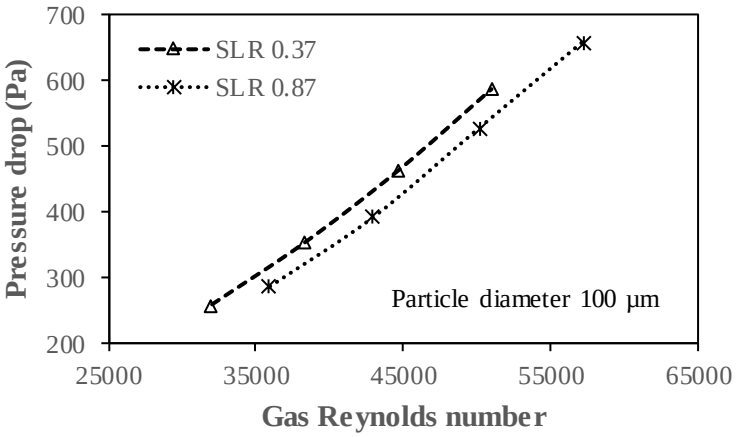

Figure 5.23: Effect of gas-phase Reynolds number on pressure drop

5.7.2 Gas Prandtl number variation

The gas Prandtl number variation with respect to the particle diameter, SLR, and gas velocity is shown in Figure 5.24(a), Figure 5.24(b), and Figure 5.24(c) respectively. It is noticed from Figures 5.24(a)–(c) that the gas phase Prandtl number variation is not affected by the flow parameters such as the particle diameter, SLR, and gas velocity, although the gas properties change with respect to the temperature. The change in the particle diameter and SLR affect

the effective properties of the gas. However, the change in the gas velocity does not affect the effective properties of the gas. Increasing the particle diameter increases the effective viscosity of the gas, increases the effective thermal conductivity of the gas, and slightly increases the effective specific heat of the gas. Increasing the SLR decreases the effective viscosity of the gas, decreases the effective thermal conductivity of the gas, and slightly decreases the effective specific heat of the gas. However, the net effect of the effective properties of the gas on gas Prandtl number is insignificant.

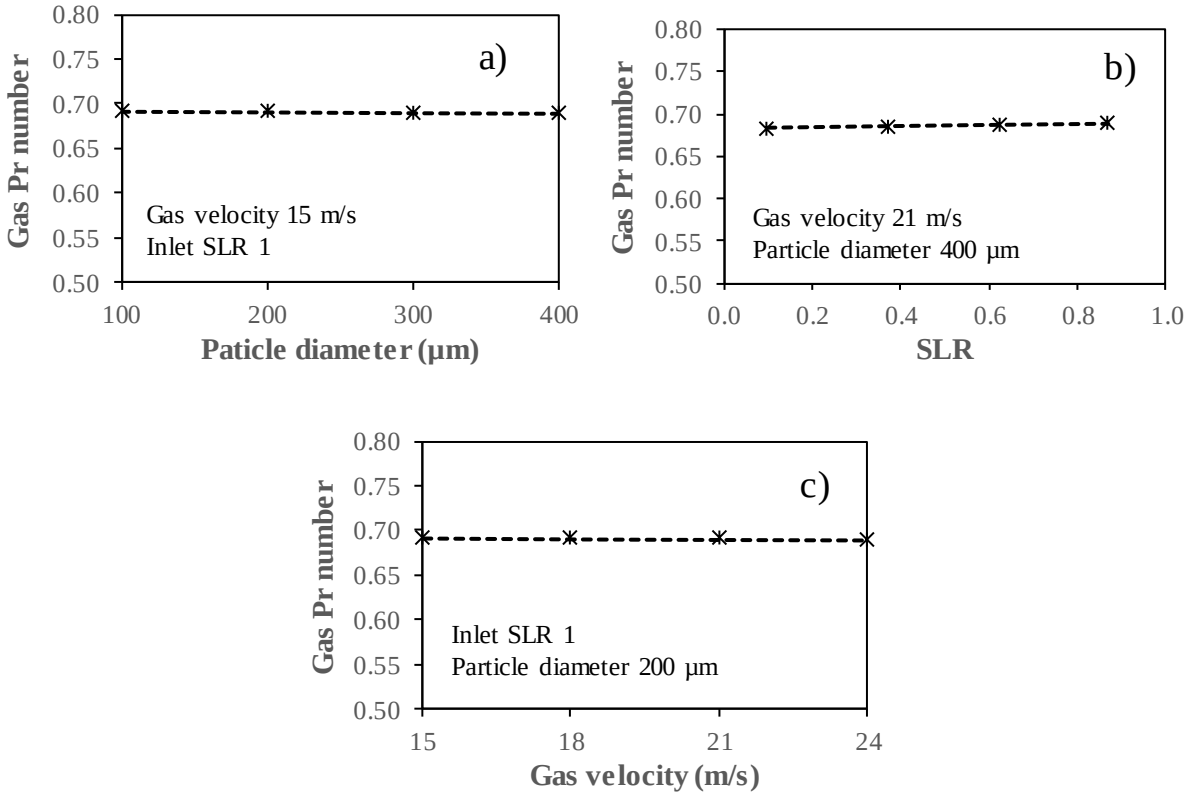

Figure 5.24: Gas Prandtl number variation

5.7.3 A correlation of gas-solid Nusselt number

A total 64 number of simulations have been conducted to find the gas-solid Nusselt number in the vertical pipe for following conditions:
$15\ \mathrm{m/s} \leq v_g \leq 24\ \mathrm{m/s}$ $(29000 \leq Re_g \leq 57300)$, $100\ \mu\mathrm{m} \leq d_s \leq 400\ \mu\mathrm{m}$, $0.1 \leq m \leq 1$.

A nonlinear regression analysis has been done to generate a correlation to calculate the gas-solid Nusselt number in the following form.

$$Nu_{avg} = b_1 \left(\frac{d_s}{D}\right)^{b_2} \times \left(Re_g\right)^{b_3} \times (m)^{b_4} \quad (5.3)$$

The optimized regression parameters are:

$b_1 = 6.427$; $b_2 = -0.337$; $b_3 = 0.336$; $b_4 = -0.036$.

The correlation presented in eq. 5.3 calculates the Nusselt number within ±15% deviations (Figure 5.25).

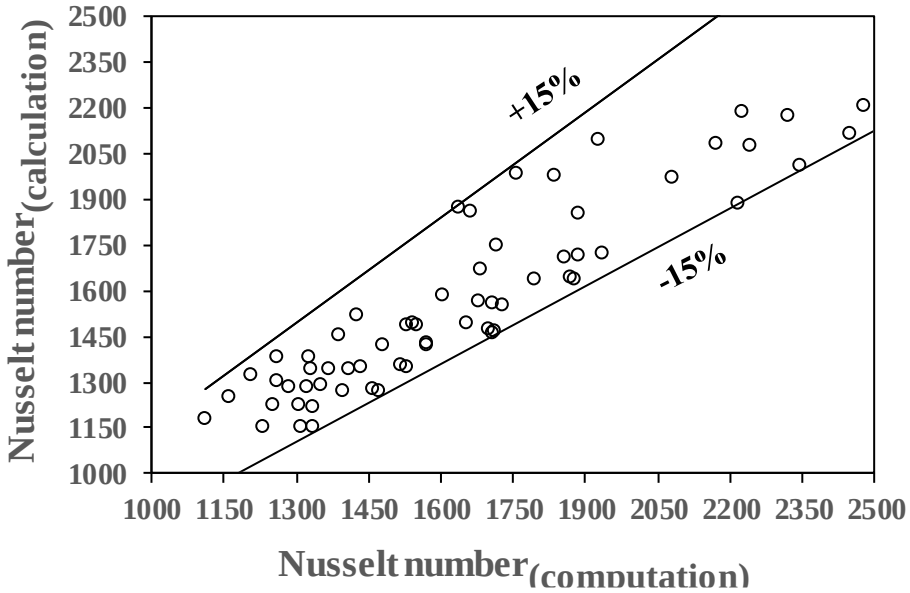

Figure 5.25: Calculated values vs computed values of Nusselt number

5.7.4 Studies of local heat transfer characteristics using sand particles

In this subsection, the local heat transfer characteristics of dilute gas-solid flows through an adiabatic, vertical pipe are studied, at a position of 100 mm from the inlet of the pipe, considering the effect of particle diameter, SLR, and inlet gas velocity.

5.7.4.1 Temperature profiles

The effect of particle size, SLR, and inlet gas velocity on gas and solid temperatures is shown in Figures 5.26–5.29. The gas and solid temperatures are taken at the location of 100 mm from the inlet (area weighted average). Figure 5.26(a) and Figure 5.26(b) show the effect of particle diameter on gas and solid temperatures at a gas velocity of 15 m/s, considering inlet

SLRs of 0.1 and 1 respectively. It is observed from Figure 5.26(a) and Figure 5.26(b) that increasing the particle diameter increases the gas temperature and decreases the solid temperature at the location (100 mm). Increasing the particle diameter decreases the heat transfer area of particles (with the same SLR), and the heat energy from the gas is absorbed by the solid particles having less surface area. Again, the particle residence time decreases with increasing the particle diameter, due to the less number of particles. The gas temperature increases due to a decrease in both heat transfer area and particle resident time. However, the solid temperature decreases due to the decreased particle resident time, despite a decrease in the heat transfer area.

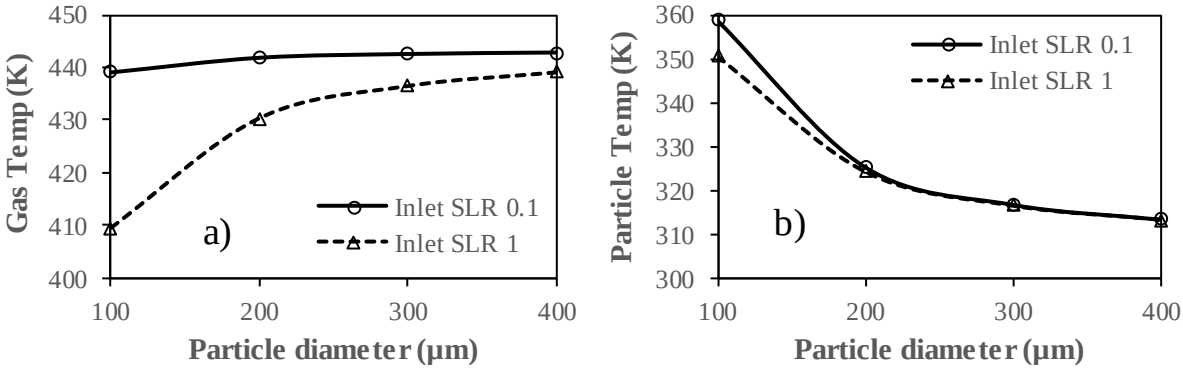

Figure 5.26: Effect of particle diameter on gas and solid temperatures at a gas velocity of 15 m/s

Figures 5.27(a) and 5.27(b) depict the effect of SLR on gas and solid temperatures at the location (100 mm) at a gas velocity of 21 m/s, for particle diameters of 100 µm and 400 µm respectively. It is noticed from Figure 5.27(a) and Figure 5.27(b) that increasing the SLR decreases the gas temperature, and decreases the solid temperature at a particle diameter of 100 µm, and slightly decreases the solid temperature at a particle diameter of 400 µm at the location (100 mm). Increasing the SLR increases the heat transfer area due to the introduction of several particles and increases the particle resident time. Due to the increased heat transfer area and particle residence time, more heat is taken from the gas, as a result, the gas temperature decreases. Because of the increased heat transfer area, the solid temperature decreases, and due to the increased particle resident time, the solid temperature increases. However, the effect of the increased heat transfer area is more than the effect of the increased particle resident time. Therefore, the solid temperature decreases at a lower particle diameter

of 100 µm. At a higher particle diameter of 400 µm, both the effects are nearly equal, and therefore, the solid temperature marginally decreases.

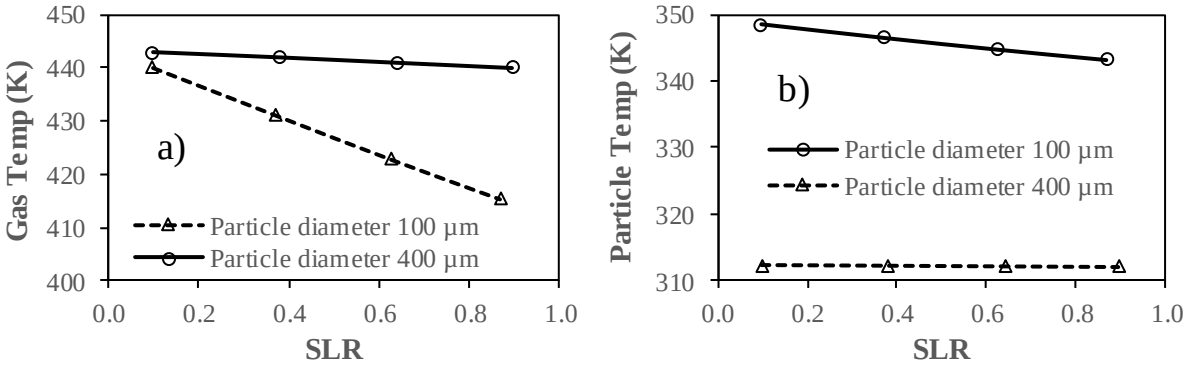

Figure 5.27: Effect of SLR on gas and solid temperatures at a gas velocity of 21 m/s

Figure 5.28 and Figure 5.29 show the effect of inlet gas velocity on gas and solid temperatures at the location (100 mm) at different particle diameters and inlet SLRs. It is noticed from Figure 5.28 and Figure 5.29 that the gas temperature increases and the solid temperature decreases with increasing the inlet gas velocity at the location (100 mm). This is due to the decreased particle resident time with increasing the inlet gas velocity.

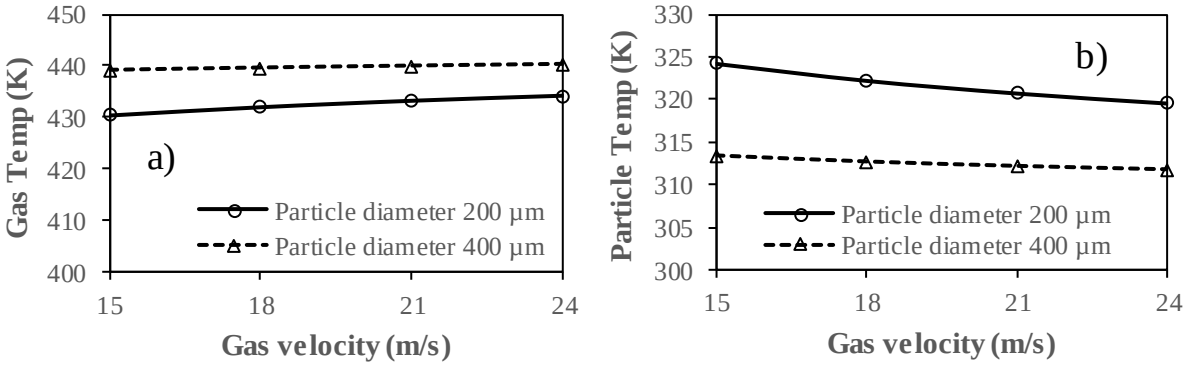

Figure 5.28: Effect of inlet gas velocity on gas and solid temperatures at an inlet SLR of 1

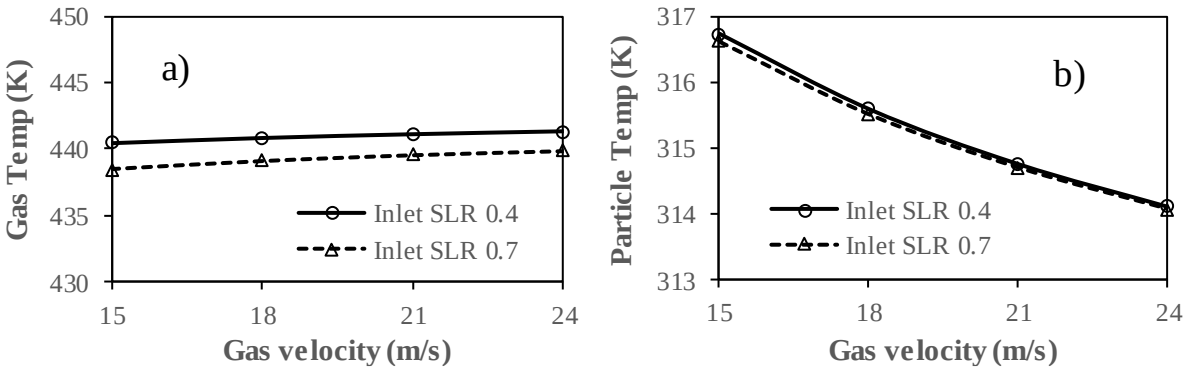

Figure 5.29: Effect of inlet gas velocity on gas and solid temperatures at a particle diameter of 300 µm

5.7.4.2 Local logarithmic mean temperature difference (LMTD) profiles

Figure 5.30 shows the effect of particle diameter on LMTD at the location 100 mm from the inlet at a gas velocity of 15 m/s, for inlet SLRs of 0.1 and 1. The local LMTD is calculated as per eq. 3.44. It is noticed from Figure 5.30 that increasing the particle diameter increases the LMTD. With increasing the particle diameter, the gas temperature at the location (100 mm) increases, and the solid temperature at the location (100 mm) decreases. Therefore, the temperature difference between the gas and solid increases at the location (100 mm), which increases the LMTD.

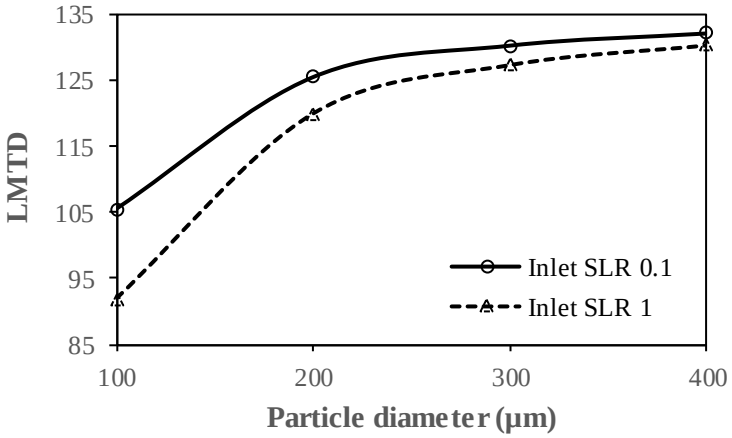

Figure 5.30: Effect of the particle diameter on the local LMTD at a gas velocity of 15 m/s

Figure 5.31 shows the effect of SLR on LMTD at the location (100 mm) at a gas velocity of 21 m/s, for particle diameters of 100 µm and 400 µm. It is noticed from Figure 5.31 that

increasing the SLR decreases the LMTD. By increasing the SLR, both the gas temperature and solid temperature decrease at the location (100 mm). However, the effect of the decreased gas temperature is more than the effect of the decreased solid temperature, which reduces the temperature difference between the gas and solid. Therefore, the LMTD decreases with increasing the SLR.

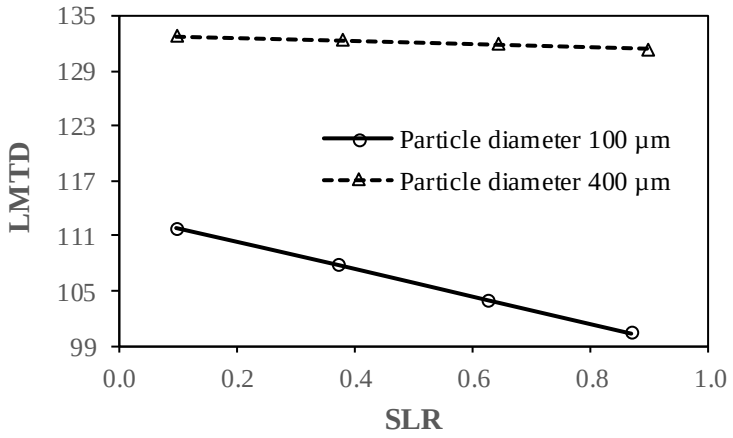

Figure 5.31: Effect of SLR on local LMTD at a gas velocity of 21 m/s

The effect of inlet gas velocity on LMTD at the location (100 mm) is shown in Figures 5.32 and 5.33. It is noticed from Figures 5.32 and 5.33 that the LMTD increases with increasing the inlet gas velocity. Increasing the inlet gas velocity increases the gas temperature and decreases the solid temperature at the location (100 mm). As a result, it increases the temperature difference between the gas and solid. Therefore, the LMTD increases with the increase of the inlet gas velocity.

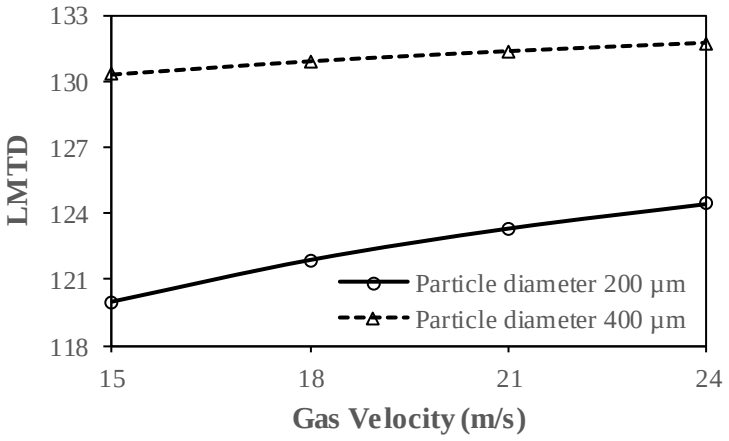

Figure 5.32: Effect of inlet gas velocity on local LMTD at an inlet SLR of 1

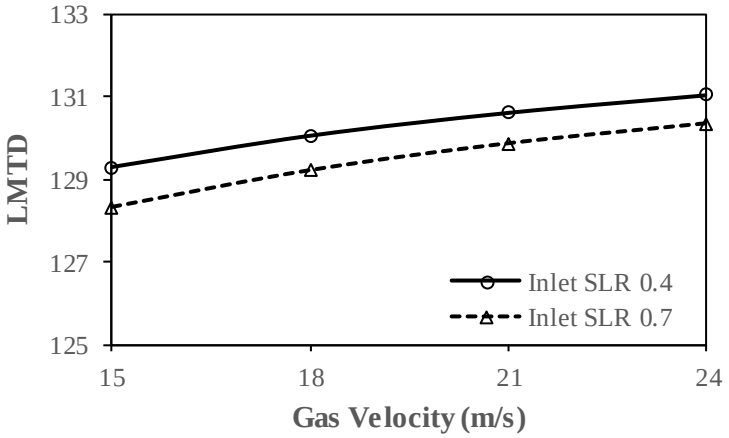

Figure 5.33: Effect of inlet gas velocity on local LMTD at a particle diameter of 300 µm

5.7.4.3 Local gas-solid Nusselt number profiles

The effect of particle diameter on local gas-solid Nusselt number at the location (100 mm) is depicted in Figure 5.34, at a gas velocity of 15 m/s, for inlet SLRs of 0.1 and 1. It is noticed from Figure 5.34 that the Nusselt number decreases with increasing the particle diameter. Increasing the particle diameter decreases the turbulent gas Reynolds number, which is also known as turbulent suppression. Therefore, the Nusselt number decreases due to the turbulent suppression.

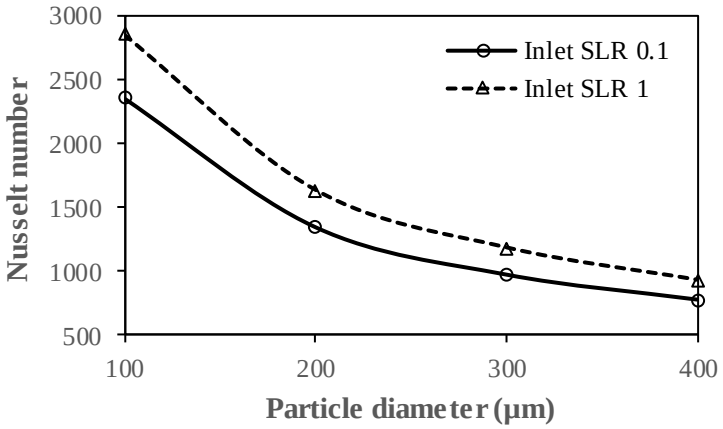

Figure 5.34: Effect of particle diameter on local gas-solid Nusselt number at a gas velocity of 15 m/s

The effect of SLR on local gas-solid Nusselt number at the location (100 mm) is shown in Figure 5.35, at a gas velocity of 21 m/s, for particle diameters of 100 µm and 400 µm. It is noticed from Figure 5.35 that the Nusselt number increases with increasing the SLR. Increasing the SLR increases the turbulent gas Reynolds number (turbulent improvement); therefore, the Nusselt number increases.

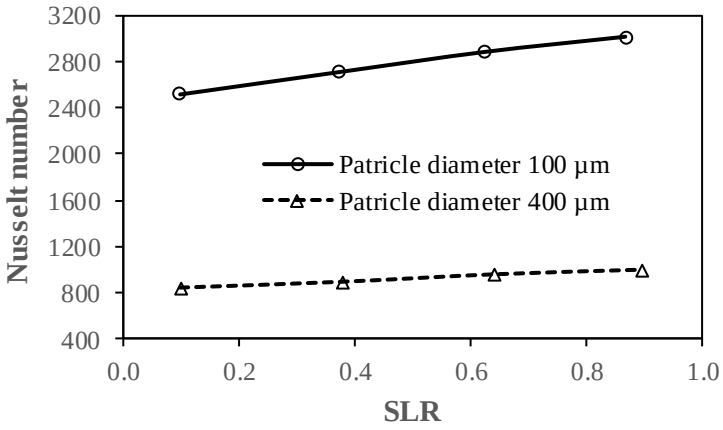

Figure 5.35: Effect of SLR on local gas-solid Nusselt number at a gas velocity of 21 m/s

The effect of inlet gas velocity on local gas-solid Nusselt number at the location (100 mm) is shown in Figures 5.36 and 5.37. It is noticed from Figures 5.36 and 5.37 that the Nusselt number increases with increasing the inlet gas velocity. This is due to the increased convection heat transfer from the gas to the particles with increasing the inlet gas velocity.

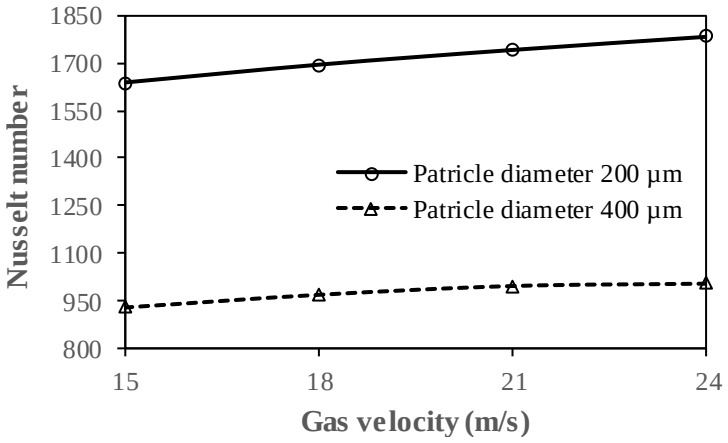

Figure 5.36: Effect of inlet gas velocity on local gas-solid Nusselt number at an inlet SLR of 1

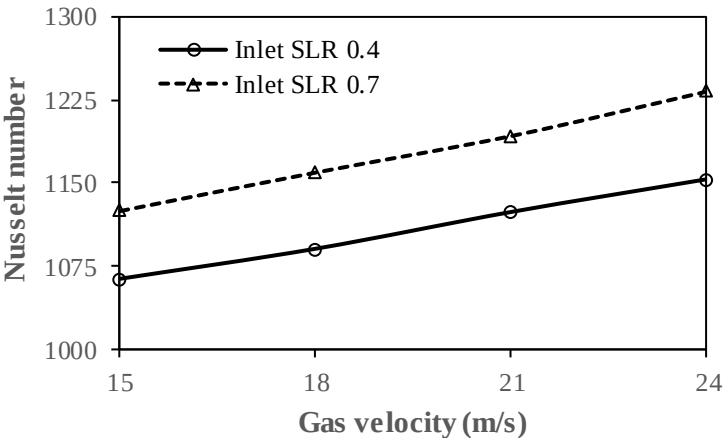

Figure 5.37: Effect of inlet gas velocity on local gas-solid Nusselt number at a particle diameter of 300 µm

5.7.4.4 Thermal effectiveness of the gas and solid

The thermal effectiveness of the gas and solid at any location is calculated using the eq. 4.9 and 4.10 respectively. The effect of particle diameter on thermal effectiveness of the gas and solid at the location (100 mm) is shown in Figure 5.38. It is observed from Figure 5.38 that the thermal effectiveness of the gas and solid decreases with increasing the particle diameter. This is due to a decrease in the mean temperature change of the phase, as the maximum possible temperature change is constant. The gas temperature increases and the solid

temperature decreases at the location (100 mm) with increasing the particle diameter. Therefore, it decreases the mean temperature change of both phases.

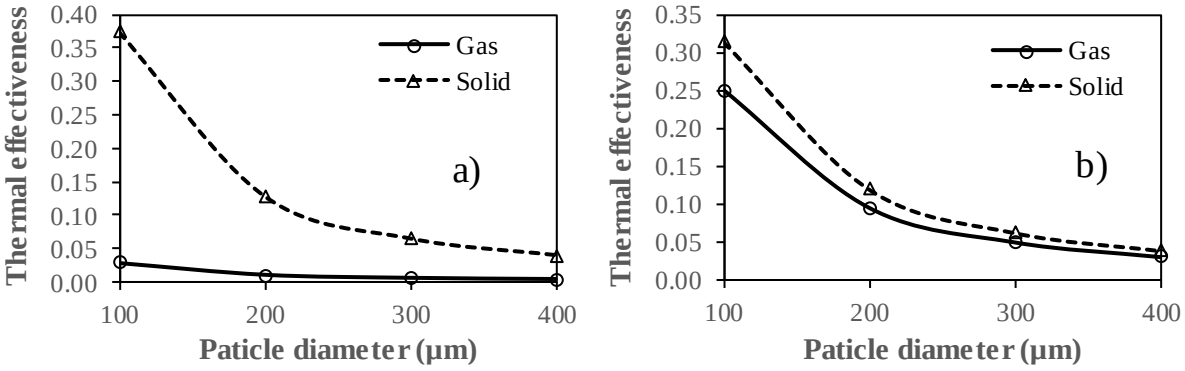

Inlet SLR 0.1 Inlet SLR 1

Figure 5.38: Effect of particle diameter on thermal effectiveness of the gas and solid at a gas velocity of 15 m/s

The effect of inlet SLR on thermal effectiveness of the gas and solid at the location (100 mm) is shown in Figure 5.39. It is seen from Figure 5.39 that, with increasing the SLR, the thermal effectiveness of the gas increases; however, the thermal effectiveness of the solid decreases at a particle diameter of 100 µm, and a slight decrease in the thermal effectiveness of the solid at a particle diameter of 400 µm. The thermal effectiveness of the gas increases at particle diameters of 100 µm and 400 µm, due to an increase in the mean temperature change of the gas. Increasing the inlet SLR decreases the gas temperature at the location (100 mm), which increases the mean temperature change of the gas. At a particle diameter of 100 µm, the thermal effectiveness of the solid decreases due to a decrease in the mean temperature change of the solid. The mean temperature change of the solid decreases due to a decrease in the solid temperature at the location (100 mm) with increasing the inlet SLR at a particle diameter of 100 µm. However, at a particle diameter of 400 µm, there is a slight decrease in the thermal effectiveness of the solid, due to a negligible variation in the mean temperature change of the solid phase. At a particle diameter of 400 µm with an increase of the inlet SLR, the mean temperature change of the solid is negligible, due to a negligible change in the solid temperature.

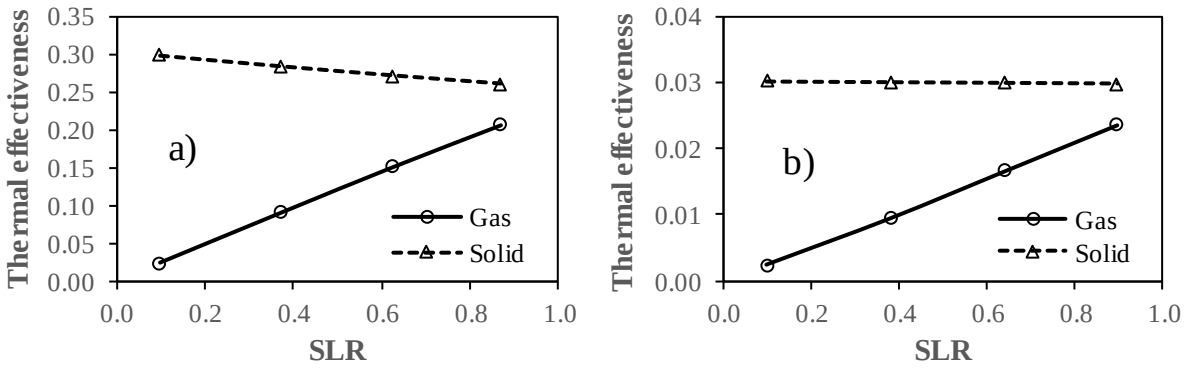

Particle diameter 100 µm Particle diameter 400 µm

Figure 5.39: Effect of SLR on thermal effectiveness of the gas and solid at a gas velocity of 21 m/s

The effect of inlet gas velocity on thermal effectiveness of the gas and solid at the location (100 mm) is depicted in Figures 5.40 and 5.41. It is observed from Figures 5.40 and 5.41 that the thermal effectiveness of the gas and solid decreases with increasing the inlet gas velocity. This is because of a decrease in the mean temperature change of the individual phase. Increasing the inlet gas velocity increases the gas temperature and decreases the solid temperature at the location (100 mm), and hence, it decreases the mean temperature change of both phases.

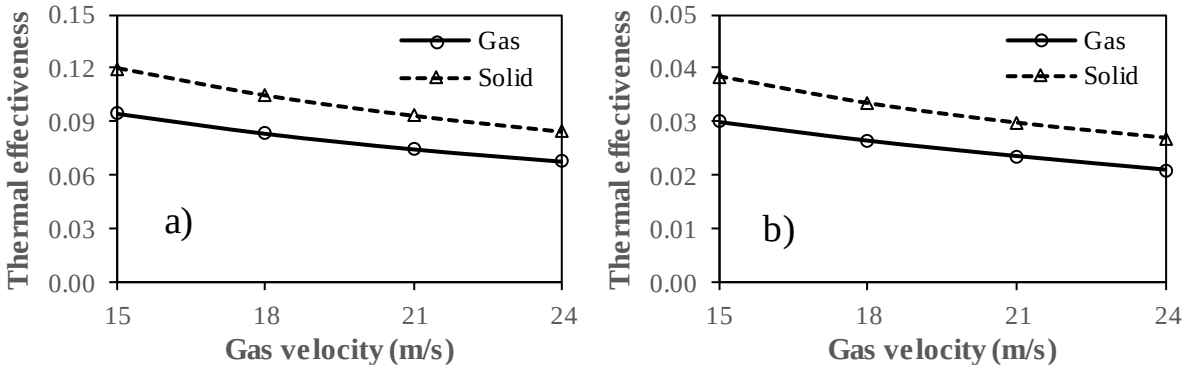

Particle diameter 200 µm Particle diameter 400 µm

Figure 5.40: Effect of inlet gas velocity on thermal effectiveness of the gas and solid at an inlet SLR of 1

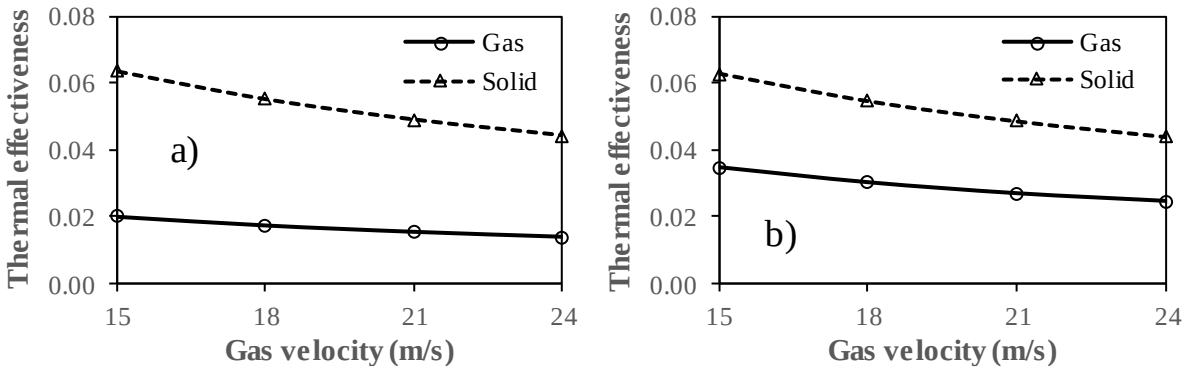

Inlet SLR 0.4 Inlet SLR 0.7

Figure 5.41: Effect of inlet gas velocity on thermal effectiveness of the gas and solid at a particle diameter of 300 µm

5.7.4.5 Contour plots of gas temperature, solid temperature, and solid volume fraction (SVF)

The contour plots of gas temperature and solid temperature at different locations at a gas velocity of 15 m/s, an inlet SLR of 1, and a particle diameter of 200 µm are shown in Figures 5.42(a) and 5.42(b) respectively. It is noticed from 5.42(a) and 5.42(b) that the gas temperature decreases and the solid temperature increases up to some distance (1 m) due to the heat transfer from the gas to the solid. Then the gas and solid temperatures remain unchanged due to the thermal equilibrium between the gas and solid.

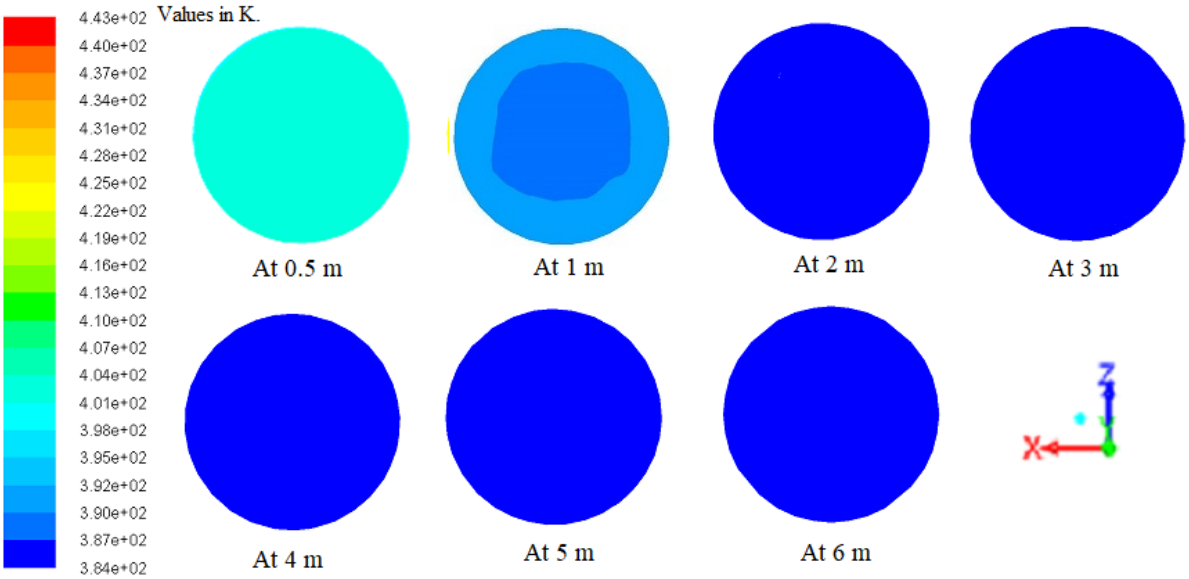

Figure 5.42(a): Contour plots of gas temperature at different locations

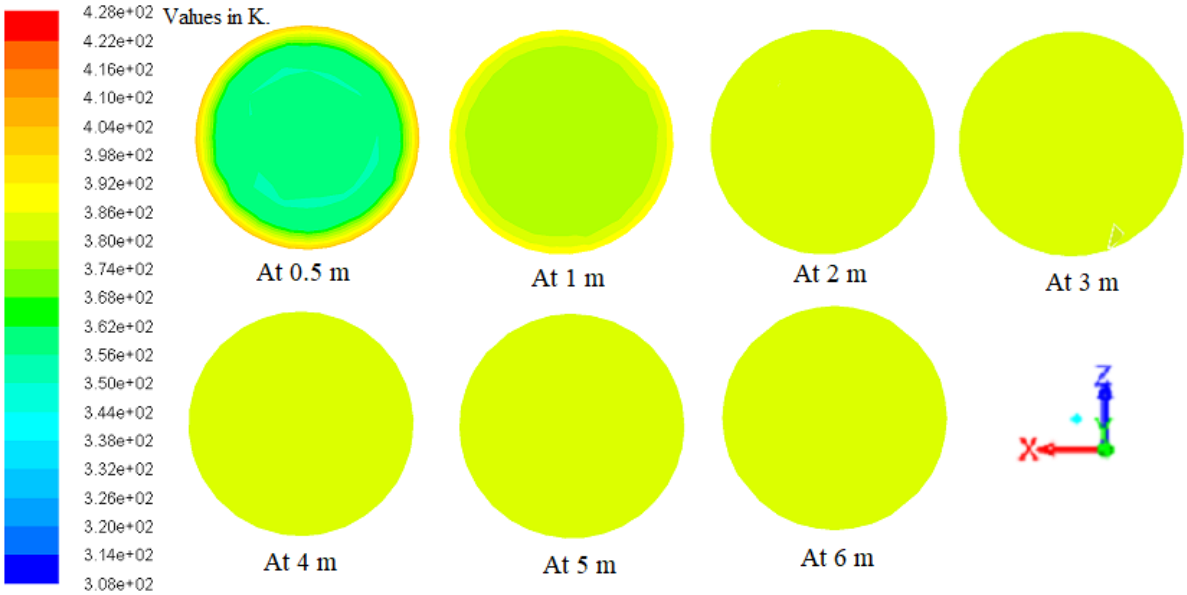

Figure 5.42(b): Contour plots of solid temperature at different locations

The contour plots of SVF at different locations at a gas velocity of 15 m/s, an inlet SLR of 1, and a particle diameter of 200 µm are shown in Figures 5.42(c). It is observed from Figure 5.42(c) that the SVFs are more at the center and least at the pipe wall. This is due to the suspension flow in the pipe by a sufficient gas velocity.

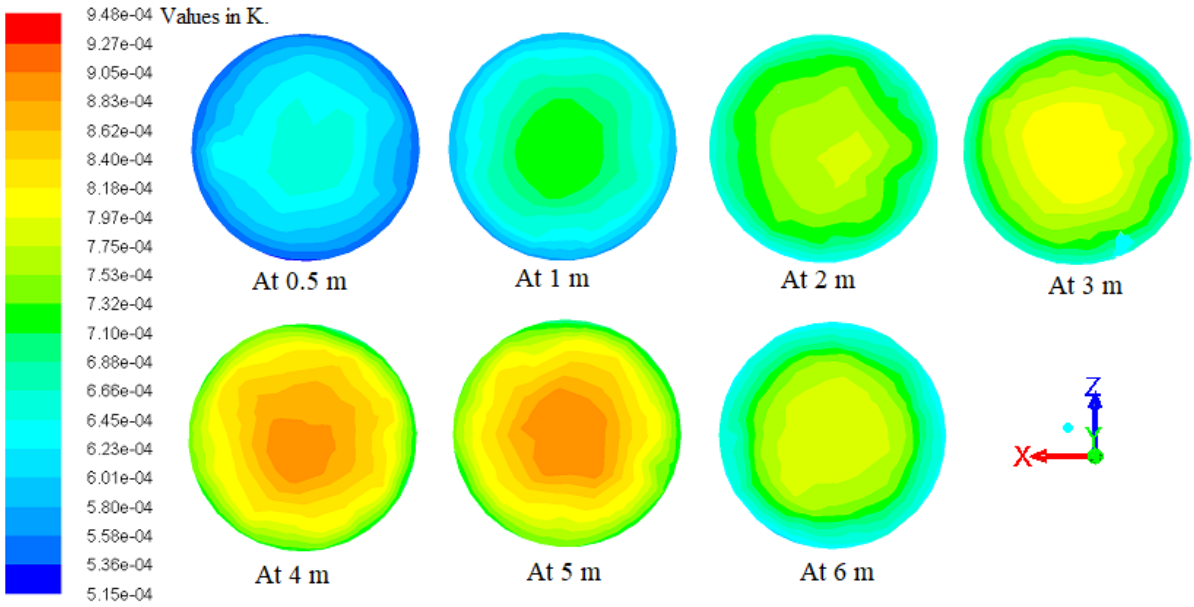

Figure 5.42(c): SVF contours at different locations along the pipe

5.7.5 Comparison of heat transfer and pressure drop results using plastic, sand, and glass particles

Plastic, sand, and glass particles are used to compare the heat transfer and pressure drop results of dilute gas-solid flows in the vertical, adiabatic pipe. The selection of these particles is due to their wide industrial applications. The properties of plastic, sand, and glass particles have already been given in Table 3.2 of chapter 3.

5.7.5.1 Comparison of temperature profiles among the flows using plastic, sand, and glass particles

The comparison of gas temperature profiles among the flows using plastic, sand, and glass particles along the axis is shown in Figure 5.43. It is noticed from Figure 5.43 that the gas temperature is higher for air-glass flow and lower for air-plastic flow along with the axial distance. Because of the higher heat properties ratio of air-glass flow and lower heat properties ratio of air-plastic flow, the gas temperature is higher for air-glass flow and lower for air-plastic flow along with the axial distance.

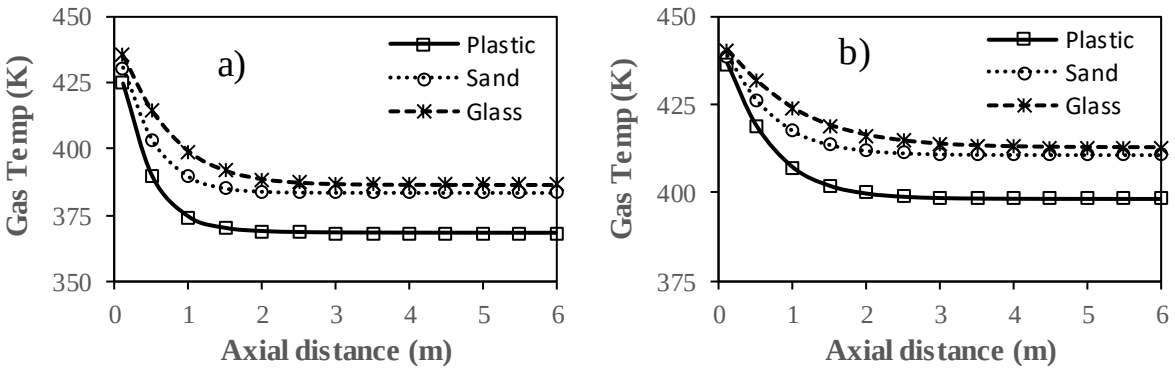

Figure 5.43: Comparison of gas temperature profiles among the flows using plastic, sand, and glass particles for, (a) $\vec{v}_g$=15 m/s, inlet SLR=1, d_s=200 µm; (b) $\vec{v}_g$=18 m/s, inlet SLR=0.4, d_s=200 µm

The comparison of particle temperature profiles among the flows using plastic, sand, and glass particles along the axis is shown in Figure 5.44. The particle temperature rises rapidly up to the initial length, and after that, it remains constant where the equilibrium temperature exists between the phases. The particle temperature is higher for air-glass flow and lower for air-plastic flow in the equilibrium temperature region. This is mainly because of the higher heat properties ratio of air-glass flow and lower heat properties ratio of air-plastic flow. However, up to a part of the initial length, the particle temperature is higher for air-sand flow and lower for air-glass flow. This depends upon the value of the heat capacity-density ratio and a lower value results in a higher temperature. This value is lower for sand particles and higher for glass particles.

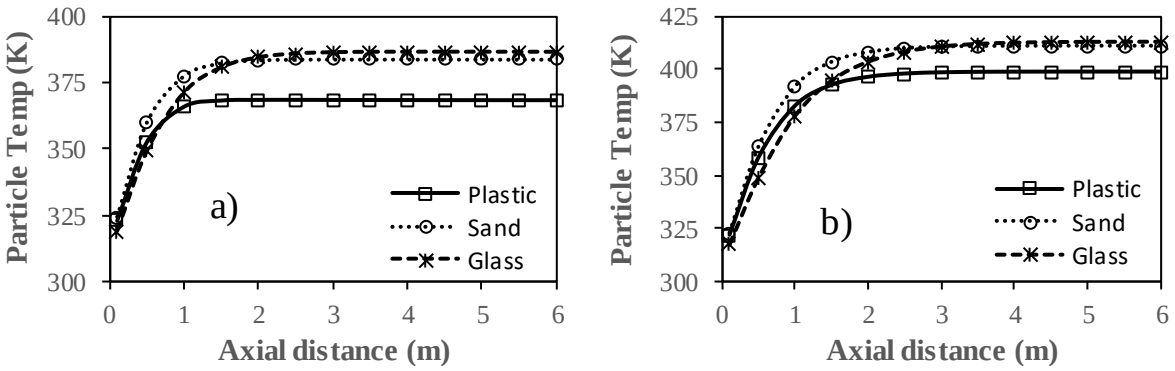

Figure 5.44: Comparison of particle temperature profiles among the flows using plastic, sand, and glass particles for, (a) $\vec{v}_g$=15 m/s, inlet SLR=1, d_s=200 µm; (b) $\vec{v}_g$=18 m/s, inlet SLR=0.4, d_s=200 µm

5.7.5.2 Comparison of heat transfer results among the flows using plastic, sand, and glass particles

The influence of particle diameter on Nusselt number at a gas velocity of 15 m/s and an inlet SLR of 0.4 for plastic, sand, and glass particles is shown in Figure 5.45. It is seen from Figure 5.45 that the Nusselt number decreases with the particle diameter increase for the three particles. The reason is the turbulence suppression by the fine particles.

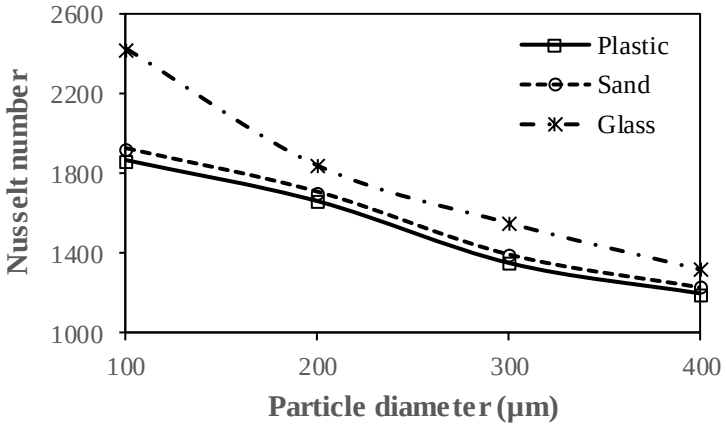

Figure 5.45: Comparison of Nusselt number among the flows using plastic, sand, and glass particles with respect to the particle diameter ($\vec{v}_g$=15 m/s; inlet SLR=0.4)

The Nusselt number is higher for glass particles and lower for plastic particles. This is due to the higher heat properties ratio of glass particles and lower heat properties ratio of plastic particles.

The influence of inlet SLR on Nusselt number at a gas velocity of 15 m/s and a particle diameter of 200 μm, for plastic, sand, and glass particles is shown in Figure 5.46. It is seen from Figure 5.46 that the Nusselt number increases for glass particles, and it first increases and then shows a negligible change for sand particles, with increasing the inlet SLR. However, for plastic particles, the Nusselt number initially increases, reaches a maximum value, and later decreases. Increasing the inlet SLR decreases the heat capacity-density ratio and effective thermal conductivity of the gas. Decreasing the heat capacity-density ratio decreases the heat transfer, whereas decreasing the effective thermal conductivity of the gas increases the heat transfer. The dominant nature of the reduction in the heat capacity-density ratio decreases the Nusselt number, and the dominant nature of the reduction in the effective thermal conductivity of the gas increases the Nusselt number. The Nusselt number shows insignificant variation in the cases where the effect of the reduction in the heat capacity-density ratio is nearly equal to the effect of the reduction in the effective thermal conductivity of the gas. Thus, the Nusselt number shows irregular behavior with the inlet SLR.

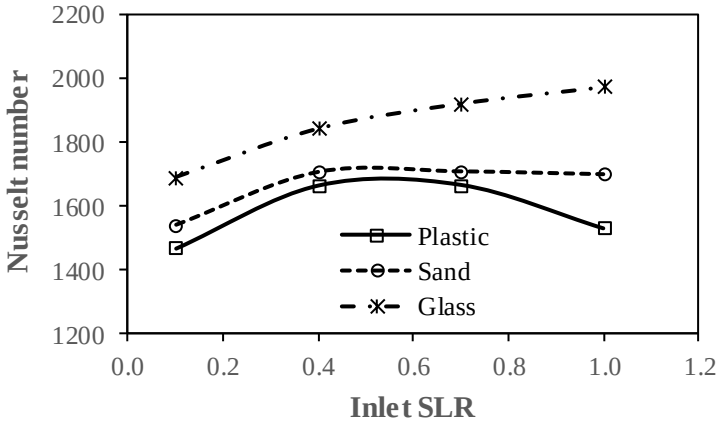

Figure 5.46: Comparison of Nusselt number among the flows using plastic, sand, and glass particles with respect to the inlet SLR ($\vec{v}_g$=15 m/s; d_s=200 μm)

The Nusselt number is higher for glass particles because of the higher heat properties ratio of glass particles. The Nusselt number is lower for plastic particles due to the lower heat properties ratio of plastic particles.

The influence of inlet gas velocity on Nusselt number for plastic, sand, and glass particles is shown in Figure 5.47. It is seen from Figure 5.47 that the Nusselt number increases as the gas velocity increases for the three particles. This is because of the increase in the convection heat transfer with increasing the gas velocity.

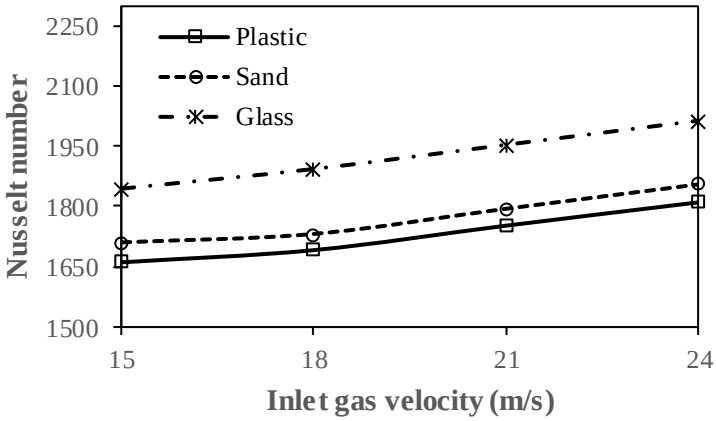

Figure 5.47: Comparison of Nusselt number among the flows using plastic, sand, and glass particles with respect to the inlet gas velocity (inlet SLR=0.4; d_s=200 µm)

Again, it is noticed from Figure 5.47 that the Nusselt number is higher for glass particles due to the higher heat properties ratio of glass particles. The Nusselt number is lower for plastic particles due to the lower heat properties ratio of plastic particles.

5.7.5.3 Comparison of pressure drop results among the flows using plastic, sand, and glass particles

The influence of particle diameter on pressure drop for plastic, sand, and glass particles is shown in Figure 5.48. It is noticed from Figure 5.48 that the pressure drop increases as the particle diameter increases for the three particles. An increase in the particle diameter increases the slip velocity between the phases which causes an increment in the drag force. An increased drag force increases the pressure drop. Therefore, the pressure drop increases with increasing the particle diameter.

The pressure drop is higher for glass particles and lower for plastic particles. This is due to the higher density of glass particles and lower density of plastic particles.

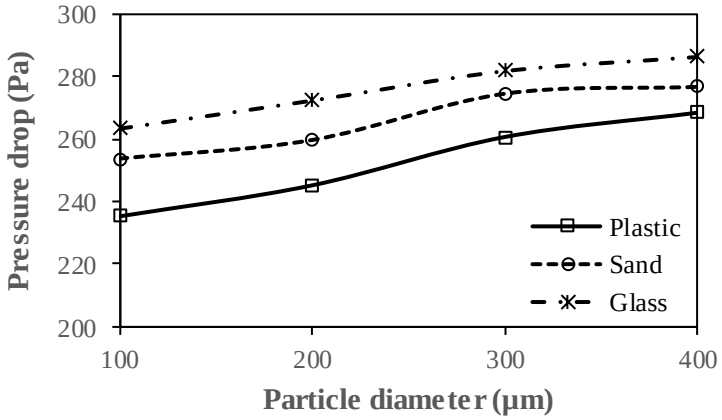

Figure 5.48: Comparison of pressure drop among the flows using plastic, sand, and glass particles with respect to the particle diameter ($\vec{v}_g$=15 m/s; inlet SLR=0.4)

The influence of inlet SLR on pressure drop for plastic, sand, and glass particles is shown in Figure 5.49, at a gas velocity of 15 m/s and a particle diameter of 200 µm. It is noticed from Figure 5.49 that the pressure increases as the inlet SLR increases for sand and glass particles. However, for plastic particles, it first increases, goes to a maximum value, and after that, it decreases. As the inlet SLR increases, more particles are introduced which increases the interparticle and particle-wall collisions. The collisions increase the pressure drop. Nevertheless, at the same time, increasing the inlet SLR modifies the effective properties of the gas (increases the effective density and decreases the effective viscosity of the gas). An increase in the effective gas density increases the pressure drop, and a decrease in the effective gas viscosity decreases the pressure drop. For sand and glass particles, the combined effect of the collisions and increased effective gas density is dominant, hence the pressure drop increases. Similarly, due to the above reason, the pressure drop increases for plastic particles at inlet SLRs of up to 0.7. However, for plastic particles at an inlet SLR of 1, the effect of the decreased effective gas viscosity is dominant, and hence, the pressure drop decreases.

The pressure drop is higher for glass particles and lower for plastic particles. This is due to the higher density of glass particles and lower density of plastic particles.

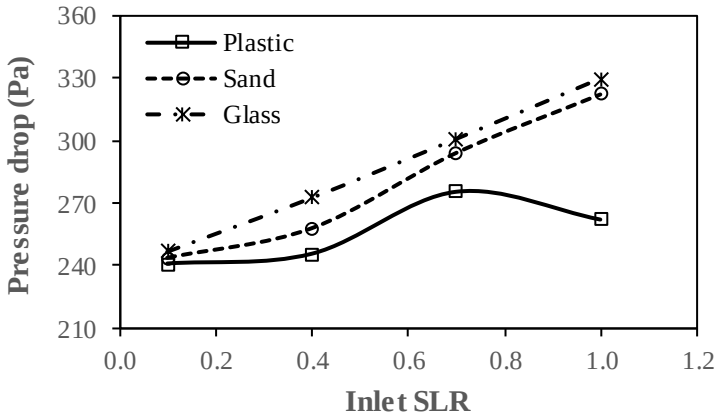

Figure 5.49: Comparison of pressure drop among the flows using plastic, sand, and glass particles with respect to the inlet SLR ($\vec{v}_g$=15 m/s; d_s=200 µm)

The influence of inlet gas velocity on pressure drop for plastic, sand, and glass particles is shown in Figure 5.50. It is seen from Figure 5.50 that the pressure drop increases as the inlet gas velocity increases for the three particles. This is due to the increase in the drag force on the solid particles with increasing the gas velocity.

The pressure drop is higher for glass particles and lower for plastic particles. This is due to the higher density of glass particles and lower density of plastic particles.

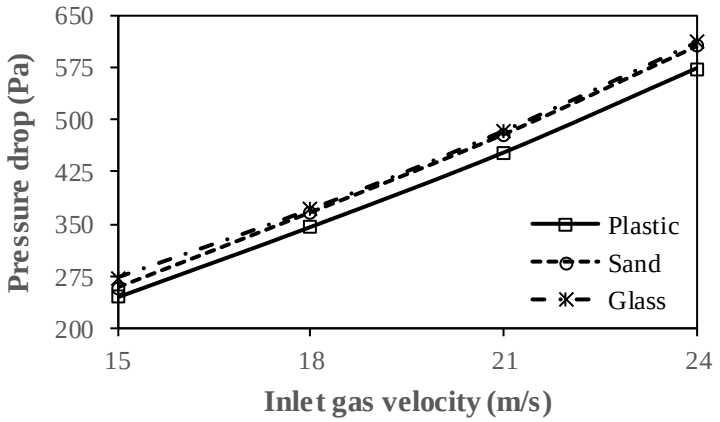

Figure 5.50: Comparison of pressure drop among the flows using plastic, sand, and glass particles with respect to the inlet gas velocity (inlet SLR=0.4; d_s=200 µm)

5.8 Closure

In the present chapter, the heat transfer and pressure drop studies of dilute gas-solid flows through a vertical, adiabatic pipe of internal diameter 0.058 m are studied. First, the pipe geometry is modeled in ANSYS 15.0 design modeler, and then, the pipe mesh is created in ANSYS 15.0 meshing tool. Moreover, the grid and time-step independence tests are conducted. The numerical model is successfully validated with the experimental results available in the literature and other theoretical data. Then, the numerical sensitivity studies are conducted, considering different drag models and different values of restitution coefficient and SC.

The effect of different flow variables such as SLR, particle diameter, and inlet gas velocity on average gas-solid Nusselt number, gas Prandtl number, and pressure drop is studied. A correlation is developed to predict the average gas-solid Nusselt number in the vertical pipe. Further, the local heat transfer characteristics such as the temperature profiles of the gas and solid, profiles of the local LMTD, local gas-solid Nusselt number, and local thermal effectiveness of the gas and solid are studied, considering the effect of SLR, particle diameter, and inlet gas velocity. Finally, the comparative studies of heat transfer and pressure drop are carried out, using three particles such as plastic, sand, and glass.

Chapter 6

Comparative Studies of Heat Transfer and Pressure Drop between the Horizontal Pipe Flow and Vertical Pipe Flow

6.1 Introduction

In this chapter, the comparative studies of heat transfer and pressure drop between the horizontal pipe flow and vertical pipe flow are discussed.

6.2 Comparative studies of heat transfer between the horizontal pipe flow and vertical pipe flow

The comparison of Nusselt number between the horizontal pipe flow and vertical pipe flow is shown in Figures 6.1–6.3. It is noticed from Figures 6.1–6.3 that the Nusselt number is higher for the vertical pipe flow than the horizontal pipe flow for plastic, sand, and glass particles. This is because of the higher overall heat transfer coefficients for the vertical pipe flow, because of more suspension flow.

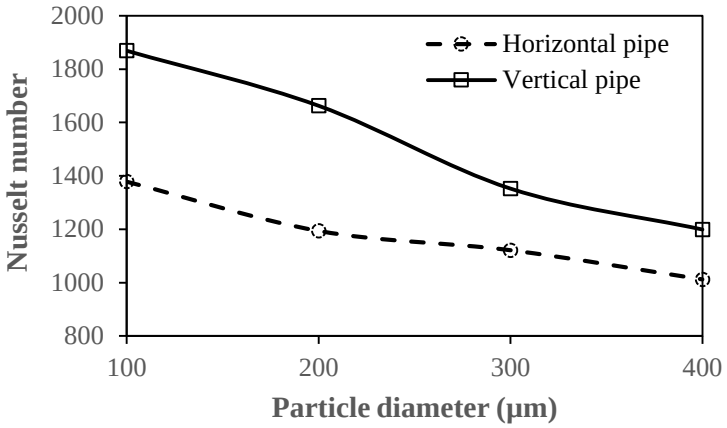

Figure 6.1: Comparison of Nusselt number between the horizontal pipe flow and vertical pipe flow using plastic particles, at a gas velocity of 15 m/s and an inlet SLR of 0.4

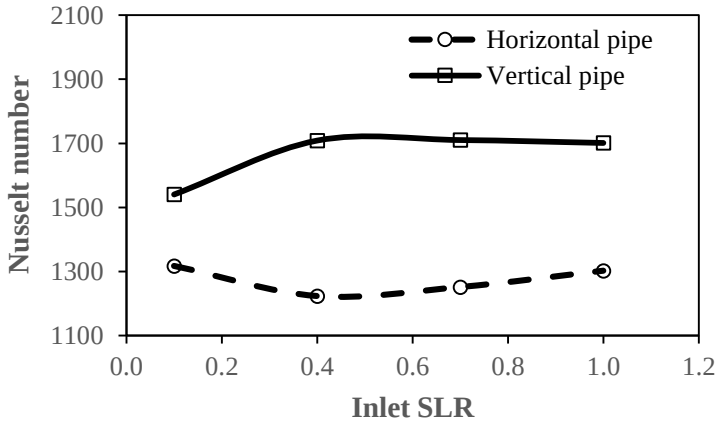

Figure 6.2: Comparison of Nusselt number between the horizontal pipe flow and vertical pipe flow using sand particles, at a gas velocity of 15 m/s and a particle diameter of 200 µm

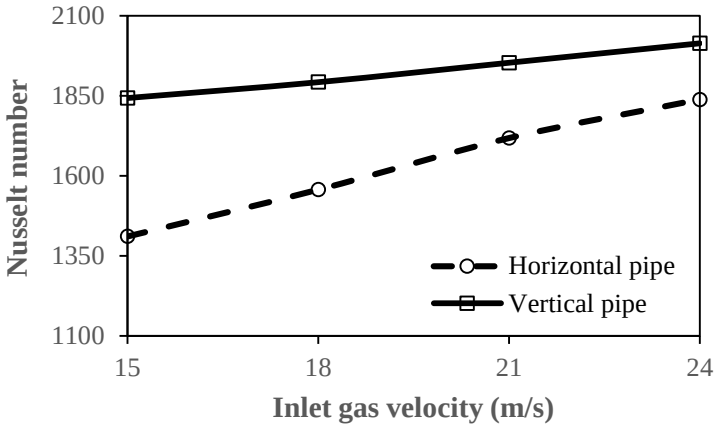

Figure 6.3: Comparison of Nusselt number between the horizontal pipe flow and vertical pipe flow using glass particles, at an inlet SLR of 0.4 and a particle diameter of 200 µm

6.3 Comparative studies of pressure drop between the horizontal pipe flow and vertical pipe flow

The comparison of pressure drop between the horizontal pipe flow and vertical pipe flow is shown in Figures 6.4–6.6. It is noticed from Figure 6.4 that the pressure drop is higher for the vertical pipe flow than the horizontal pipe flow for plastic particles. This is due to the higher gravitational pressure drop for the vertical pipe flow than the horizontal pipe flow.

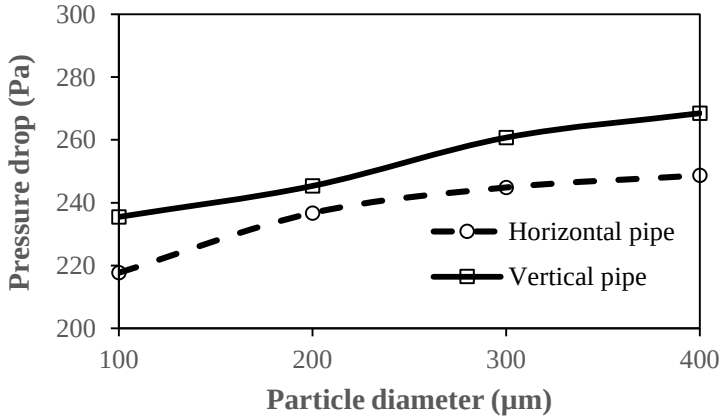

Figure 6.4: Comparison of pressure drop between the horizontal pipe flow and vertical pipe flow using plastic particles, at a gas velocity of 15 m/s and an inlet SLR of 0.4

In Figure 6.4, the difference of pressure drop between the horizontal flow and vertical is minimum at 200 µm particle size. This could be due to the application of gravity and how they collide with the particles and with the wall.

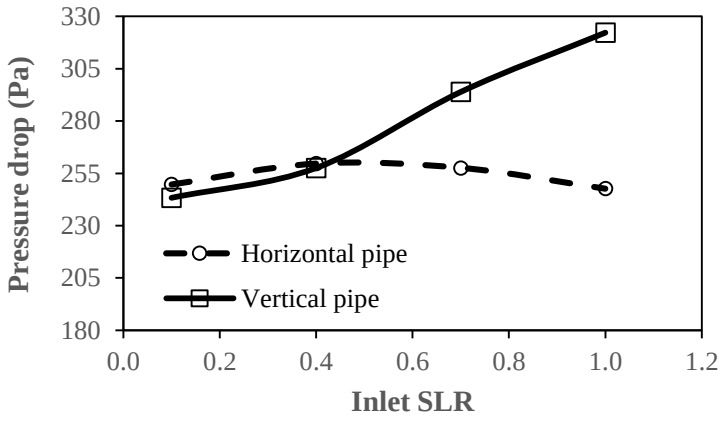

Figure 6.5: Comparison of pressure drop between the horizontal pipe flow and vertical pipe flow using sand particles, at a gas velocity of 15 m/s and a particle diameter of 200 µm

In Figure 6.5, for the horizontal pipe, the pressure drop appears to reach a maximum value and then decreases with respect to the inlet SLR. As the SLR increases, more solids are introduced which increases the intersolid and solid-wall collisions. The intersolid and solid-wall collisions increase the pressure drop. Nevertheless, at the same time, increasing the SLR increases the effective density of the gas and decreases the effective viscosity of the gas. An increased effective density of the gas increases the pressure drop and a decreased effective viscosity of the gas decreases the pressure drop. The pressure drop increases to a maximum value due to the combined effects of the increased collisions and increased effective density of the gas. After the maximum value, the pressure drop decreases due to the dominant nature of the decreased effective viscosity of the gas. For the vertical pipe, as the SLR increases, the pressure drop increases with the SLR. This is due to the gravitational force to be overcome to maintain the flow by the increased collisions.

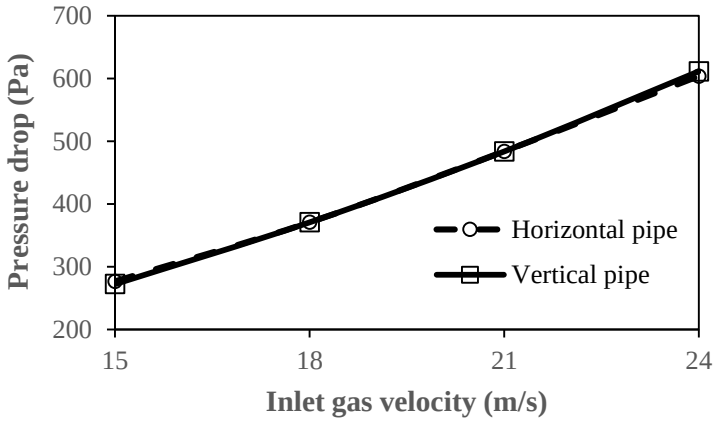

Figure 6.6: Comparison of pressure drop between the horizontal pipe flow and vertical pipe flow using glass particles, at an inlet SLR of 0.4 and a particle diameter of 200 µm

For sand particles (Figure 6.5), the pressure drop is higher for the horizontal pipe flow than the vertical pipe flow at low inlet SLRs (0.1 and 0.4); and it is higher for the vertical pipe flow than the horizontal pipe flow at high inlet SLRs (0.7 and 1). At low inlet SLRs, the frictional pressure drop in the horizontal pipe flow is dominant; however, the gravitational pressure drop in the vertical pipe flow is dominant at high inlet SLRs. The frictional pressure drop is due to fluid friction. In gas-solid flows, it consists of two components i.e. one is for the gas phase and the other is for the solid phase. The details of the frictional pressure drop are given in eq. 4.4. The gravitational pressure drop comes into play due to gravity (pipe elevation). The gravitational force needs to be overcome to maintain the flow, which leads to a pressure drop. The detail of the gravitational pressure drop is given in eq. 5.2. For glass particles (Figure 6.6), the pressure drop variation is insignificant between the horizontal pipe flow and vertical pipe flow. This is due to the insignificant net effects of frictional pressure drop and gravitational pressure drop.

6.4 Closure

The heat transfer and pressure drop results between the horizontal pipe flow and vertical pipe flow are compared. It is noticed that the Nusselt number is higher for the vertical pipe flow than the horizontal pipe flow for plastic, sand, and glass particles. However, the pressure drop is higher for the vertical pipe flow than the horizontal pipe flow for plastic particles. For sand particles, the pressure drop is higher for the horizontal pipe flow than the vertical pipe flow at

low inlet SLRs (0.1 and 0.4); and it is higher for the vertical pipe flow than the horizontal pipe flow at high inlet SLRs (0.7 and 1). For glass particles, the pressure drop variation is insignificant between the horizontal pipe flow and vertical pipe flow.

Chapter 7

Conclusions and Scope for Future Work

7.1 General

In the present chapter, the overall conclusions of the present research work are discussed. Moreover, the scope for future work is presented.

The heat transfer and pressure drop studies of gas-solid flows have been conducted in the horizontal and vertical, adiabatic pipes, using a variable gas property two-fluid model of ANSYS FLUENT 15.0. The grid and time-step independence tests are conducted before carrying out the final simulations for both horizontal and vertical pipes. The present computational model is well validated with the benchmark experimental data and other theoretical results, and is found satisfactory agreements. The numerical sensitivity studies are conducted considering different drag models, particle-particle restitution coefficients, particle-wall restitution coefficients, and SCs. Moreover, the computational results for heat transfer and pressure drop are compared with the variable and constant gas properties models.

The subsequent outcomes are obtained from the present research work, based on the studied parameters.

7.1.1 Horizontal pipe gas-solid flows

The computational results show that the variable gas properties model significantly affects both heat transfer and pressure drop when compared with the constant gas properties model. Moreover, it is noticed that the restitution coefficients (for particle-particle and particle-wall collisions) and SC do not affect much the temperature difference between the gas and particle and pressure variation results.

It is advisable to do numerical sensitivity tests considering different model parameters before conducting the final simulations.

7.1.1.1 Heat transfer and pressure drop studies using sand particles

- The Nusselt number decreases and the pressure drop increases when the particle diameter increases.
- The Nusselt number decreases with an increase in the SLR at a particle diameter of 100 µm. However, at a particle diameter of 200 µm, the Nusselt number initially decreases up to a specific SLR (0.63), and after that, it increases with an increase in the SLR.
- When the SLR increases, the pressure drop first increases, and after that, it decreases at a gas velocity of 21 m/s for particle diameters of 100 µm and 200 µm. However, at a gas velocity of 15 m/s, the pressure drop continuously decreases at a particle diameter of 100 µm and shows a negligible effect at a particle diameter of 300 µm. Here, it is observed that the effective gas properties (effective density and effective viscosity) expressively influence the pressure drop.
- The Nusselt number as well as the pressure drop increases when the inlet gas velocity increases.
- The gas Prandtl number variation is not affected by the flow parameters such as particle diameter, SLR, and gas velocity.
- A correlation, in the following form: $\mathrm{Nu_{avg}} = 1.485\left(\frac{\mathrm{d_s}}{\mathrm{D}}\right)^{-0.172} \times \left(\mathrm{Re_g}\right)^{0.548} \times (\mathrm{m})^{-0.083}$, is generated to predict the Nusselt number. This correlation can be used to calculate the Nusselt number in horizontal, adiabatic pipes based on the studied conditions.

7.1.1.2 Local heat transfer characteristic studies using sand particles

- At a lower inlet gas velocity (15 m/s) with a higher inlet SLR (1) and a higher particle diameter (400 µm), the maximum solid temperature is found near the top and bottom walls. However, at a higher inlet gas velocity (24 m/s) with a higher inlet SLR (1) and a higher particle diameter (400 µm), the maximum solid temperature is found near the bottom wall. Again, at a higher inlet gas velocity (24 m/s) with a lower inlet SLR (0.1)

and a lower particle diameter (100 μm), the solid temperature is nearly equal at all positions.

- The gas and solid temperatures are lower at the lower half of the pipe up to the thermal equilibrium length. At or after the thermal equilibrium length, the gas and solid temperatures are unchanged.
- The gas temperature increases and the solid temperature decreases with increasing the particle diameter and inlet gas velocity.
- The gas temperature and solid temperature decrease with increasing the SLR. The decrease in the solid temperature at 400 μm particle size is marginal.
- The SVFs are more towards the bottom of the pipe and least towards the top of the pipe.
- The local LMTD increases with increasing the particle diameter and gas velocity. But the local LMTD decreases with increasing the SLR.
- The local Nusselt number first increases up to a certain distance, and then, it starts decreasing. The local Nusselt number decreases with increasing the particle diameter. But the local Nusselt number increases with increasing the SLR and gas velocity.
- The thermal effectiveness of the gas and solid decreases with increasing the particle diameter and inlet gas velocity. However, the thermal effectiveness of the gas increases, and the thermal effectiveness of the solid decreases with increasing the SLR.

7.1.1.3 Comparison of heat transfer and pressure drop results using plastic, sand, and glass particles

- The gas temperature is higher for air-glass flow and lower for air-plastic flow along with the axial distance.
- A new concept which is called the heat properties ratio is defined in gas-solid flows. The heat properties ratio is defined as the ratio of the multiplication of the density, specific heat, and thermal conductivity of the solid to the gas $((\rho C_p k)_{solid} / (\rho C_p k)_{gas})$. Because of the higher heat properties ratio of air-glass flow and lower heat properties ratio of air-plastic flow, the gas temperature is higher for air-glass flow and lower for air-plastic flow along with the axial distance. The heat properties ratio is important when different solids having different properties are used.

- The particle temperature is higher for air-glass flow and lower for air-plastic flow in the equilibrium temperature region. However, up to a part of the initial length, the particle temperature is higher for air-sand flow and lower for air-glass flow.
- The Nusselt number decreases as the particle diameter increases for the three particles (plastic, sand, and glass). The Nusselt number is higher for glass particles and lower for plastic particles.
- The pressure drop increases as the particle diameter increases for the three particles. The pressure drop is higher for glass particles and lower for plastic particles.
- The Nusselt number first decreases, goes to a bottom, and after that, it increases as the inlet SLR increases for the three particles. The Nusselt number is higher for glass particles. However, the Nusselt number is lower for plastic particles at lower inlet SLRs (0.1 and 0.4) and lower for sand particles at higher inlet SLRs (0.7 and 1).
- The pressure drop decreases as the inlet SLR increases for plastic particles. For sand particles, it initially increases, goes to a maximum, and after that, it decreases. However, for glass particles, it first increases and after that, it shows insignificant effects. The pressure drop is higher for glass particles and lower for plastic particles.
- The Nusselt number increases with the inlet gas velocity increase for the three particles. The Nusselt number is higher for glass particles. However, the Nusselt number is lower for sand particles at lower inlet gas velocities (15 and 18 m/s) and lower for plastic particles at higher inlet gas velocities (21 and 24 m/s).
- The pressure drop increases with the increase of the inlet gas velocity for the three particles. The pressure drop is higher for glass particles and lower for plastic particles.

7.1.2 Vertical pipe gas-solid flows

The computational results show that there is an insignificant deviation in the results of heat transfer, but there is a significant deviation in the pressure drop data between the variable and constant gas properties models.

7.1.2.1 Heat transfer and pressure drop studies using sand particles

- The Nusselt number decreases when the particle size increases.
- The pressure drop shows different behavior with increasing the particle size at different particle flow rates.

- The Nusselt number decreases when the SLR increases at a particle size of 100 µm. Nevertheless, the Nusselt number initially increases, reaches a maximum, and later decreases with increasing the SLR at a particle size of 400 µm.
- The pressure drop increases when the SLR increases at a particle size of 100 µm. However, the pressure drop initially increases, reaches a maximum, and later decreases with increasing the SLR at a particle size of 400 µm.
- The Nusselt number as well as the pressure drop increases when the gas Reynolds number increases.
- The gas Prandtl number variation is not affected by changing the particle diameter, SLR, and gas velocity.
- A correlation, in the following form: $\mathrm{Nu_{avg}} = 6.427\left(\frac{\mathrm{d_s}}{\mathrm{D}}\right)^{-0.337} \times \left(\mathrm{Re_g}\right)^{0.336} \times (\mathrm{m})^{-0.036}$, is generated to predict the Nusselt number. This correlation can be used to calculate the Nusselt number in vertical, adiabatic pipes based on the studied conditions.

7.1.2.2 Local heat transfer characteristic studies using sand particles

- The gas temperature increases and the solid temperature decreases with increasing the particle diameter and inlet gas velocity.
- The gas temperature and solid temperature decrease with increasing the SLR. The decrease in the solid temperature at 400 µm particle size is marginal.
- The local LMTD increases with increasing the particle diameter and gas velocity. But the local LMTD decreases with increasing the SLR.
- The local Nusselt number decreases with increasing the particle diameter. But the local Nusselt number increases with increasing the SLR and gas velocity.
- The thermal effectiveness of the gas and solid decreases with increasing the particle diameter and inlet gas velocity. However, the thermal effectiveness of the gas increases, and the thermal effectiveness of the solid decreases with increasing the SLR.

7.1.2.3 Comparison of heat transfer and pressure drop results using plastic, sand, and glass particles

- The gas temperature is higher for air-glass flow and lower for air-plastic flow along with the axial distance.

- The particle temperature is higher for air-glass flow and lower for air-plastic flow in the equilibrium temperature region. However, up to a part of the initial length, the particle temperature is higher for air-sand flow and lower for air-glass flow.
- The Nusselt number decreases as the particle diameter increases for the three particles (plastic, sand, and glass). The Nusselt number is higher for glass particles and lower for plastic particles.
- The pressure drop increases as the particle diameter increases for the three particles. The pressure drop is higher for glass particles and lower for plastic particles.
- With increasing the inlet SLR, the Nusselt number increases for glass particles, it first increases and then shows insignificant variation for sand particles, and it initially increases, goes to a maximum, and later decreases for plastic particles. The Nusselt number is higher for glass particles and lower for plastic particles.
- With increasing the inlet SLR, the pressure drop increases for sand and glass particles, and it initially increases, goes to a maximum, and later decreases for plastic particles. The pressure drop is higher for glass particles and lower for plastic particles.
- The Nusselt number increases with the inlet gas velocity increase for the three particles. The Nusselt number is higher for glass particles and lower for plastic particles.
- The pressure drop increases with the increase of the inlet gas velocity for the three particles. The pressure drop is higher for glass particles and lower for plastic particles.

7.1.3 Comparison of heat transfer and pressure drop results between the horizontal pipe flow and vertical pipe flow

- The Nusselt numbers are higher for the vertical pipe flow than the horizontal pipe flow.
- The pressure drop is higher for the vertical pipe flow than the horizontal pipe flow for plastic particles. Nevertheless, for sand particles, the pressure drop is higher for the horizontal pipe flow than the vertical pipe flow at low inlet SLRs (0.1 and 0.4); and it is higher for the vertical pipe flow than the horizontal pipe flow at high inlet SLRs (0.7 and 1). For glass particles, the pressure drop variation is insignificant between the horizontal pipe flow and vertical pipe flow.

7.2 Scope for future work

The scope for future work is presented below.

- The present study may be extended to inclined pipes.
- Higher SLRs (more than one) may be used.
- Other solid materials such as iron beads, flyash, aluminum powder, and many more may be used to investigate the heat transfer and pressure drop behavior.

7.3 Closure

The overall conclusions of the present research work and the scope for future work are presented.

References

[1] M. Maeda, T. Saigusa, S. Ikai, Study on heat transfer to gas-solids suspension: Part 1, influence of free turbulence on heat transfer, Bulletin of JSME 19 (1976) 1317–1325.

[2] G.E. Klinzing, R.D. Marcus, F. Rizk, L.S. Leung, Pneumatic conveying of solids – A theoretical and practical approach (second edition), Chapman & Hall, UK, 1997.

[3] H. Cui, J.R. Grace, Pneumatic conveying of biomass particles : A review, China Particuology 4 (2006) 183–188.

[4] E. Peirano, B. Leckner, Fundamentals of turbulent gas-solid flows applied to circulating fluidized bed combustion, Progress in Energy and Combustion Science 24 (1998) 259–296.

[5] P.D.S. de Vasconcelos, A.L.A. Mesquita, Gas-solid flow applications for powder handling in industrial furnaces operations, Chapter 10, Heat Analysis and Thermodynamic Effects, Dr. Amimul Ahsan (Ed.), ISBN: 978-953-307-585-3, Intech open access Publisher, Rijeka, 2011.

[6] H.A. Stoess, Pneumatic conveying (second edition), John Wiley & Sons, New York, 1983.

[7] O.A. Williams, Pneumatic and hydraulic conveying of solids, Marcel Dekker, New York, 1983.

[8] K. Konrad, Dense-phase pneumatic conveying: A review, Powder Technology 49 (1986) 1–35.

[9] R.D., Marcus, L.S. Leung, G.E. Klinzing, F. Rizk, Pneumatic conveying of solids, Chapman & Hall, New York, 1990.

[10] S.L. Soo, Multiphase fluid dynamics, Science Press, Beijing, 1990.

[11] D.S. Azbel, N.P. Cheremisinoff, Fluid mechanics and unit operations, Ann Arbor Science Publishers, 1983.

[12] W. Wang, G. Chen, A.S. Mujumdar, Physical interpretation of solids drying: An overview on mathematical modeling research, Drying Technology 25 (2007) 659–668.

[13] W. Kaensup, S. Kulwong, S. Wongwises, A small-scale pneumatic conveying dryer of

rough rice, Drying Technology, 24 (2006) 105–113.

[14] Z.R. Gorbis, Determination of the coefficient of heat transfer from graphite powder to pipe walls, Odessa Technological Institute Report, 1957.

[15] D. Schluderberg, R. Whitelaw, R. Carlson, Gaseous suspensions- A new reactor coolant, 1961. https://www.osti.gov/biblio/4843136

[16] R. Pfeffer, S. Rossetti, S. Lieblein, Analysis and correlation of heat-transfer coefficient and friction factor data for dilute gas-solid suspensions, NASA Technical Note D-3603, Washington, DC, September 1966.

[17] B. Zhou, Y. Yang, M.A. Reuter, U.M.J. Boin, CFD-based process modelling of a rotary furnace for aluminium scrap melting, Progress in Computational Fluid Dynamics 7 (2007) 195–208.

[18] C.A. Depew, T.J. Kramer, Heat transfer to flowing gas-solid mixtures, Advances in Heat Transfer 9 (1973) 113–180.

[19] L. Farbar, M.J. Morley, Heat transfer to flowing gas-solids mixtures in a circular tube, Industrial and Engineering Chemistry 49 (1957) 1143–1150.

[20] W.J. Danziger, Heat transfer to fluidized gas-solids mixtures in vertical transport, Industrial & Engineering Chemistry Process Design and Development 2 (1963) 269–276.

[21] Z.R. Gorbis, R.A. Bakhtiozin, Investigation of convection heat transfer to a gas-graphite suspension under conditions of internal flow in vertical channels, The Soviet Journal of Atomic Energy 12 (1962) 402–409.

[22] S. Matsumoto, D.C.T. Pei, A mathematical analysis of pneumatic drying of grains—I. Constant drying rate, International Journal of Heat and Mass Transfer 27 (1984) 843–849.

[23] R.G. Boothroyd, Flowing gas-solids suspensions, Chapman and Hall, London, 1971.

[24] Stephen Hall, Pneumatic Conveying, in book: Branan's rules of thumb for chemical engineers (fifth edition), 2012, pp. 244-256.

[25] M. Sommerfeld, Analysis of collision effects for turbulent gas-particle flow in a horizontal channel: Part 1. Particle transport, International Journal of Multiphase Flow

29 (2003) 675–699.

[26] W.C. Yang, Pneumatic transport in a 10-cm pipe horizontal loop, Powder Technology 49 (1987) 207–216.

[27] R. Avila, J. Cervantes, Analysis of the heat transfer coefficient in a turbulent particle pipe flow, International Journal of Heat and Mass Transfer 38 (1995) 1923–1932.

[28] Z. Mansoori, M. Saffar-Avval, H.B. Tabrizi, G. Ahmadi, Modeling of heat transfer in turbulent gas-solid flow, International Journal of Heat and Mass Transfer 45 (2002) 1173–1184.

[29] P. Patro, Computation of wall to suspension heat transfer in vertical pipes, Drying Technology 34 (2016) 703–712.

[30] J.R. Grace, in: Circulating fluidized bed technology (P. Basu, Ed.), Pergamon Press, Toronto, 1986, pp. 63–80.

[31] P. Basu, P.K. Nag, An investigation into heat transfer in circulating fluidized beds, International Journal of Heat and Mass Transfer 30 (1987) 2399–2409.

[32] R.L. Wu, C.J. Lim, J. Chaouki, J.R. Grace, Heat transfer from a circulating fluidized bed combustor to membrane waterwall surfaces, AIChE Journal 33 (1987) 1888–1893.

[33] H.T. Bi, Y. Jin, Z.Q. Yu, D. Bai, An investigation on heat transfer in circulating fluidized beds, in: J.R. Grace, L.W. Shemilt, M.A. Bergougnou (Eds.), Fluidization VI, Engineering Foundation, New York, 1989, pp. 701–708.

[34] R.L. Wu, C.J. Lim, J.R. Grace, The measurement of instantaneous local heat transfer coefficients in a circulating fluidized bed, The Canadian Journal of Chemical Engineering 67 (1989) 301–307.

[35] P. Basu, P.K. Nag, Heat transfer to walls of a circulating fluidized-bed furnace, Chemical Engineering Science 51 (1996) 1–26.

[36] L.R. Glicksman, Heat transfer in circulating fluidized beds, in: J.R. Grace, A.A. Avidan, T.M. Knowlton (Eds.), Circulating fluidized beds, Springer, Dordrecht, 1997, pp. 261–311. https://doi.org/10.1007/978-94-009-0095-0_8

[37] Y. Ma, J.X. Zhu, Heat transfer between gas-solids suspension and immersed surface in an upflow fluidized bed (riser), Chemical Engineering Science 55 (2000) 981–989.

[38] J. Li, G.M. Campbell, A.S. Mujumdar, Discrete modeling and suggested measurement of heat transfer in gas-solids flows, Drying Technology 21 (2003) 979–994.

[39] J. Li, D.J. Mason, A.S. Mujumdar, A numerical study of heat transfer mechanisms in gas-solids flows through pipes using a coupled CFD and DEM model, Drying Technology 21 (2003) 1839–1866.

[40] J. Li, D.J. Mason, A computational investigation of transient heat transfer in pneumatic transport of granular particles, Powder Technology 112 (2000) 273–282.

[41] C. Crowe, M. Sommerfeld, Y. Tsuji, Multiphase flows with droplets and particles, CRC Press, USA, 1998.

[42] S. Sundaresan, Modeling the hydrodynamics of multiphase flow reactors: Current status and challenges, AIChE Journal 46 (2000) 1102–1105.

[43] A. Levy, I. Borde, Two-fluid model for pneumatic drying of particulate materials, Drying Technology, 19 (2001) 1773–1788.

[44] I. Skuratovsky, A. Levy, I. Borde, Two-fluid, two-dimensional model for pneumatic drying, Drying Technology 21 (2003) 1645–1668.

[45] X. Liu, J. Chen, M. Liu, D. Zhu, R. Yi, G. Liu, One-dimensional two-fluid model for pneumatic drying wet alumina particle, in: International Conference on Computing, Control and Industrial Engineering, 2010. https://doi.org/10.1109/CCIE.2010.19

[46] C.L. Tien, Heat transfer by a turbulently flowing fluid-solids mixture in a pipe, Journal of Heat Transfer 83 (1961) 183–188.

[47] R. Briller, R.L. Peskin, Gas solids suspension convective heat transfer at a Reynolds number of 130,000, Journal of Heat Transfer 90 (1968) 464–468.

[48] C.A. Depew, E.R. Cramer, Heat transfer to horizontal gas-solid suspension flows. Journal of Heat Transfer 92 (1970) 77–82.

[49] S.R. Sunderesan, N.N. Clark, Local heat transfer coefficients on the circumference of a tube in a gas fluidized bed, International Journal of Multiphase Flow 21 (1995) 1003–1024.

[50] T. Aihara, K. Yamamoto, K. Narusawa, T. Haraguchi, M. Ukaku, A. Lasek, F. Feuillebois, Experimental study on heat transfer of thermally developing and developed,

turbulent, horizontal pipe flow of dilute air-solids suspensions, Heat and Mass Transfer 33 (1997) 109–120.

[51] J. Li, D.J. Mason, Application of the discrete element modelling in air drying of particulate solids, Drying Technology 20 (2002) 255–282.

[52] Y. Zheng, J.R. Pugh, D. McGlinchey, R.O. Ansell, Simulation and experimental study of gas-to-particle heat transfer for non-invasive mass flow measurement, Measurement 41 (2008) 446–454.

[53] T. Brosh, A. Levy, Modeling of heat transfer in pneumatic conveyer using a combined DEM-CFD numerical code, Drying Technology 28 (2010) 155–164.

[54] Y. Zheng, J.R. Pugh, D. McGlinchey, E.A. Knight, Q. Liu, Numerical analysis of heat transfer mechanisms to pneumatically conveyed dense phase flow, Powder Technology 208 (2011) 231–236.

[55] P. Patro, B. Patro, S. Murugan, Prediction of two-phase heat transfer and pressure drop in dilute gas-solid flows: A numerical investigation, Drying Technology 32 (2014) 1167–1178.

[56] B. Patro, Computational thermo-hydrodynamic studies of dilute gas-solid flows in a horizontal pipe using a higher value of solid volume fraction, Journal of Enhanced Heat Transfer 23 (2016) 449–463.

[57] S.K. Senapati, S.K. Dash, Computation of pressure drop and heat transfer in gas-solid suspension with small sized particles in a horizontal pipe, Particulate Science and Technology 38 (2020) 985–998.

[58] C.A. Depew, L. Farbar, Heat transfer to pneumatically conveyed glass particles of fixed size, Journal of Heat Transfer 85 (1963) 164–171.

[59] L. Farbar, C.A. Depew, Heat transfer effects to gas-solids mixtures using solid spherical particles of uniform size, Industrial & Engineering Chemistry Fundamentals 2 (1963) 130–135.

[60] R.G. Boothroyd, H. Haque, Fully developed heat transfer to a gaseous suspension of particles flowing turbulently in ducts of different size, Journal of Mechanical Engineering Science 12 (1970) 191–200.

[61] S.E. Sadek, Heat transfer to air-solids suspensions in turbulent flow, Industrial & Engineering Chemistry Process Design and Development 11 (1972) 133–135.

[62] W.J. Danziger, S.E. Sadek, Heat transfer to air-solids suspensions in turbulent flow, Industrial & Engineering Chemistry Process Design and Development 11 (1972) 634–638.

[63] S.E. Sadek, Heat transfer to air-solids suspensions in turbulent flow. Modified equations, Industrial & Engineering Chemistry Process Design and Development 12 (1973) 397–398.

[64] W.J. Danziger, Heat transfer to air-solids suspensions in turbulent flow. Modified correlation, Industrial & Engineering Chemistry Process Design and Development 12 (1973) 396–397.

[65] S. Matsumoto, S. Ohnishi, S. Maeda, Heat transfer to vertical gas-solid suspension flows, Journal of Chemical Engineering of Japan 11 (1978) 89–95.

[66] J.M. Kim, J.D. Seader, Heat transfer to gas-solids suspensions flowing cocurrently downward in a circular tube, AIChE Journal 29 (1983) 306–312.

[67] E.E. Michaelides, Heat transfer in particulate flows, International Journal of Heat and Mass Transfer 29 (1986) 265–273.

[68] K.S. Han, H.J. Sung, M.K. Chung, Analysis of heat transfer in a pipe carrying two-phase gas–particle suspension, International Journal of Heat and Mass Transfer 34 (1991) 69–78.

[69] M. Haim, Y. Weiss, H. Kalman, Numerical model for heat transfer in dilute turbulent gas-particle flows, Particulate Science and Technology 25 (2007) 173–196.

[70] S. Park, Heat transfer in countercurrent gas-solid flow inside the vertical pipes, KSME Journal 5 (1991) 125–129.

[71] Y. Molodtsof, Hydrodynamics and heat transfer to vertically flowing gas-solids suspensions, KONA 10 (1992) 41-57.

[72] Y. Molodtsof, D.W. Muzyka, Wall to suspension heat transfer in the similar profile regime, International Journal of Heat and Mass Transfer 35 (1992) 2665–2613.

[73] P. Boulet, B. Oesterle, A. Taniere, Prediction of heat transfer in a turbulent gas-solid pipe flow using a two-fluid model, Particulate Science and Technology 17 (1999) 253–267.

[74] Y.J. Kim, J.H. Bang, S.D. Kim, Bed-to-wall heat transfer in a downer reactor, The Canadian Journal of Chemical Engineering 77 (1999) 207–212.

[75] Y. Ma, J.X. Zhu, Characterizing gas and solids distributors with heat transfer study in a gas-solids downer reactor, Chemical Engineering Journal 72 (1999) 235–244.

[76] Y.L. Ma, J. Zhu, Heat transfer in the downer and the riser of a circulating fluidized bed – A comparative study, Chemical Engineering & Technology 24 (2001) 85–90.

[77] R.A. Sorensen, J.D. Seader, B.S. Brewster, Pressure drop and heat transfer for cocurrent upflow of dilute gas-coal particle suspensions in a circular tube, Industrial & Engineering Chemistry Research 40 (2001) 457–464.

[78] E.S. Bourloutski, A.M. Bubenchikov, A.V. Starchenko, The comparison of two approaches to numerical modelling of gas-particles turbulent flow and heat transfer in a pipe, Mechanics Research Communications 29 (2002) 437–445.

[79] V. Chagras, S. Moissette, P. Boulet, B. Oesterle, Numerical investigation of the influence of the particle / pipe diameter ratio in a non-isothermal gas-solid flow, in: Proceedings of ASME Fluids Engineering Division Summer Meeting, July 14-18, Montreal, Quebec, Canada, 2002.

[80] Z. Jin-song, L. Zhong-yang, G. Xiang, M. Ming-jian, C. Ke-fa, Thermo-mechanical modeling of turbulent heat transfer in gas-solid flows including particle collisions, Journal of Zhejiang University Science 3 (2002) 381–386.

[81] Z. Mansoori, M. Saffar-Avval, H.B. Tabrizi, G. Ahmadi, S. Lain, Experimental study of turbulent gas-solid heat transfer at different particles temperature, International Journal of Heat and Fluid Flow 23 (2002) 792–806.

[82] Z. Mansoori, M. Saffar-Avval, H.B. Tabrizi, G. Ahmadi, Experimental study of turbulent gas-solid heat transfer at different particles temperature, Experimental Thermal and Fluid Science 28 (2004) 655–665.

[83] W. Namkung, M. Cho, Pneumatic Drying of iron ore particles in a vertical tube, Drying

Technology 22 (2004) 877–891.

[84] Z. Mansoori, M. Saffar-Avval, H.B. Tabrizi, B. Dabir, G. Ahmadi, Inter-particle heat transfer in a riser of gas–solid turbulent flows, Powder Technology 159 (2005) 35–45.

[85] K. Everaert, J. Baeyens, K. Smolders, Heat transfer from a single tube to the flowing gas-solid suspension in a CFB riser, Heat Transfer Engineering 27 (2006) 66–70.

[86] K.S. Rajan, S.N. Srivastava, B. Pitchumani, B. Mohanty, Simulation of gas-solid heat transfer during pneumatic conveying: Use of multiple gas inlets along the duct, International Communications in Heat and Mass Transfer 33 (2006) 1234–1242.

[87] C.P. Narimatsu, M.C. Ferreira, J.T. Freire, Drying of coarse particles in a vertical pneumatic conveyor, Drying Technology 25 (2007) 291–302.

[88] K.S. Rajan, B. Pitchumani, S.N. Srivastava, B. Mohanty, Two-dimensional simulation of gas–solid heat transfer in pneumatic conveying, International Journal of Heat and Mass Transfer 50 (2007) 967–976.

[89] M. Saffar-Avval, H.B. Tabrizi, Z. Mansoori, P. Ramezani, Gas–solid turbulent flow and heat transfer with collision effect in a vertical pipe, International Journal of Thermal Sciences 46 (2007) 67–75.

[90] M. Haim, H. Kalman, The effect of internal particle heat conduction on heat transfer analysis of turbulent gas–particle flow in a dilute state, Granular Matter 10 (2008) 341–349.

[91] K.S. Rajan, S.N. Srivastava, B. Pitchumani, K. Dhasandhan, Experimental study of thermal effectiveness in pneumatic conveying heat exchanger, Applied Thermal Engineering 28 (2008) 1932–1941.

[92] K.S. Rajan, K. Dhasandhan, S.N. Srivastava, B. Pitchumani, Studies on gas-solid heat transfer during pneumatic conveying, International Journal of Heat and Mass Transfer 51 (2008) 2801–2813.

[93] Z. Mansoori, A. Dadashi, M. Saffar-Avval, F. Behzad, G. Ahmadi, Three-dimensional simulation of turbulent gas-solid flow and heat transfer in a pipe, in: Proceedings of ASME Fluids Engineering Division Summer Meeting, August 2-6, Vail, Colorado USA, 2009.

[94] F. Behzad, Z. Mansoori, M. Saffar-Avval, H.B. Tabrizi, G. Ahmadi, Thermal stochastic collision model in turbulent gas–solid pipe flows, International Journal of Heat and Mass Transfer 53 (2010) 1175–1182.

[95] M. Hamzehei, H. Rahimzadeh, G. Ahmadi, Computational and experimental study of heat transfer and hydrodynamics in a 2D gas-solid fluidized bed reactor, Industrial & Engineering Chemistry Research 49 (2010) 5110–5121.

[96] K.S. Rajan, S.N. Srivastava, B. Pitchumani, V. Surendiran, Thermal conductance of pneumatic conveying preheater for air–gypsum and air-sand heat transfer, International Journal of Thermal Sciences 49 (2010) 182–186.

[97] S.M. El-Behery, W.A. El-Askary, M.H. Hamed, K.A. Ibrahim, Hydrodynamic and thermal field analysis in gas-solid two phase flow, International Journal of Heat and Fluid Flow 32 (2011) 740–754.

[98] S. Azizi, M. Taheri, D. Mowla, Numerical modeling of heat transfer for gas-solid flow in vertical pipes, Numerical Heat Transfer, Part A: Applications 62 (2012) 659–677.

[99] S.M. El-Behery, W.A. El-Askary, M.H. Hamed, K.A. Ibrahim, Numerical and experimental studies of heat transfer in particle-laden gas flows through a vertical riser, International Journal of Heat and Fluid Flow 33 (2012) 118–130.

[100] K.A. Ibrahim, M.H. Hamed, W.A. El-Askary, S.M. El-Behery, Swirling gas-solid flow through pneumatic conveying dryer, Powder Technology 235 (2013) 500–515.

[101] Y. Zheng, D. McGlinchey, J. Pugh, Y. Li, Experimental investigation on heat transfer mechanisms of pneumatically conveyed solids' plugs as a means to mass flow rate measurement, Flow Measurement and Instrumentation 40 (2014) 232–237.

[102] L. Bertoli, C.K. de Souza, J.C.S.C. Bastos, J. de Almeida, J. de Almeida Jr., S. Licodiedoff, V.R. Wiggers, Lumped parameter analysis criteria for heat transfer in a co-current moving bed with adiabatic walls, Powder Technology 317 (2017) 381–390.

[103] S.M. El-Behery, A.A. El-Haroun, M.R. Abuhegazy, Prediction of pressure drop in vertical pneumatic conveyors, Journal of Applied Fluid Mechanics 10 (2017) 519–527.

[104] A.K. Sahu, V. Raghavan, B.V.S.S.S. Prasad, Temperature effects on hydrodynamics

of dense gas-solid flows: Application to bubbling fluidized bed reactors, International Journal of Thermal Sciences 124 (2018) 387–398.

[105] T. Arvind, R. Thiyagu, H. Nelson, Effect of performance parameters on the pneumatic conveying solid-gas heat transfer, International Journal of Ambient Energy 40 (2019) 413–416.

[106] R. Dhurandhara, J.P. Sarkar, B. Das, Elucidation of hydrodynamics and heat transfer characteristic of converging and equivalentuniform riser for dilute phase gas-solid flow, Chemical Engineering Research and Design 151 (2019) 120–130.

[107] M.F. Watkins, R.D. Gould, Experimental characterization of heat transfer to vertical dense granular flows across wide temperature range, Journal of Heat Transfer 141 (2019) 032001.

[108] W. Wanchan, P. Khongprom, S. Limtrakul, Study of wall-to-bed heat transfer in circulating fluidized bed riser based on CFD simulation, Chemical Engineering Research and Design 156 (2020) 442–455.

[109] M.H.M. Tawfik, M.R. Diab, H.M. Abdelmotalib, Heat transfer and hydrodynamics of particles mixture in swirling fluidized bed, International Journal of Thermal Sciences 147 (2020) 106134.

[110] A.K. Popuri, P. Garimella, Heat transfer studies in a laboratory vertical riser system suitable for waste heat recovery from industrial waste exhaust gases, Chemical Engineering Communications 207 (2020) 1616–1623.

[111] J. Li, X. Yao, L. Liu, X. Zhong, C. Lu, Bed-to-wall heat transfer in a gas-solid fluidized bed with external solids circulation: Modified packet renewal model, Powder Technology 383 (2021) 19–29.

[112] M.K. Wahi, Heat transfer to flowing gas-solid mixtures, Journal of Heat Transfer 99 (1977) 145–148.

[113] R.S. Kane, R. Pfeffer, Heat transfer in gas-solids drag-reducing flow, Journal of Heat Transfer 107 (1985) 570–574.

[114] V. Chagras, B. Oesterle, P. Boulet, On heat transfer in gas–solid pipe flows: Effects of collision induced alterations of the flow dynamics, International Journal of Heat and Mass Transfer 48 (2005) 1649–1661.

[115] A. Ebadi, Z. Mansoori, M. Saffar-Avval, G. Ahmadi, Wall roughness effect on heat transfer rate of the turbulent gas-solid flow in inclined pipes, in: Proceedings of ASME 4th Joint US-European Fluids Engineering Division Summer Meeting, August 3-7, Chicago, Illinois, USA, 2014.

[116] M. Pishvar, M.S. Avval, Z. Mansoori, M. Amirkhosravi, Three dimensional heat transfer modeling of gas-solid flow in a pipe under various inclination angles, Powder Technology 262 (2014) 223–232.

[117] N. Mokhtarifar, F. Saffaraval, M. Saffar-Avval, Z. Mansoori, A. Siamie, Experimental modeling of gas-solid heat transfer in a pipe with various inclination angles, Heat Transfer Engineering 36 (2015) 113–122.

[118] B.E. Launder, D.B. Spalding, The numerical computation of turbulent flows, Computer Methods in Applied Mechanics and Engineering 3 (1974) 269–289.

[119] D. Gidaspow, Multiphase flow and fluidization: Continuum and kinetic theory descriptions, Academic Press, Boston, 1994.

[120] C.L. Tien, Transport processes in two-phase turbulent flow, Technical Report PR-91-T-R, Project SQUID, ONR, 1959.

[121] C.K.K. Lun, S.B. Savage, D.J. Jeffrey, N. Chepurniy, Kinetic theories for granular flow: inelastic particles in Couette flow and slightly inelastic particles in a general flowfield, Journal of Fluid Mechanics 140 (1984) 223–256.

[122] M. Syamlal, W. Rogers, T.J. O`Brien, MFIX documentation: Theory guide, DOE/METC-94/1004, U.S. Department of Energy, 1993.

[123] S. Swain, S. Mohanty, A 3-dimensional Eulerian-Eulerian CFD simulation of a hydrocyclone, Applied Mathematical Modelling 37 (2013) 2921–2932.

[124] P. Patro, S.K. Dash, Numerical simulation for hydrodynamic analysis and pressure drop prediction in horizontal gas-solid flows, Particulate Science and Technology 32 (2014) 94–103.

[125] P. Patro, S.K. Dash, Prediction of acceleration length in turbulent gas-solid flows, Advanced Powder Technology 25 (2014) 1643–1652.

[126] S.E. Elghobashi, T.W. Abou-Arab, A two-equation turbulence model for two phase

flows, Physics of Fluids 26 (1983) 931–938.

[127] J. Ding, D. Gidaspow, A bubbling fluidization model using kinetic theory of granular flow, AIChE Jornal 36 (1990) 523–538.

[128] J. Cao. G. Ahmadi, Gas-particle two-phase turbulent flow in a vertical duct, International Journal of Multiphase Flow 21 (1995) 1203–1228.

[129] D. Gidaspow, R. Bezburuah, J. Ding, Hydrodynamics of circulating fluidized beds: Kinetic theory approach, in: O.E. Potter, D.J. Nicklin (Eds.), Proceedings of the 7th Engineering Foundation Conference on Fluidization, New York, May 3–8, 1992, pp. 75–82.

[130] C.Y. Wen, Y.H. Yu, Mechanics of fluidization, Chemical Engineering Progress Symposium Series 162 (1966) 100–111.

[131] S. Ergun, Fluid flow through packed columns, Chemical Engineering Progress 48 (1952) 89–94.

[132] D.A. Drew, R.T. Lahey, Particulate two-phase flow, Butterworth-Heinemann, Boston, 1993.

[133] R. Mei, J.F. Klausner, Shear lift force on spherical bubbles, International Journal of Heat Fluid Flow 15 (1994) 62–65.

[134] D.J. Gunn, Transfer of heat or mass to particles in fixed and fluidised beds, International Journal of Heat and Mass Transfer 21 (1978) 467–476.

[135] Ansys Fluent Inc., Fluent 15.0 user guide, Canonsburg, PA, USA, 2015.

[136] J.C. Dixon, The shock absorber handbook (second edition), John Wiley & Sons, England, 2007.

[137] P.C. Johnson, R. Jackson, Friction-collisional constitutive relations for granular materials, with application to plane shearing, Journal of Fluid Mechanics 176 (1987) 67–93.

[138] S.A. Vasquez, V.A. Ivanov, A phase coupled method for solving multiphase problem on unstructured meshes, in: Proceedings of ASME Fluids Engineering Division Summer Meeting, Boston, June 11–15, 2000.

[139] Fluent Inc., Fluent 6.3 user guide, Lebanon, NH, USA, 2003.

[140] Y. Tsuji, Y. Morikawa, LDV measurements of an air-solid twophase flow in a horizontal pipe, Journal of Fluid Mechanics 120 (1982) 385–409.

[141] M. Syamlal, T.J. O'Brien, Computer simulation of bubbles in a fluidized bed, AIChE Symposium Series 85 (1989) 22–31.

[142] Y. Tsuji, Y. Morikawa, H. Shiomi, LDV measurements of an air-solid two-phase flow in a vertical pipe, Journal of Fluid Mechanics 139 (1984) 417–434.

Publications

Journals:

- Brundaban Patro, Kiran K. Kupireddi, and Jaya K. Devanuri (2021) Computation of flow and heat transfer in horizontal gas-solid flows through an adiabatic pipe, **Proceedings of the Institution of Mechanical Engineers Part C: Journal of Mechanical Engineering Science**, 235(5), pp. 934–945. (SCI)
- Brundaban Patro, Kiran Kumar Kupireddi, and Jaya Krishna Devanuri (2020) Comparison of heat transfer and pressure drop results of horizontal gas-solid flows in an adiabatic pipe using plastic, sand and glass particles, **Powder Technology**, 374, pp. 314–322. (SCI)
- Brundaban Patro, K. Kiran Kumar, and D. Jaya Krishna (2019) Prediction of local heat transfer characteristics of dilute gas-solid flows through an adiabatic, horizontal pipe, **Heat Transfer–Asian Research**, 48(6), pp. 1987–2006. (ESCI)
- Brundaban Patro, K. Kiran Kumar, and D. Jaya Krishna (2019) Computational fluid dynamics studies of gas-solid flows in a horizontal pipe, subjected to an adiabatic wall, using a variable gas properties Eulerian model, **Chemical Product and Process Modeling**, 14(3), 20180063. (ESCI)
- Brundaban Patro, K. Kiran Kumar, and D. Jaya Krishna (2019) Computational modelling of gas-to-solid heat transfer in an adiabatic, vertical pipe, **International Journal of Advanced Trends in Computer Applications**, Special Issue 1 (1), pp. 83–88. (Peer Review)

Conference:

- Brundaban Patro, K. Kiran Kumar, and D. Jaya Krishna, Computational studies of air-glass particle flows for the prediction of heat transfer and pressure drop, Proceedings of the 2nd International Conference on New Frontiers in Chemical, Energy, and Environmental Engineering, 15th - 16th Feb. 2019, NIT Warangal, India.